Determining the role of murine hyaluronidase 2 in hyaluronan catabolism

By

Biswajit Chowdhury

A Thesis submitted to the Faculty of Graduate Studies of

The University of Manitoba

in partial fulfilment of the requirements of the degree of

Doctor of Philosophy

Department of Biochemistry and Medical Genetics

Faculty of Health Sciences

University of Manitoba

Winnipeg

Abstract

Hyaluronidase 2 (HYAL2) is a GPI-linked protein that is proposed to initiate the degradation of hyaluronan (HA), a major extracellular matrix component of many vertebrate tissues. *Hyal2* knockout (KO) mice displayed craniofacial abnormalities and severe preweaning lethality. 54% of the surviving KOs developed a grossly dilated left or right atrium, requiring euthanasia, by 3 months of age. We hypothesize that the absence of HYAL2 leads to the accumulation of HA in organs/tissues where HA is normally abundant resulting in developmental defects and organs dysfunction.

Molecular and histological analysis of HYAL2 KO hearts demonstrated extracellular accumulation of high molecular mass (HMM) HA in the heart valves, myocardium, serum and lungs which was associated with severe cardiopulmonary dysfunction. Further, structural and functional analyses of *Hyal2* KO mouse hearts using high-frequency ultrasound revealed atrial dilation accompanied by diastolic dysfunction that was evident as early as 4 weeks of age, and progressed with age. Further, 50% of HYAL2 KO mice exhibited a triatrial heart (cor-triatriatum). Histological analyses revealed that the atrial dilation was the result of excess tissue, and did not correlate with the presence of cor triatrium. *Hyal2* KO mice were found to have increased numbers of mesenchymal cells at early stages of development, presumably due to the presence of excess HA, that lead to cardiac dysfunction. Further examination of HYAL2 distribution in a broad range of mouse tissues, and accumulation of HA in its absence demonstrated that HYAL2 is mainly localized to endothelial cells and some specialized epithelial cells, and plays a major role in HMM-HA degradation. These studies demonstrated that HYAL2 is important for HA degradation and organ development. In the longer term, our findings will be valuable for understanding pathologies associated

with the disruption of HA catabolism, and potentially in the identification of HYAL2-deficient patients.

Dedication

Dedicated to my parents,

Mr. Biraj Kanti Chowdhury

&

Mrs. Juthika Chowdhury

They have taught me to keep my dreams big, to work hard to chase my dreams, never give up my patience; ultimately the results will be big

Acknowledgements

For me, this thesis is a life changing journey and became possible only with the support and love of many. First and foremost, I would like to thank my supervisor, Prof. Barbara Triggs-Raine. Words cannot express my appreciation to her for all her highly valued guidance throughout the entire process. She has taught me how to be organized, focused and collaboratively perform a project in research. Due to the countless hours she dedicated to me I have developed great critical thinking, problem-solving and academic writing skills. Her intellectual prowess, professional resolve and continuous patience all along has helped me to achieve high merit during the course of this degree.

Apart from my supervisor I would like to thank my present and past committee members Dr. Ian Dixon, Dr. Jeffrey Wigle, Dr. David Merz, and Dr. Steve Pind for their time, encouragement and valuable suggestions throughout my Ph.D. work. Special thanks to our collaborators Dr. Sabine Hombach-Klonish, Dr. Brian Blakely, Dr. Vernon W. Dolinsky, Dr. Andrew Crosby, and Dr. Bruno Flamion for their excellent insight and assistance. I am also very grateful to the BMG office staff for their kind support throughout my PhD work. I would also like to acknowledge Xiaoli Wu for her technical assistance with unfamiliar laboratory equipment and techniques. The ultrasound imaging studies discussed in this thesis would not have been possible without the help of Dr. Bo Xiang. I gratefully acknowledge the funding sources including University of Manitoba, Faculty of Graduate Studies, Department of Biochemistry and Medical Genetics, Manitoba Health Research Council, and Children Hospital Research Institute of Manitoba that assisted my PhD studies.

Present and past members of BTR lab's had played an enormous role in my professional life during my stay at University of Manitoba. Special thanks go out to Dr. Rick Hemming, Dr. Joy Armistead, Lara Gushulak, Ramya Vinith, Dr. Gagandeep Singh Basra, Naderah Altaleb

and Naimul Hasan for their continuous support and encouragement during my studies. I would like to thank Rick for all his help and expert technical advice in various experiments. I really appreciate the minute technical details that he would tell me while training and I appreciate the hard work and enthusiasm he put - in was a learning experience for me. I would like to thank Joy for all her feedback on various occasions and for being a wonderful lab mate.

I must acknowledge the wonderful friends I have made in this journey. My life at the University of Manitoba and especially Winnipeg was made memorable and enjoyable in large part due to my friends. I would like to thank Subhankar Ghosh, Triparna Lahari, Raja Chackroborty, Shivika Gupta, Aruni Jha, Nivedita Seshadri, Anurag and his family, for their support during my stay in Winnipeg. I would like to thank Tuntun Sarkar enormously, who has not only guided me professionally but has also been a motherly figure, and never let me feel homesick over the last six years. Lastly, I would like to thank my Baba, Biraj Kanti Chowdhury, Maa, Juthika Chowdhury, my Sister, Anuradha Chowdhury Samanta and Brother-in-law, Ashim Samanta. It is because of their blessings, unconditional love, and tremendous support from 8000 miles away that I dared to dream this journey and now finally finish it.

Table of contents

List of abbreviations

α-SMA	alpha smooth muscle actin
AA	amino acid
ADAMTS	a disintegrin and metalloproteinase with thrombospondin motifs
AVC	atrioventricular canal
Asp	aspartate
BM	basement membrane
Bmps	bone morphogenetic proteins
CHD	congenital heart disease
CO	cardiac output
CPC	hexadecylpyridinium chloride
CS	chondroitin sulphate
CD44	cluster of differentiation antigen 44
Da	Dalton
DAB	diaminobenzidine
DS	dermatan sulphate
ECM	extracellular matrix

EC-SOD	extracellular superoxide dismutase
EF	ejection fraction
EMT	epithelial to mesenchymal transition
endoEMT	endothelial to mesenchymal transition
ERBB2	receptor tyrosine kinase erbB-2
ERK	extracellular signal-regulated kinase
ERT	enzyme replacement therapy
Fgfs	fibroblast growth factors
FACE	fluorophore assisted carbohydrate electrophoresis
FS	fractional shortening
GAG	glycosaminoglycan
GlcNAc	N-acetylglucosamine
GalNAc	N-acetylgalactosamine
GlcUA	glucuronic acid
Glu	glutamate
GPI	glycosylphosphatidylinositol
GT	glycosyltransferase
HA	hyaluronan
HAS	hyaluronan synthase

HABP	HA binding protein
HARE	HA receptor for endocytosis
HMM	high molecular mass
HS	heparin sulphate
HYALs	hyaluronidases
HYAL/Hyal	human/mouse gene
Hyal2$^{+/+}$	wild type mouse
Hyal2$^{+/-}$	heterozygous mouse
IdoA	iduronic acid
IHC	immunohistochemistry
IVRT	isovolumetric relaxation time
KO	knockout
kDa	kilo Dalton
LMM	low molecular mass
LN	lymph node
LYVE-1	lymphatic vessel endothelial receptor-1
MEF	mouse embryonic fibroblast
Micro-CT	micro computed tomography
MPI	myocardial performance index

MPS	mucopolysaccharidosis
NCC	neural crest cells
NK	natural killer
NI	none identified
OFT	outflow tract
PBS	phosphate buffer saline
PG	proteoglycan
RHAMM	receptor for hyaluronic acid mediated motility
SEM	standard error mean
SPAM1	sperm adhesion molecule 1
Tgfβ	transforming growth factor β
UDP	uridine diphosphate
VEGF	vascular endothelial growth factor
VIC	valve interstitial cells

List of figures

List of tables

List of copyrighted material with permission

Figure 3.1. Apical 4-chamber view of *Hyal2* KO and control hearts

Reprinted with permission *International Journal of Cardiology*, Volume 209, 15 April 2016, Pages 281-283 *License number*- 3813920767340 © by Elsevier Ltd

Chapter 4. Hyaluronidase 2 (HYAL2) is expressed in endothelial cells, as well as some specialized epithelial cells, and is required for normal hyaluronan catabolism.

Reprinted with permission *Histochemistry and Cell Biology* Volume January 2016, Volume 145, Issue 1, pp 53-66 *License number*- 3814280244582 © by Springer Ltd

Chapter 1: Introduction

1.1 The extracellular matrix (ECM)

One of the most significant transitions in evolution is the formation of a multicellular organism from a single-celled ancestor. The extracellular matrix (ECM) is central to multicellularity as it connects cells, provides structural support, regulates physiological functions, and is essential for proliferation and differentiation during development [1,2]. The constituents of the ECM are synthesized by highly conserved pathways and secreted by mesodermal cells including fibroblasts, chondroblasts, and osteoblasts [3]. The importance of the ECM is demonstrated by the multiple pathologies that result from genetic abnormalities of an ECM molecule.

1.1.1 ECM structure

In connective tissues, the ECM is composed of proteins and polysaccharides that interact to form a dense meshwork between cells [4]. There are more than one hundred genes that are involved in the synthesis of ECM components in the vertebrate genome [1]. Many ECM components are ubiquitously present, while others exhibit tissue-specific expression. Vertebrate connective tissues are highly varied. For example, the connective tissue is flexible and tough in tendons and dermis, hard and dense in bone, soft and transparent in heart and eye, and resilient and shock-absorbing in cartilage. The tensile strength of the connective tissues depends on the amount and types of a fibrous protein called collagen, together with its organization with other molecules such as elastin and polysaccharides [4].

In vertebrates, the most abundant fibrous proteins are collagen and elastin, which play an important role in determining the mechanical properties of the tissue [2]. Collagens are

well characterised triple helical proteins that provide tensile strength, regulate cell migration and adhesion, and participate directly in the development of many tissues, including tendon, skin, heart valves, cartilage and blood vessels [5]. More than 40 collagen genes are transcribed, and result in 28 different subtypes of collagen [6]. Abnormalities in these genes are the cause of several human connective tissue disorders including Marfan syndrome, osteogenesis imperfecta and Ehlers-Danlos syndrome [5].

Elastin is secreted as tropoelastin and is cross-linked by members of the lysyl oxidase family of enzymes. It is a major component of some connective tissues including blood vessels, heart valves and skin. In these tissues, elastin provides elasticity during repetitive stretching and relaxation. It regulates the activity of transforming growth factor β (TGFβ) through association with fibrillins [7]. Elastin also play a role in different cell signalling events. For example, tropoelastin inhibits proliferation of arterial smooth muscle cells and act as a chemotactic agent to induce organization of actin fibers [8]. Mutations in the elastin-encoding gene cause supravalvular aortic stenosis in Williams syndrome, which is characterised by narrowing of the aorta and pulmonary arteries [9]. The importance of elastin during development has been characterized by elastin knockout (KO) mice. These mice die soon after birth due to severe cardiovascular abnormalities including aortic stiffness and low cardiac output [10].

The non-protein parts of the ECM are the long-chain polysaccharides known as glycosaminoglycans (GAGs). These GAGs are typically covalently linked to ECM proteins in the form of proteoglycans (PGs). In the ECM, polysaccharides provide a hydrated environment where protein molecules are embedded. A more detailed discussion of PGs and GAGs is provided in the subsequent sections.

1.1.1.1 **Glycosaminoglycans (GAGs)**

GAGs are negatively-charged carbohydrate polymers that consist of repeating units of an amino sugar (either N-acetylglucosamine [GlcNAc] or N-acetylgalactosamine [GalNAc]) and a uronic acid (glucouronic acid [GlcUA] or Iduronic acid [IdoA]). These disaccharide units are often modified by sulfation of the amino sugar at position 4 or 6 [11]. Hyaluronan (HA) is the only non-sulfated GAG, whereas chondroitin, dermatan, keratan, and heparin are all sulfated. With the exception of HA, the GAGs are linked to core proteins via a serine residue [11]. The disaccharide composition, modification and origin of synthesis of all the GAGs are described in Table 1.1.

Table 1.1. Characteristic features of GAGs

GAG Type	Disaccharide composition	Sulfation position [12]	Synthesis location	Distribution in tissues [11]
HA	GlcUA & GlcNAc	None	Plasma membrane	Ubiquitous
Chondroitin sulfate (CS)	GlcUA & GalNAc	IdoA-2S , 3S GalNac 4S & 6S	Endoplasmic reticulum and Golgi	Cartilage, tendon, ligament and aorta
Dermatan sulfate (DS)	IdoA or GlcUA & GalNAc	IdoA-2S , 3S GalNac 4S & 6S	Endoplasmic reticulum and Golgi	Skin, blood vessels and heart valves
Heparin and heparin sulfate (HS)	IdoA or GlcUA & GlcNAc	IdoA-2S GlcA-2S GlcNAc-3S, 6S	Endoplasmic reticulum and Golgi	Basement membrane (BM), mast cells
Keratan sulfate (KS)	Gal & GlcNAc	GlcNac -6S Gal-6S	Endoplasmic reticulum and Golgi	Eye, cartilage

1.1.1.2. **Proteoglycans (PGs)**

Proteoglycans (PGs) are composed of core proteins that are covalently attached to GAGs other than HA. Based on the GAGs that are attached, PGs are categorized into three groups including CS/DS (aggrecan, versican, neurocan and brevican), HS (syndecans and betaglycans), and KS (fibromodulin) proteoglycans. Most mammalian cells synthesize PGs that are transported into either the ECM, plasma membrane, or stored as secretory granules. In the ECM, PGs may be linked with a small number of GAG chains or carry more than 100 GAG chains. Plasma membrane PGs including CD44 (cluster of differentiation antigen 44) and syndecan, possess either a transmembrane domain or a glycosylphosphatidylinositol (GPI) anchor. Cell surface and ECM PGs bind with several growth factors. Serglycin is a secretory PG, and it is synthesized by immune cells including mast cells, natural killer cells and basophils [13]. The tissue distribution, major function and diseases associated with all PGs are described in Table 1.2

Table 1.2. Characteristic features of PGs

Proteoglycans	**Tissue distribution**	**Major functions**	**Human disease associated with mutation in PGs**
Versican V0, V1, V2, V3 isoforms	Blood vessels, brain skin, cartilage	ECM assembly, cell signalling events, collagen fibrillogenesis	NI (none identified)
Aggrecan	Cartilage, brain, blood vessels	Cartilage development, growth and homeostasis	Spondyloepiphyseal dysplasia [14]
Neurocan & Brevican	Brain	Inhibition of neuronal attachment and neurite outgrowth	NI
Perlecan	BM, cartilage, connective tissue stromas	Signaling, pro-angiogenic, collagen fibrillogenesis, apoptosis; C-terminal domain: Endorepellin, anti-angiogenic	Dyssegmental dysplasia, Silver Handmacher type; Schwartz-Jampel syndrome [15]

1.1.2 Role of ECM in tissues/organs

ECM molecules play important roles in regulating tissue integrity, branching morphogenesis, cell signalling events and determining the identity of neighbouring cells [2]. Therefore, homeostasis of ECM components is necessary for the maintenance of normal tissue integrity and cross-talk between cells of the stroma. Different tissue remodelling enzymes including matrix metalloproteinases (MMPs), tissue inhibitor matrix metalloproteinases (TIMPs), and hydrolases play important roles in the degradation/activation of ECM molecules [16].

Although many roles for the ECM in organ morphogenesis and tissue homeostasis are known to exist, their mechanisms of action are still unclear. Therefore, it is compelling to define the role of the ECM components that contribute to the complex series of events governing organ development. Errors in development leading to congenital birth defects in humans are associated with defects in several ECM components. Determining the molecular basis/causes of the diseases associated with ECM dysregulation in mouse models is an important step in understanding the normal role of the ECM and potentially improving disease outcome in the longer term.

1.2 Hyaluronan (HA)

In 1934 Karl Meyer and his colleague John Palmer isolated hyaluronic acid from the vitreous body of bovine eyes. Initially, it was characterized as an unknown chemical

substance composed of sugar molecules and uronic acid and proposed its name ‘hyaluronic acid’. The name hyaluronic acid was derived from the Greek word ‘hyalos’, which means glass, and uronic acid. The term ‘hyaluronan’ was introduced by Endre Balazs, to represent all forms of this molecule, both the free acid and salt conjugated forms [17]. Later on, HA was also isolated from various other sources including skin, synovial fluid, rooster comb and umbilical cord. Twenty years after the initial characterization, the same group identified the chemical structure of HA as a negatively charged GAG composed of a repeating unit of D-GlcUA and GlcNAc linked by β1-3 and β1-4 glycosidic bonds (Figure 1.1). The carboxyl groups of HA attract water into the extracellular space whereas newly formed hydrogen bonds along the polysaccharide creates hydrophobic patches that allow close association with other HA molecules and cell surface receptors [18]. The number of disaccharide units in an HA molecule can reach 10,000 or more with a molecular mass of several million Daltons (Da). The average molecular mass of HA in synovial fluid is 7×10^6 Da and if it is linearized, the length would be extended to approximately 15 μm [19]. At a physiological pH, HA attracts solvent due to its anionic charge, and forms a continuous network.

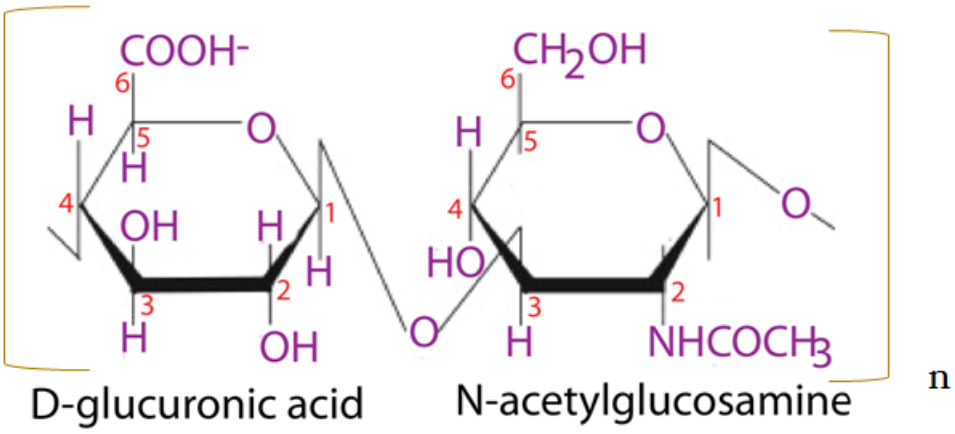

Figure 1.1. Molecular structure of HA

It is composed of a repeating unit of D-GlcUA and D-GlcNAc with alternating β1-3 and β1-4 glycosidic bonds.

1.2.1 HA distribution and function

HA is ubiquitously present in all vertebrate ECM as well as in the capsule of gram positive and gram negative bacteria such as *Strepococci pyogenes, and Pasteurella multocida* respectively [20]. It is an abundant component of the ECM in many vertebrate tissues including heart valves, umbilical cord, vitreous humour of the eye, palate, skin and synovial fluid. The careful study of HA content in the rat provided an overview of HA distribution in mammals [21]. Almost 50% of the HA in the body was present in the skin, 25% in the skeleton and joints, and the remaining HA was equally distributed in the muscle and viscera [21]. In humans, the highest HA concentrations are present in umbilical cord (4.1 mg/g), synovial fluid (1.4 mg/g), skin (0.2 mg/g) and vitreous body (0.14 mg/g) [19]. The levels of HA are also high in brain, lung, kidney and liver [19]. HA is primarily thought to be present in the extracellular space and pericellular coat, although recent studies have also shown it to be intracellular [22]. Within tissues, HA is connected via link proteins with PG-associated

GAGs and plays important roles in cell motility, signal transduction, embryogenesis, and regulation of many disease pathologies [23]. The role of HA in organ development and tissue homeostasis will be discussed in a subsequent section.

1.2.2 **Link protein or hyaladherins**

In the ECM, the interaction between HA and HA binding protein (HABP) are mediated by a common protein domain known as a link module. The molecular structure of the link module is comprised of two alpha helices and two beta helices, as well as positively charged amino acids (aa) that bind HA [24]. The presence of the link module has been found in the core protein of several PGs, including aggrecan, versican, neurocan and brevican. The interaction of HA and PGs play important roles in the formation of the pericellular matrix and provide structural integrity in the ECM.

The link module was also found to be present in the cell surface receptor for HA, and other proteins including tumor necrosis factor stimulating gene-6 (TSG-6). The interaction between HA and the cell surface receptor via link module initiated cell signaling events or the local degradation of HA by endocytosis. However, no link module has been identified in some molecules. In this case, a consensus sequence $B(X_7)B$ has been identified as a HA binding motif, where B represents a basic lysine or arginine and X represents any aa [25].

1.2.3 HA synthesis

HA differs from other GAGs in that it is not synthesized in the endoplasmic reticulum/Golgi. HA is synthesised at the plasma membrane and then exported into the ECM (Figure 1.2). HA synthases are plasma membrane associated glycosyltransferases that

polymerize nucleotide sugars, uridine diphosphate (UDP)-GlcUA and UDP-GlcNAc to generate a long chain of HA [26]. HA chain elongation does not require an additional protein backbone like other GAGs; the presence of nucleotide sugars alone can initiate a new chain. In 1993, characterization of the *Streptococcus hasA* gene led to the identification of HAS genes in other organisms including vertebrates. HASs are classified into two categories based on their architecture, predicted topology, and whether the sugars were added to the reducing or non-reducing terminus [26]. Class I HAS is an integral membrane proteins present in vertebrates and some gram-positive bacteria. The HAS molecules contain one glycosyltransferase (GT) module and can add newly synthesized sugar molecules either to reducing or non-reducing ends. Type II HAS is present mainly in gram-negative bacteria such as *Pasteurella multocida*; it has two GT modules and always adds sugar molecules at non-reducing ends. It is a peripheral membrane protein with no affinity for lipid bilayers and no requirement of lipid for its activity [26].

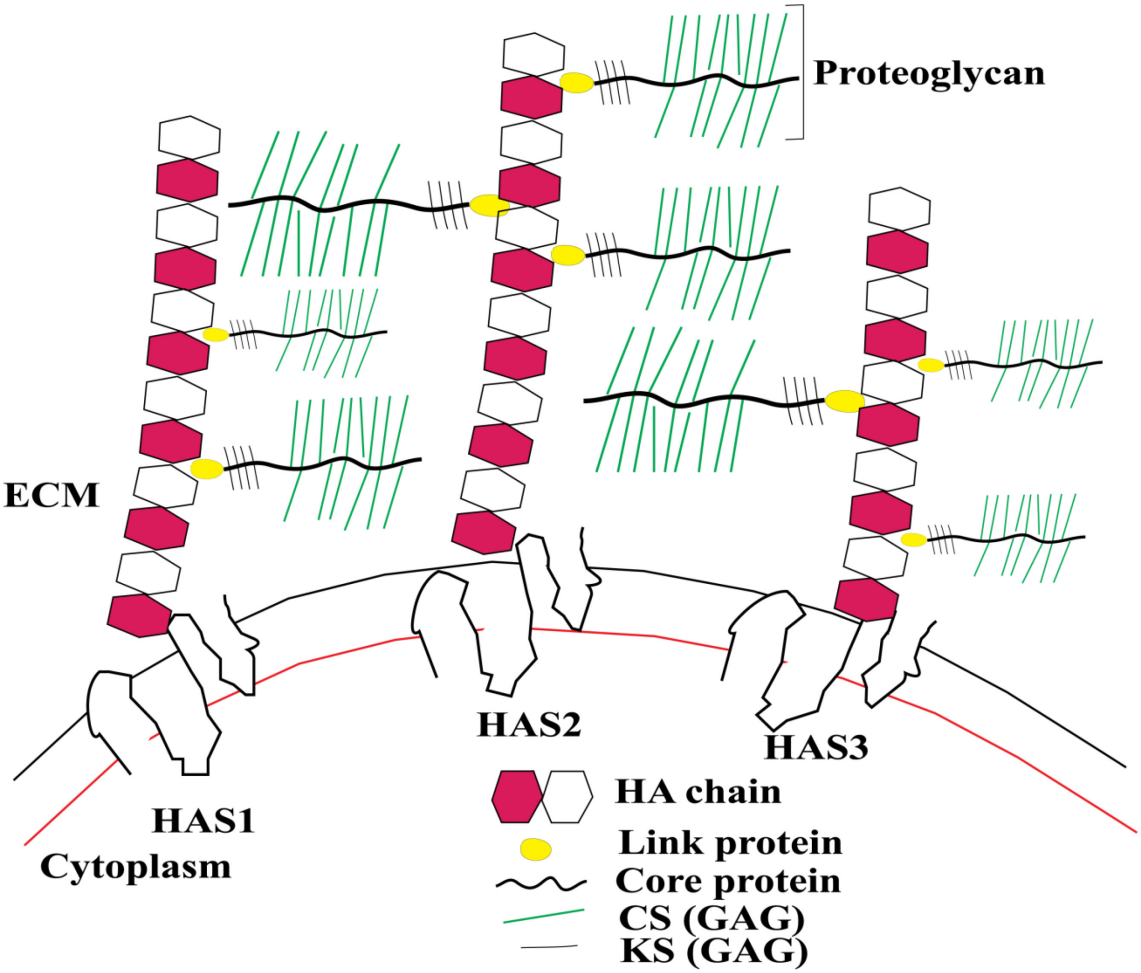

Figure 1.2. Interaction of HA with PGs.

In the ECM, newly synthesized HA from plasma membrane associated HAS enzymes is directly secreted into the matrix. The molecular mass of newly synthesized HA by HAS3 is lower than that of the other two enzymes. In the matrix, the core protein of PGs bind with HA via the link module. The GAGs are covalently attached to the core protein.

1.2.4 Mammalian HA synthase

There are three mammalian HA synthases, *HAS1*, *HAS2*, and *HAS3*, which are evolutionarily conserved in mammals. These enzymes are encoded by genes on three different chromosomes. The chromosomal distribution of the three *HAS* genes suggests that they may have arisen in vertebrates from an ancestral *HAS* gene by duplication events. Although they share more than 90% sequence similarity and catalyse the same reaction, they differ in the chain length they synthesize, enzyme stability and specific enzyme activity [27]. Differential expression of *HAS* genes during development and in adult tissues indicates that each gene has an important role [28].

1.2.4.1 *HAS1*

The human *HAS1* gene is located on chromosome 19q13.3, whereas the mouse *Has1* gene is on chromosome 17 [27]. Mouse *Has1* has five exons and shares 95% aa identity with human HAS1 [27]. The HAS1 protein is less stable than the other two human HASs and generates high molecular mass HA (2 x 10^6 Da) [29]. *In vitro* studies have been shown that HAS1 needs a higher concentration of UDP-GlcNAc for its activity than the other HAS proteins [30]. Although HAS1 is highly expressed during early gastrulation in mouse [28], *Has1*- deficient mice are viable and fertile [31]. A recent study of *Has1* KO mice showed that they had mild epileptic seizures [32].

1.2.4.2 *HAS2*

Human and mouse *HAS2*/*Has2* genes are located on chromosome 8 and 15 respectively and synthesize HA chains similar in size to HAS1, 2 x 10^6 Da [27]. Human and mouse HAS2 proteins share 98 % identity to each other [27]. HAS2 is more active and widely expressed during embryonic development than is HAS1 [28]. HAS2 is known to be

the major somatic HA synthase. The examination of a KO mouse for *Has2* clearly demonstrated that HA has a key role in heart development (21). These mice die during embryogenesis because of extensive abnormalities of the developing cardiovascular system, a defect that can be corrected by the addition of exogenous HA. Since the *Has2* KO mice are embryonic lethal, conditional KO studies were required to determine its role in the development of other organs. Skeletal tissue-specific inactivation of *Has2* in a mouse model demonstrated that HA is also required for normal development and growth of the limb [33]. Brain-specific conditional *Has2* KO mice revealed reduced HA in the cortex led to abnormal brain development and an epileptic phenotype [32]. The conditional deletion of *Has2* in other tissues will be necessary to determine its full role in development.

1.2.4.3 *HAS3*

Human and mouse *HAS3*/*Has3* genes are located on chromosomes 16 and 8 respectively. The mouse *Has3* gene is comprised of 4 exons [27]. Unlike HAS1, HAS3 is the most active enzyme and synthesizes comparatively low molecular mass HA (2 $X10^5$ Da). During embryonic development, HAS3 expression was evident in ectodermal derived organs such as the nervous system, tooth and epidermis [28]. Like *Has1*, *Has3* KO mice are also viable and fertile. Further, *Has1* and *Has3* double KO mice also did not demonstrate any developmental abnormalities [34]. To determine the function of HAS3 in the development of ectodermal derived organs, *Has3* conditional KO mice were generated. The characterization of *Has3* KO mice demonstrated HAS3 plays a role in normal brain development and its absence results in frequent epileptic seizures [32].

1.3 HA turnover

HA has a high rate of constitutive turnover, with ~1/3 of the 15 g of HA estimated to be present in a 70 kg person turned over daily. The half-life of HA is tissue dependent. For example, the degradation rate of HA is 2-3 min in serum, 1-2 days in skin, and 2-3 weeks in cartilage. Turnover of circulating HA in various animal models showed that after local degradation, approximately 50-90% of processed HA enters the lymphatic system for further removal, and the remaining HA is removed from the blood primarily by the liver and spleen [35,36]. The molecular mass of HA is systematically reduced in each step of removal. HA that enters the lymph nodes (LN) has an average mass lower than that in the local tissue (10^5 or 10^6 Da) and when it leaves through the efferent lymphatic vessels it has an average mass of 10^4 Da. Unlike other GAGs, the amount of HA excreted in urine is minimal, only 330 μg per day [37].

1.3.1 Hyaluronidases (HYALs)

Hyaluronidases (HYALs) are a group of enzymes responsible for the majority of HA degradation that also have weak activity toward chondroitin and CS. In 1928, Duran-Reynals identified HYALs from mammalian testes as a 'spreading factor' which can promote the diffusion of injected substances [38]. Based on their enzymatic properties, Karl Meyer categorised them into three groups; lyases, mammalian hydrolases and hydrolases found in leeches and in certain crustaceans [39]. Bacterial hyaluronidases (EC 4.2.2.1 or EC 4.2.99.1) are lyases that cleave the β-1-4 linkage between GlcNAc and GlcUA to produce unsaturated disaccharides. Mammalian hyaluronidases are hyaluronate-4-glycanohydrolases (EC 3.2.1.35) which have been found in mammalian spermatozoa, lysosomes and venoms of various insects and snakes. The third group of hyaluronidases are 3-glycanohydrolases (EC

3.2.1.36) that are produced by leeches and some hookworms [40]. Unlike the bacterial hyaluronidase, these enzymes hydrolyze the β 1→4 linkages between GlcNAc and GlcUA and the end product is tetrasaccharide. It becomes the substrate for an exoglycosidase that hydrolases the HA to single monomer units.

Six genes encoding HYAL-related enzymes have been identified in humans; they are grouped as a two tightly linked triplets on human chromosomes 3p21.3 (*HYAL1*, *HYAL2*, *HYAL3*) and 7q31.3 (*HYALP1*, *HYAL4*, *SPAM1*) [41]. These sequences all share approximately 40% aa identity and appear to have evolved by duplication to form a cluster of three genes on one chromosome that was duplicated again to form a second cluster on another chromosome [42]. *HYALP1* is a non-coding pseudogene because of the presence of a premature stop codon.

The mouse orthologous genes are found on chromosome 9 (*Hyal1*, *Hyal2*, *Hyal3*) and chromosome 6 A2 (*Hyal4*, *Spam1* and *Hyalp1*) [43]. Along with these six genes, another homologous gene, *Hyal5*, was found downstream of *Spam1* [44]. Details of each of these genes and their encoded enzymes are described in the following sections.

1.3.1.1 HYAL1

HYAL1, also known as the plasma hyaluronidase, is an acid-active hyaluronidase that degrades HA to tetrasaccharides. It was the first hyaluronidase to be isolated, cloned and sequenced from mammalian tissues [45]. Human *HYAL1* has 7 exons (Gene ID: 3373) and encodes a 2507 bp mRNA, which is translated into a protein of 435 aa with a predicted molecular mass of 43.5 kDa. *HYAL1* mRNA is present in almost all human tissues [46]. However, it is most highly expressed in liver, kidney, spleen, and bone marrow the major

sites of HA degradation [41,47]. A recent study of the subcellular localization of HYAL1 in murine macrophages showed that HYAL1 is synthesized as a 52 kDa protein that is processed to a 48 kDa form by proteolytic maturation when it reaches the lysosome [48]. The crystal structure of human HYAL1 has been determined. Like other glycosidases, the active site region is found in the centre of an alpha/beta barrel. Two residues, Asp129 and Glu131 are the key catalytic residues required for hydrolysis although several aromatic amino acids and some key amino acids lining the substrate binding groove are also important [49]. During the catalytic reaction, glutamate acts as a proton donor and the N-acetyl group of HA provides the nucleophile [50]. Therefore, the activity of HYAL1 is dependent on acidic environments (pH 3.8) and it can breakdown any size of HA to produce tetrasaccharide units [45]. The mouse orthologue shares approximately 73% aa similarity with human HYAL1 [45].

A deficiency in HYAL1 results in a lysosomal storage disorder in humans, mucopolysaccharidosis (MPS) IX, that is characterized by joint abnormalities due to HA accumulation [51]. Histological examination of affected tissue demonstrated the accumulation of HA in the lysosomes of macrophage and fibroblasts [51]. Studies of HYAL1 deficiency in a mouse model demonstrated a similar phenotype to that of the human disease [52]. To date, four patients (two males and two females) have been diagnosed with MPS IX. They exhibit chronic joint pain and pathological studies showed mild hyperplasia of the synovium and macrophage infiltration [53] that in one patient has led to bilateral joint replacement. Considering the broad distribution of HA and its role during development, this phenotype is unexpectedly mild and suggests that other enzymes play a role in constitutive HA degradation.

1.3.1.2 HYAL3

Human *HYAL3* has 5 exons and encodes a 1492 bp mRNA which is translated into a protein of 417 aa with a predicted molecular weight 41.7 kDa. HYAL3 is weakly expressed in most tissues, except in the testes and bone marrow, where it is highly expressed [47]. *In vitro* transfection of murine HYAL3 in baby hamster kidney cells resulted in 45 and 56 kDa isoforms that localised in late endosomes/lysosomes [54]. Although no HYAL3 activity is detected [55], its overexpression resulted in an elevation in HYAL1 activity suggesting a role for HYAL3 in HA metabolism [54]. *Hyal3* KO mice appeared healthy and did not exhibit any skeletal abnormalities or HA accumulation [56]. The only pathology was a mild morphological difference in the lungs of *Hyal3* KO mice. A recent study reported that HYAL3 had an acidic enzymatic activity in sperm that might facilitate the penetration of the sperm through the cumulus cells surrounding the oocytes [57].

1.3.1.3 HYAL2

The *HYAL2* gene has six exons (Gene ID: 8692) and encodes a 1909 bp mRNA that is translated to form a 473 aa (GenBank: AAH00692.1). Initially, HYAL2 was proposed to be a lysosomal enzyme [58]. Amino acid sequence similarity of human HYAL2 with its mouse orthologue is 82%. Analysis of the primary structure of HYAL2 using bioinformatics revealed the presence of an N-terminal signal sequence that would be expected to target the protein to the endoplasmic reticulum. A signal for a GPI linkage was also predicted that would replace the c-terminal 27 aa [59]. Later, HYAL2 was identified as a GPI linked protein in HEK293 cells [60], and in bronchial epithelium [61]. Subcellular localization of HYAL2 has been reported in association with lipid rafts [59]. HYAL2 can also be translocated from a

organelle in the cytoplasm to the plasma membrane. In activated platelets, HYAL2 is transported from α-granules to the membrane [62].

1.3.1.3.1 HYAL2 expression

An initial study of *HYAL2* revealed that it is broadly expressed in all human tissues except in adult brain [58]. Further, expression analysis using quantitative RT-PCR in adult and embryonic mouse tissues demonstrated ubiquitous expression of *Hyal2* mRNA including in the brain [63]. The expression of HYAL2 is also evident during development. For example, HYAL2 levels varied during development and it was assumed to promote blastocyst formation of bovine embryos *in vitro* [64]. The expression of HYAL2 in microvascular endothelial cells indicated it may play an important role in tubulogenesis [65]. However, further research is necessary to determine where HYAL2 is localized in tissues to improve our understanding of the cellular involvement of this enzyme in HA catabolism.

1.3.1.3.2 HYAL2 in HA catabolism

HYAL2 is thought to be involved in the regulation of HA turnover and size, as it partially cleaves long chain HA molecules to produce ~ 20 kDa fragments [39]. *In vitro* studies in an HEK293 cell line stably transfected with HYAL2 demonstrated that HYAL2 acts extracellularly, and its activity depends on a cell surface receptor, CD44 [55]. The interaction and colocalization between HYAL2 and CD44 have been also reported in both vesicles and plasma membrane of chondrocytes from arthritis patients [66]. The activity of HYAL2- mediated HA cleavage depends on an acidic microenvironment [67]. HYAL2 can act at the cell surface and is also presumed to be active in the ECM. For example, CD44

shedding in bovine chondrocytes increases the release of HYAL2 from the membrane of these cells to the ECM where weak HYAL2 activity has been demonstrated [66]. The activity of a soluble form of HYAL2 has been also reported in human bronchial epithelial cells [68]. Therefore, it appears HYAL2 can either act at the cell membrane or as a soluble form.

1.3.1.3.3 Other functions of HYAL2

HYAL2 does not only have a major role in HA catabolism, but also acts as a cell surface receptor for the jaagsiekte sheep retrovirus. The envelope protein of this virus mediates oncogenesis in lungs of sheep [60]. It also acts as a critical modulator of the way cells interact with their microenvironment and regulates cell motility by a direct interaction between HYAL2 and the CD44- ezrin-radixin-moesin complex [69]. The function of HYAL2 in cell survival and death has been demonstrated in murine fibroblast cells [70]. In this study, the interaction of HYAL2 and transforming growth factor β 1 (TGF-β1) recruited the tumor suppressor WW domain-containing oxidoreductase. The resulting complex then translocated into the nuclei and activated SMAD signaling, resulting in an increase in SMAD-driven expression of cell growth and death [70]. These suggested that HYAL2 has functions other than in HA catabolism.

1.3.1.3.4 HYAL2 in disease pathology

HYAL2 is proposed to play an important role in the pathology of many inflammatory diseases and tissue repair. *In vitro* study of exogenous HA fragments has shown several functions, such as induction of the synthesis of inflammatory cytokines [71], MMP [72] and recognition of injury through the activation of endothelial cells [73]. Proinflamatory

cytokines also regulate the expression of HYAL2. In human knee explants, HYAL2 expression was up-regulated by IL-1 and TNF cytokines [74]. Recently a study has been reported that *HYAL2* mRNA expression can also be upregulated by mechanical stimuli in articular chondrocytes [75]. Elevated HYAL2 expression has also been reported in the synovial fluid of rheumatoid arthritis and osteoarthritis patients [76]. Increased expression of HYAL2 is also associated with the pathology of the post-ischemic kidney in rat [77]. Taken together, HYAL2 could be a potential therapeutic target in the treatment of disease where modulation of HA catabolism is necessary. However, further study of HYAL2's function *in vivo* and whether exogenously added HA mimics fragments produced by HYAL2 are a prerequisite.

1.3.1.3.5 HYAL2 in cancer

There is growing evidence suggesting HYAL2 is a modulator in the pathophysiology of different cancers including breast [78,79], skin [80], endometrial [81] and ovarian carcinoma [82]. Decreased *HYAL2* methylation is proposed to be a prognostic marker for early diagnosis of breast cancer [83]. An elevated level of *Hyal2* mRNA and protein has been correlated with highly invasive breast cancer cells [78,79], and an increased level of HYAL2 expression has been reported in tumor metastasis in highly aggressive breast cancer [79]. Along with breast cancer, increased expression of HYAL2 has also been reported in advanced colorectal cancer *in vitro* [84]. In addition, immunohistochemistry (IHC) demonstrated increased HYAL2 in both premalignant and malignant skin cancer [80]. In ovarian cancer, increased HYAL2 expression was found post-chemotherapy, but not to pre-chemotherapy [82]. In a recent study of cells from the naked mole rat, the overexpression of *Hyal2* induced malignant transformation and tumor formation by removing HMM-HA [85].

In contrast, down-regulation of HYAL2 was also associated with several carcinomas, including endometrial, lung and kidney [81,86]. More studies are needed to determine whether HYAL2 has a direct role in the progression of cancer and what characterizes the types of cancers for which it appears to be a negative or positive prognostic factor.

1.3.1.3.6 Animal model of HYAL2 deficiency

The generation of a mouse model with HYAL2 deficiency was recognized as a valuable way to try to characterize its role in HA catabolism. Unfortunately, the initial attempt to generate *Hyal2* KO mice suggested HYAL2-deficiency was embryonic lethal [87]. However, our laboratory and collaborators were successful in generating *Hyal2* KO mice on an outbred background (129/Ola/CD1/C57BL/6) which was then backcrossed for 6 generations onto the C57BL/6 background. Initial characterization of the HYAL2 KO mice revealed craniofacial abnormalities, apparent decreased survival rate, increased serum HA, and mild anemia compared to control mice [63]. In contrast to HYAL1 KO mice [52], there was an increased level of HA in *Hyal2* KO serum suggesting that HYAL2 played a role in maintaining normal plasma HA in mice. However, a survey of the distribution of HYAL2 in major mouse tissues was not performed, and initial studies failed to identify broad HA accumulation in its absence [63].

1.3.1.4 Other HYALs

Besides the HYALs that are expressed in somatic tissues, there are three additional HYAL-related genes (*HYAL4*, *PHYAL1* and *SPAM1*) on human chromosomes 7q31.3 that do not appear to contribute to HA turnover on a broad level. *HYAL4* expression is limited to the

placenta and skeletal muscle, and it encodes a chondroitinase rather than a hyaluronidase [41]. In humans, *HYALP1* is a pseudogene that is broadly expressed in human tissues at the mRNA level [41], but a premature stop codon prevents the production of a protein. The mouse orthologue, *Hyalp1* is expressed in testes, brain, liver, fat and skeletal muscle [88,89]. However, the catalytic activity of HYALP1 is controversial [88]. The last gene in this group, *SPAM1*, is expressed specifically in the testes, where it appears to function in fertilization.

Sperm adhesion molecule 1 (SPAM1), also known as PH20, is the testicular hyaluronidase. It resembles HYAL2 in that it is found on the membrane surface as a GPI-linked neutrally active hyaluronidase. Unlike HYAL2 which degrades high molecular mass (HMM) HA to 20 kDa fragments, SPAM1 can degrade any length of HA to generate tetrasaccharides [88]. During fertilization, SPAM1 on the surface of sperm facilitates penetration of the HA-rich cumulus of the oocytes [88]. However, during the acrosome reaction, SPAM1 is cleaved to form a smaller, acid-active form. Whether, the formation of a similar soluble form through proteolytic cleavage applies to HYAL2 is currently uncertain.

Despite the apparent role of SPAM1 in fertilization, SPAM1 null mice are fertile, suggesting redundancy with other HYALs. It was suggested that in mice, this was due to the presence of *Hyal5,* a second testicular HYAL that is absent in humans. HA zymography showed that HYAL5 was active at physiological, but not at an acidic pH [88]. Like SPAM1 KO mice, HYAL5 KO mice are fertile and produce litters of normal size. *In vitro* fertilization studies of both *Spam1* and *Hyal5* KOs demonstrated that HYAL5 is not essential for fertilization [90]. Whether HYAL2 may also play a role in fertilization is yet to be determined, although it is present on the sperm surface [91].

Recently, another gene encoding a protein involved in HA degradation in skin fibroblasts, KIAA1199, was identified [92]. Initially, mutations in this gene were identified as

a cause of hearing loss [93]. Indeed, it is highly expressed in the cochlea, and is required for normal ear development [93]. *In vitro* studies have demonstrated that KIA1199 can bind to HA and depolymerise HA through the clathrin-coated pathway [92]. HA accumulation has been reported in cultured cells from a hearing loss patient with a mutation in KIA1199 [92]. However, the relationship between KIAA1199 and the HYALs in currently unexplored.

1.3.1.5 Exoglycosidases

For decades, the exoglycosidases have been recognized as having the potential to contribute to the degradation of HA through the sequential removal of terminal sugar units [94]. There are two lysosomal exoglycosidases, β-hexosaminidase and β-glucuronidase that have the potential to act on HA by removing terminal GlcNac and GlcUA, respectively. The contribution of these enzymes to overall HA degradation has been controversial although mice deficient in all forms of β-hexosaminidase do exhibit an MPS-like phenotype with accumulation of both GAGs and gangliosides in several tissues. The types of GAGs that were accumulating in tissues were not known. To determine the types of GAGs, and assess the potential for the exoglycosidases to compensate for HYAL1 deficiency, triple KO ($Hexa^{KO}/Hexb^{KO}/Hyal1^{KO}$), and double KO($Hexa^{KO}/Hexb^{KO}$) mouse models were generated and their GAG storage was assessed. These studies clearly demonstrated more accumulation of HA in the triple KO as compared to double KO tissues, demonstrating that the exoglycosidases contribute significantly to HA catabolism in the mouse [95]. Although these studies were performed using β-hexosaminidase deficiency in combination with HYAL1 deficiency, one might expect a similar outcome in a combined β-glucuronidase/HYAL1 deficiency as these two exoglycosidases work alternately in the degradation of HA.

1.4 Model of HA degradation

Although HA is an abundant component of the vertebrate ECM, and plays important roles in tissue homeostasis, development and remodelling, the pathway of HA degradation is still unclear. A model for HA catabolism has been proposed (Figure 1.3). In this model, HYAL2 initiates the degradation of HMM-HA to smaller fragments that bind with cell surface receptors for endocytosis and degradation in lysosomes by HYAL1 and the exoglycosidases, β-hexosaminidase and β-glucuronidase [43]. This model suggests that HYAL2 is important for the degradation of HMM-HA for systematic degradation in lysosomes. There are several cell surface receptors, including CD44, LYVE-1 (lymphatic vessel endothelial receptor 1), and HARE (HA receptor for endocytosis), which bind HA *in vitro* and promote its endocytosis. Most recently, *in vitro* studies of prostate cancer cells have been shown that overexpression of HYAL1 promotes endocytosis of extracellular HA into lysosomes, suggesting HYAL1 alone can degrade HMM-HA into fragments for entry into the cytoplasm [96]. Therefore, further studies are required to elucidate the role of these enzymes in HA breakdown.

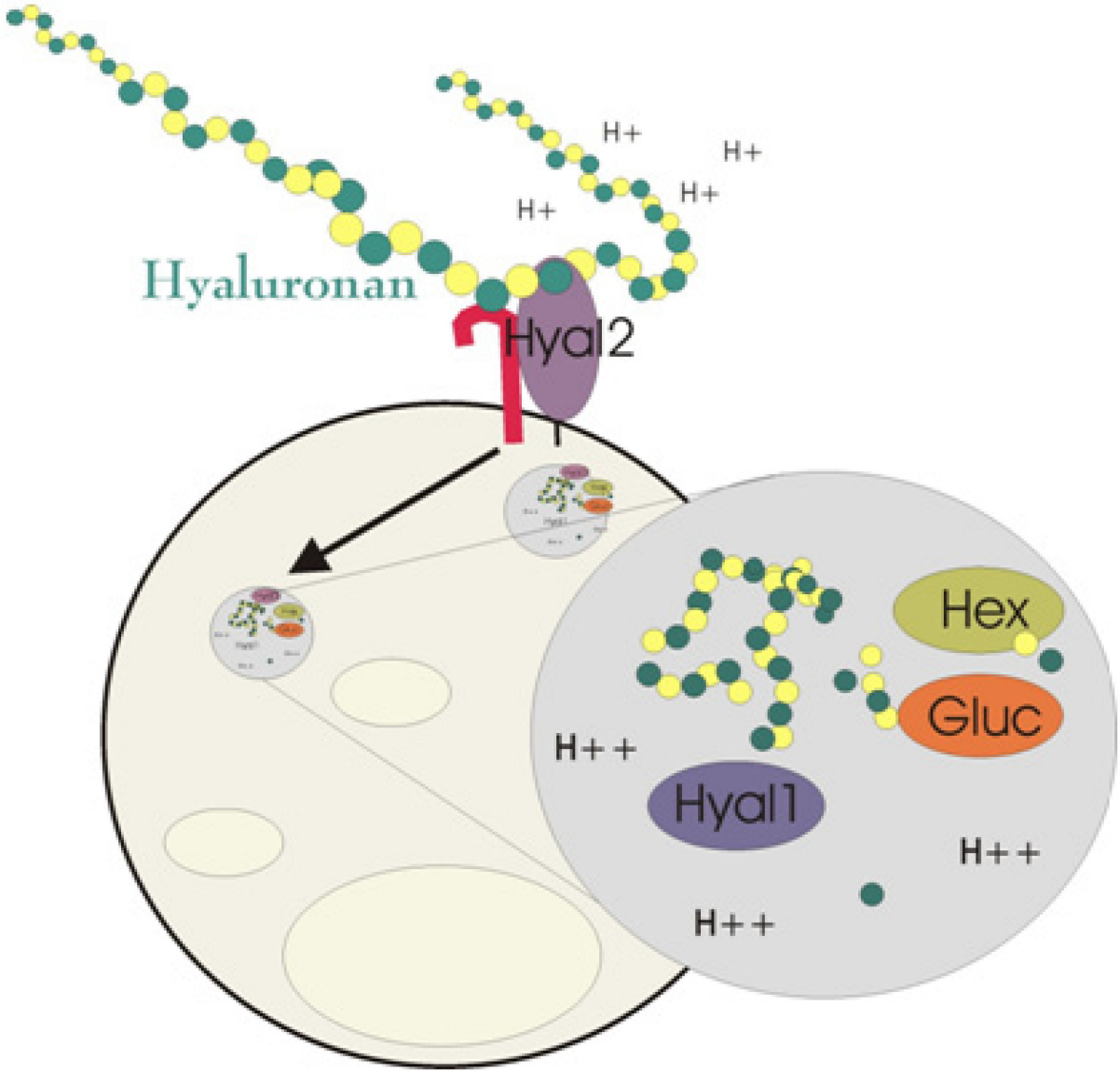

Figure 1.3. Proposed working model for HA degradation.

Proposed working model for HA degradation. In this model, HYAL2 initiates the breakdown of long chain HA to short fragments at the cell surface, which are endocytosed to lysosomes by a receptor-mediated pathway for further degradation. In the lysosome, other enzymes such as HYAL1 degrade short fragments of HA to generate disaccharides which are further degraded to monomers by the exoglycosidases, β-hexosaminidase and β-glucuronidase. H^+, hydrogen ion; *Hyal2*, hyaluronidase 2; *Hyal1*, hyaluronidase1; Hex, hexosaminidase A and B; Gluc, glucuronidase (Modified from [43], Courtesy of Dr. Barbara Triggs-Raine).

1.4.1 Non-enzymatic HA degradation

In addition to endoglycosidases and exoglycosidases, HA can be degraded by ultrasonication, acid or alkaline hydrolysis, high temperature and reactive oxygen species [97]. In recent studies of extracellular superoxide dismutase (EC-SOD) KO mice, severe pulmonary inflammation was detected which was presumed to be due to free radical degradation of extracellular HA to short pro-inflammatory fragments [98]. Zelko *et al* also demonstrated that EC-SOD attenuated the release of interstitial HA which protected from bleomycin-induced lung injury [99]. These studies suggest that free radicals play an important role in HA degradation in some situations.

1.5 HA receptors

Cell surface molecules are required for HA uptake prior to degradation. There are several cell surface receptor proteins including CD44, RHAMM (receptor for hyaluronic acid mediated motility), LYVE-1, and HARE, which bind with HA and promote its endocytosis and/or initiate cellular signalling events.

1.5.1 CD44

CD44 is the principal cell surface receptor for HA. This transmembrane glycoprotein is widely expressed in many different mammalian tissues and plays important roles in embryogenesis [100], tumor progression [101], inflammation, immune cell activation [102] and fibrosis [103]. It consists of intracellular, transmembrane and extracellular domains. Alternative splicing of CD44 exons form multiple isoforms that are the basis of functional

and structural diversity of this protein [104]. The amino-terminal region of the extracellular domain binds with HA via link modules and regulates downstream signalling pathways. For instance, *in vitro* studies have demonstrated that a CD44-HA interaction regulates the proliferation and adhesion of endothelial cells [105]. Along with downstream signalling functions, CD44 also plays an important role in HA internalization [106]. It binds with pericellular HA molecules and promotes their internalization into cytoplasmic organelles.

CD44 is expressed during embryonic development and in adult tissues. In early embryonic development, IHC showed that CD44 localizes to the myocardium and endocardial cushions of the heart, blood vessels, and craniofacial tissues [100]. Another study of CD44 expression in adult mouse tissues showed its presence in kidney, spleen, thymus, intestine and choroid of eyes [107]. However, *Cd44* KO mice do not exhibit any obvious phenotype, suggesting redundancy with other molecules in this pathway during development and in adult life [108].

1.5.2 Lymphatic vessel endothelial receptor-1 (LYVE-1)

LYVE-1 is also a transmembrane protein and has 41% amino acid sequence similarity with CD44 [109]. It also binds HA through an extracellular domain, endocytoses HA and participates in downstream cell signalling events. Northern blot analysis of *LYVE-1* in human tissues revealed its abundant expression in liver, spleen, LN, and heart [109]. In embryonic and adult tissues, LYVE-1 is mainly expressed endothelial cells of blood vessels and hepatic sinusoids respectively [110,111]. *In vitro* studies have shown that LYVE-1 binds with HMM-HA and may play a role in its uptake and degradation [109].

To determine its function in development and HA turnover, an LYVE-1 KO mouse model was generated. *Lyve-1* KO mice were viable and displayed no apparent phenotype and no difference in HA accumulation when compared to controls [112]. To determine if there was functional redundancy between LYVE-1 and its homologue CD44, LYVE-1/ CD44 double KO mice were generated [113]. However, double KO mice also displayed no obvious phenotype suggesting that other receptors might replace their function in HA endocytosis and signalling events. Further studies are needed to understand LYVE-1‘s role in HA catabolism/function.

1.5.3 HA receptor for endocytosis (HARE)

HARE also known as stabilin-2 is known to be a major receptor for rapid internalization of HA in the lymph nodes, spleen and liver [114]. The human 315 kDa HARE protein was purified from human spleen [114]. It is encoded by a single gene on chromosome 12 and contains 69 exons. The *HARE* mRNA was detected in human liver, spleen, and lymph nodes [115]. Immunohistochemical localization of HARE in mouse tissues using an antibody toward stabilin-2 demonstrated intense staining of the endothelial cells in liver, lymph nodes, bone marrow, and epithelial cells in eye, brain, kidney and the mesenchymal cells of the heart valves [116]. *In vitro* studies indicated that the HARE-HA interaction mediated intracellular signal transduction through the extracellular signal-regulated kinase 1 and 2 (ERK1/2) pathway [117]. Interestingly, *Hare* KO mice have recently been reported to show high levels of serum HA, dilated cardiomyopathy, and premature mortality [118].

1.5.4 Receptor for HA mediated motility (RHAMM)

RHAMM is widely distributed on the cell surface, in the cytoplasm and the nucleus in human breast cancer cells [119,120]. HA-RHAMM interaction mediates cell signalling pathways and promotes cell migration, proliferation and differentiation. In the cytoplasm, the HA-RHAMM interaction might play an important role in mitosis by reorganising the centromeres and microtubules [120].

1.6 HA in organ development

Despite the simple structure of HA, it has been demonstrated to have several molecular functions and to influence the physiochemical structure of tissues/organs during development and remodelling. HA provides mechanical support and contributes to tissue homeostasis. It interacts with PGs via link modules which are of key importance to the integrity of pericellular matrices and ECM. In addition to this structural role, interactions between HA and its receptors, regulate different cell signalling events such as proliferation, migration and differentiation [121]. For example, during mitosis HA-dependent pericellular matrices create a hydrated environment surrounding cells that promotes partial separation and rounding of dividing cells [22].

HA has been found in the stem cell niche and it thought to assist in stem cell proliferation, migration and differentiation [122]. One example is neural crest cell (NCC) migration and differentiation. During early embryonic development, NCCs are made up of a population of pluripotent cells that migrate into the branchial arches and produce various cell types including nervous system, connective tissues, skeletal, dermal and mesenchymal cell types. Epithelial to mesenchymal transition (EMT) is a central process in NCC migration

[123]. The EMT processes involves biochemical changes in epithelial cells and enable it to assume a mesenchymal cell phenotype that includes increased production of ECM, resistance to apoptosis,enhanced invasiveness and migratory capacity [124]. EMT begins with the down-regulation of the intercellular adhesion complex, promoting the transition from a tightly linked epithelium to motile mesenchyme. There are several transcription factors which regulate the expression of adhesion proteins. For example, SNAIL1 and 2 repress the expression of E-cadherin and induce EMT [125]. Once NCC reaches a final destination, they then start to proliferate and differentiate into specific cell types [123]. HA synthesis is also altered during EMT [126] and migration [22]. The role of HA in NCC migration has been characterised in *Xenopus laevis*. This study showed the HA-rich ECM promoted NCC migration and differentiation into chondrocytes during craniofacial development [127]. Consistent with an important role for HA in promoting EMT, HAS3 and HAS2 overexpression in human pancreatic cancer cells resulted in accumulation of extracellular HA that inhibited E-cadherin expression and increased the accumulation of cytoplasmic β-catenin, promoting EMT [128]. Once the transition is completed the mesenchymal cells express the intermediate filament protein, vimentin.

The physiochemical properties of HA influence the development of several organs including the heart [126], limb [129], kidney [130], ear [131], palate [132] and neural tube [133]. During development, HA appears to regulate various physiological processes by interacting with cell surface receptors. For example, an HA- CD44 or HA- RHAMM interaction drives changes in the cytoskeleton and activates various intracellular signalling pathways including phosphoinositide 3 kinase (PI3K), nuclear factor kappa B (NF-kB) and receptor tyrosine kinase erbB-2 (ERBB2), which cause cell proliferation, invasion and motility [121]. The degradation of HA and its associated PGs is also a key step in these developmental processes [134]. In mice, defects in the degradation of the HA-binding PG

versican result in heart, limb and palate abnormalities [135]. *In vitro* studies have shown that this developmental process can be inhibited by degradation of HA itself or using blocking antibodies for its cell surface receptor CD44 [130,136]. In fact, the occurrence of developmental mistakes can lead to craniofacial abnormalities, which in humans account for one-third of all congenital birth defects [137,138]. However, currently the field lacks information regarding how disruption of normal HA degradation impacts organ development *in vivo*.

The role of HA in heart development is examined further in the following section.

1.6.1. HA in heart development

The heart is the very first organ to develop during embryogenesis. In the developing mouse embryo the cardiac primordia forms a single heart tube at E8.5 that consists of two layers of cardiac cells, an inner layer of endocardium and an outer layer of myocardium which are separated by cardiac jelly (Figure 1.4). Cardiac jelly is rich in HA and PGs. HA binds water and promotes swelling of cardiac jelly within the cardiac cushion and forms the future atrioventricular canal (AVC) and outflow tract (OFT) that separate the atria from the ventricles at E9.5. Endothelial to mesenchymal transition (endoEMT) within atrioventricular cushions form the valve primordia [139,140]. An important role for HA during cardiac embryogenesis has been demonstrated through *Has2* KO mice; these mice die at E9.5 due to failure to form HA within the cardiac jelly [126]. HYALs are also thought to be important as very early studies in cardiac cushions and myocardium of the chick embryo suggested HYALs depolymerized HMM-HA to low molecular mass (LMM) HA during cardiac morphogenesis [141]. *In vitro* studies of cardiac explants from mice showed that removal of HMM-HA is required to attenuate EMT and induce vascular endothelial growth factor (VEGF) expression needed for further heart development (Figure 1.4) [142]. Although no

requirement for HYALs has been demonstrated *in vivo*, these findings suggest an important role.

NCC-derived ectomesenchyme is also important in the development of the heart [143]. NCC-derived ectomesenchyme is required for the patterning of the aortic arch and generating the smooth muscle layers in the tunica media of blood vessels [143]. As we mentioned earlier, the migration of NCC-derived cells also depends on HA-rich matrix [127]. There may be important roles for HA and HYALs in multiple stages of heart development where EMT is important, but the early embryonic death in *Has2* KO mice has prevented such studies.

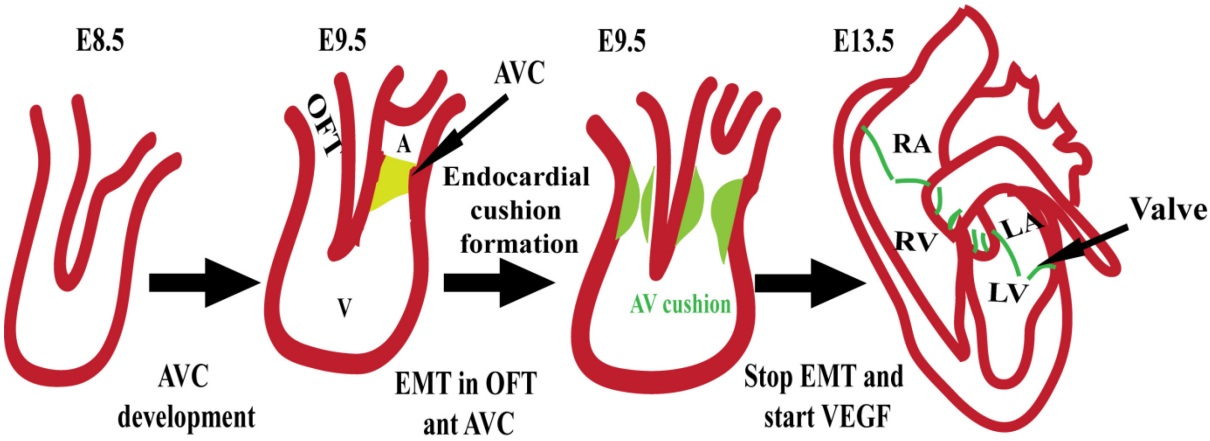

Figure 1.4. Stages of mouse embryonic heart development

The formation of the heart tube in mouse cardiac embryogenesis starts at E8.5. The heart tube consists of an inner layer of endothelial cells and an outer layer of myocardial cells. This tube then expands and undergoes rightward looping. At this time, the heart is remodelled from a linear tube to four distinct chambers of the heart through a series of complex steps between E9.5 to 13.5. This involves formation of the OFT, AVC between the atrium (A) and ventricle (V) and the endocardial cushions in the OFT and AVC. The endocardial cushions act as a precursor for all heart valves. EMT is an essential step between E8.5 and 9.5 to form the endocardial cushions. Following, this stage, activation of the VGEF pathway is required to inhibit EMT to develop four distinct structures within the heart (modified from [144]).

Mature cardiac valves consist of three distinct layers of tissue; these include the collagen-rich fibrosa, which is responsible for the structural integrity, the spongiosa which regulates the activity of the valve interstitial cells (VICs), and the elastin-rich ventricularis which gives shape to the valve (Figure 1.5) [145]. The spongiosa layer consists primarily of PGs and GAGs [145]. One of the major GAGs in the spongiosa layer is HA which regulates the flexibility of the valve leaflet [146]. *In vitro* studies of VICs, which are responsible for the synthesis and remodelling of ECM components of the valve, have shown a relationship between HA fragments and VIC activity [147]. In this study, HA fragments increased the proliferation of VICs and production of elastin, but, decreased the collagen production. These findings suggest that HYALs and other proteins involved in HA turnover, as well as the regulation of HA size, might have an effect on the normal function of heart valves.

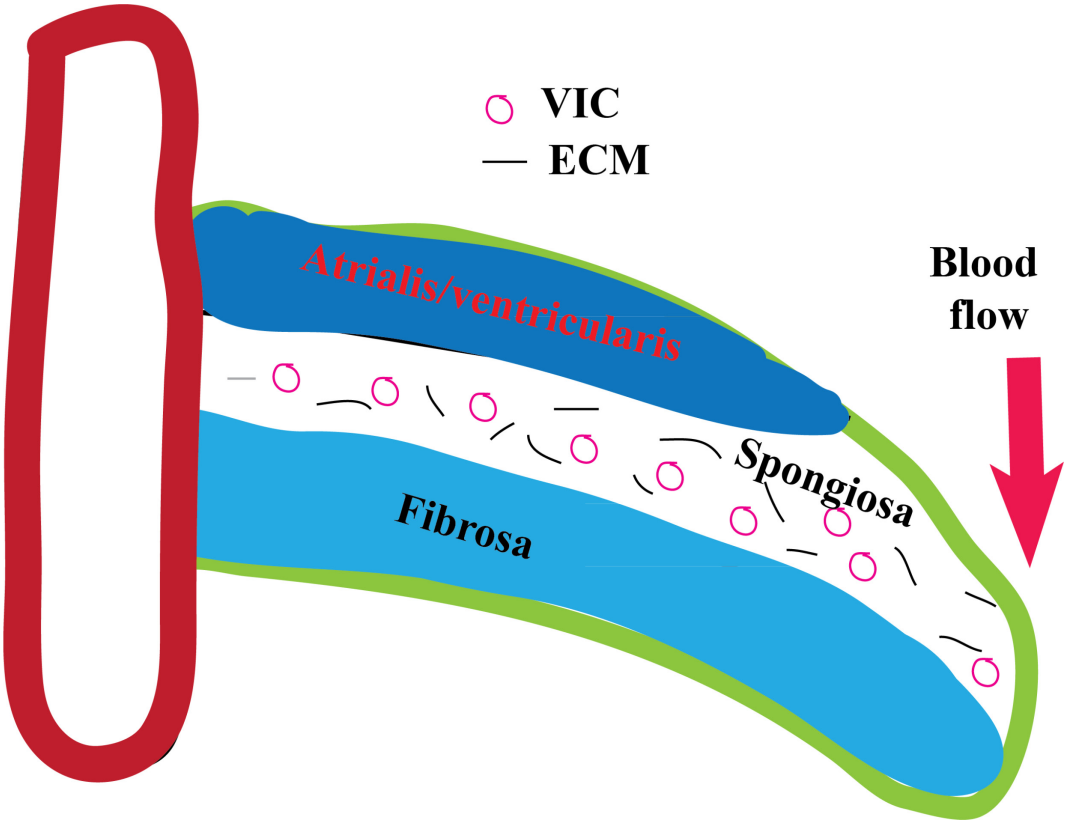

Figure 1.5. Model of the heart valve structure.

The mitral valve of the normal heart has three layers. The fibrosa consists of collagen, the atrialis/ventricularis is rich in elastin and the middle spongiosa layer is rich in GAGs. (modified from [139]).

1.7 HA in disease pathology

The biological function of HA depends on its size and amount in a spatiotemporal manner. The alteration of HA level and size has been identified in kidney disease, cancer, lung injury and stroke [148-150]. This alteration in the HA size can be used as a prognostic marker for various cancers including breast, lung, ovary and prostrate carcinoma [78,151-153]. The role of HA size in tissue injury and repair has been well characterized in wound healing. HMM-HA initiates clotting and then LMM HA promotes the requitment of fibroblasts at wound sites to synthesize new ECM for remodelling of tissue [154]. HA size is also associated with tissue fibrosis. LMM-HA promotes myofibroblast conversion from fibroblasts and production of excessive matrix components, whereas HMM-HA dampens fibrosis in lamb wound healing [155]. The presence of excessive HA in the extracellular space affects the production of other ECM components, as a result, causes disruption of tissue homeostasis. For example, biochemical and histological analysis of myxomatous mitral valves demonstrated the presence of excessive HA [156] and abundance of the three PGs versican, decorin, and biglycan when compared to controls [157]. *In vitro* studies of trabecular meshwork cells from open-angel glaucoma patients has also shown that HA level regulates the production of tissue remodelling enzymes like MMP9 and MMP2 in a dose-dependent manner; a higher concentration of HA promotes synthesis of excessive MMPs [158]. The importance of HA size and levels in determining its function suggests HYALs might play an important role in disease pathology by regulating HA size and/or abundance.

1.9 Diseases associated with defects in GAG degradation

The MPS are a group of lysosomal storage disorders; each results from the deficiency of a lysosomal enzyme that contributes to the systematic degradation of GAGs (Table 1.3). The accumulation of GAGs in the lysosome causes lysosomal dysfunction and cell death; this accumulation is greatest in those tissues where the GAG levels are highest [159]. Clinically, MPSs are categorised as heterogeneous and progressive disorders. The severity of the disorder is typically inversely correlated to the level of residual enzyme activity. At birth, patients appear normal but later develop disease symptoms, including joint, skeletal, pulmonary and cardiac symptoms, vision and hearing impairment and in some cases neurological impairment [160]. Currently, two kinds of treatment options are available; haematopoietic stem cell transplantation (HSCT) and enzyme replacement therapy (ERT) [160]. The list of MPSs, the clinical symptoms, available treatment and the accumulated substrates associated with a specific disease are listed in Table 1.3.

Table 1.3. Features of MPS

Disease	Enzyme deficiency	Substrate accumulation	Clinical features	references
MPS I Hurler (H) Hurler -Scheie (H/S) Scheie (S)	α-L-iduronidase	DS, HS	dysostosis multiplex, organomegaly, corneal clouding, heart disease; mental retardation; death in childhood.	[161]
MPS II Hunter	iduronate sulfatase	DS, HS	organomegaly, mental retardation, short stature, normal intelligence, death before 15 years (severe)	[162]
MPS III Sanfilippo A Sanfilippo B Sanfilippo C Sanfilippo D	heparan-N-sulfatase α-N-acetylglucosaminidase heparan acetyl-CoA α-glucosaminide N-acetyltransferase	HS	relatively mild somatic manifestations, hyperactivity, profound mental deterioration	[163,164]
MPS IV Morquio A Morquio B	galactose 6-sulfatase β-galactosidase	KS and CS KS	distinctive skeletal abnormalities, corneal clouding, odontoid hypoplasia, milder forms known to exist.	[164,165]

MPS VI (Maroteaux-Lamy)	arylsulfatase B (N-acetylglucosamine 4-sulfatase)	DS	dysostosis multiplex, corneal clouding, normal intelligence, survival to teens in severe form, milder forms also documented.	[166]
MPS VII (Sly)	β-glucuronidase	KS, DS, CS	dysostosis multiplex, hepatomegaly, wide spectrum of severity including fetal hydrops and neonatal form	[164,167]
MPS IX	HYAL1	HA	mild short stature, periarticular soft masses.	[51]

1.9.1 Cardiovascular disease

GAGs are one of the major ECM components of heart valves and large blood vessels [156]. Due to its hydrated nature, GAGs absorb shear force during valve leaflet/cup movement [168]. Therefore, the disruption of GAG degradation results in cardiac abnormalities in neonates and adults. The appearance of cardiovascular diseases including valve and myocardium thickening, pulmonary hypertension, and narrowing of the major blood vessels are the most prominent features in all MPSs. The onset of cardiac disease pathology appears early in life and progresses rapidly to heart failure and sudden death. Between 60-90% of patients with MPS experience valve disease [169], and 30% of MPS I and II patients are diagnosed with coronary artery disease due to the accumulation of GAGs in the vessels [170]. The accumulation of GAGs in VIC, changes the shape of the cells from fusiform to round causing thickened leaflets and chordae tendineae which affect normal cardiac function, resulting in valvular disease [159,171]. Accumulation of GAGs in the subvalvular region results in dysmorphic and stiff leaflets that may lead to left atrial/ventricular volume overload, left ventricular dilation, hypertrophy and ultimately to systolic and diastolic dysfunction [170]. Surgical replacement of heart valves and continuous monitoring of cardiac function through echocardiograms are standard practice in the treatment of MPS patients with cardiovascular disease. Detection of the enzyme responsible for the cardiac manifestation in MPSs will systematically improve the management of cardiac disease by restoring the functional enzyme. For example, long-term enzyme replacement therapy preserves the cardiac function in adults and children with MPS I and II [172,173].

1.9.2 Skeletal abnormalities

Skeletal abnormalities are common clinical features in MPSs. Accumulation of GAGs in the chondrocytes, articular cartilage, synovial fluid and surrounding tissues leads to joint stiffness and poor mobility in patients [174]. Since these abnormalities develop early in life, it also affects normal growth, resulting in growth retardation in most MPS patients. The current therapeutic options for the treatment of bone associated disease are ERT and bone-marrow transplantation [174]. However, the success of current treatment interventions is limited. A better understanding of pathophysiological events will enable us to pursue treatment aimed at improving the lives of MPS patients.

1.10 Diseases associated with PG deficiency

In the ECM, PGs have a diverse range of functions due to their multi-domain structure. In some cases, these domains mediate interactions with cells and matrices. Some domains participate in cell signalling events that regulate cellular behaviour. The function of PGs is highly regulated by a family of a disintegrin and metalloproteinase with thrombospondin motifs (ADAMTS) enzymes. Mutation in these enzymes results in the abnormal proteolysis of PGs causing disorganization of the matrix, hindering cell-cell communication and altering the biomechanical properties of the matrix [175]. For example mutation in ADAMTS2 results in abnormal collagen fibrillation in Ehlers– Danlos syndrome type VIIc [176]. A mutation in ADAMTS10 causes cardiac valvular disease, growth retardation, and ectopic lens in Weill–Marchesani syndrome [177]. Animal models of ADAMTS deficiencies have been generated to characterize their function and identify new

treatment approaches [178]. *Adamts 9* KO mice are embryonic lethal at E7.5 and haploinsufficiency of the same gene resulted in cardiac, including aortic abnormalities [178,179]. Therefore, proper regulation of PGs are necessary for normal development and to maintain tissue homeostasis.

1.11. Study objectives and hypothesis

The overall goal of the work in this thesis was to determine the role of HYAL2 in HA catabolism using *Hyal2* KO mice generated as part of a previous study. Initial studies of the HYAL2 KO mice revealed craniofacial abnormalities and chronic anemia, as well as unexplained pre-weaning lethality [63]. However, in addition to these features, our studies of *Hyal2* KO mice on an outbred background (*C129/Ola;CD1;C57BL/6)* have revealed severe pre-weaning lethality (only 9% survived after weaning) and of the surviving KOs, 54% showed a gross enlargement of either the left or right atrium compared to control mice. These findings indicated that HYAL2 likely had a much more significant role in HA catabolism than suggested in the initial investigation of the KO phenotype and set the stage for the studies described in this thesis.

Overall Hypothesis: HYAL2 normally degrades extracellular HA in a broad range of tissues and deficiency of HYAL2 during development results in HA accumulation leading to abnormal organ development and pre-weaning lethality.

To test this hypothesis, a series of molecular, histochemical and functional studies were performed on HYAL2 KO and control mice. This study had three objectives

Specific Objective 1.

To characterize the cardiac phenotype in adult *Hyal2* KO mice.

Rationale and approach.

The gross atrial enlargement observed in 54% of *Hyal2* KO mice appeared to be the cause of death. Mice with atrial dilation followed an acute course of apparent heart failure and ultimately required euthanasia at an average age of 3 months. The remaining 46% of

Hyal2 KO mice followed a sub-acute (chronic) course that required euthanasia at an average age of 5.6 months. In Chapter 2, we describe the histological and biochemical characterization of the cardiac phenotypes in the adult *Hyal2* KO mice. We demonstrate an accumulation of HA in serum, interstitium of myocardium, lungs, heart valves (100% of mice) and pulmonary fibrosis (54% of mice) that appear to be the cause of the cardiopulmonary dysfunction and premature death in *Hyal2* KO mice.

Specific Objective 2.

To characterize the cardiac functional and developmental abnormalities in *Hyal2 KO* mice.

Rationale and approach.

The severe atrial enlargement in *Hyal2* KO mice suggested that there was abnormal development. However the cause of this morphological abnormality and how it impacted cardiac function in the adult *Hyal2* KOs was not known. In Chapter 3, we describe the cardiac developmental and functional abnormalities in *Hyal2* KO mice. We provide strong evidence to indicate that increased EMT in *Hyal2* KO mice is the cause of morphological abnormalities and this structural defect leads to diastolic dysfunction in adult mice.

Specific Objective 3.

To characterize the distribution of HYAL2 in mouse tissues/organs and the tissue HA accumulation in *Hyal2* KO mice.

Rationale and approach.

HA accumulation in *Hyal2* KO heart, serum and lungs suggested a role for this protein in HA catabolism. However, a survey of the cellular distribution of HYAL2 in either human or mouse tissues was not available. In the Chapter 4, we describe the localization of HYAL2 in a broad range of mouse tissues/organs and further correlate it with HA accumulation in *Hyal2* KO mice using biochemical and histochemical approaches. We demonstrate that HYAL2 is mainly localized to endothelial cells and some specialized epithelial cells, and plays a significant role in local HA degradation.

Chapter 2: Murine hyaluronidase 2 deficiency results in extracellular hyaluronan accumulation and severe cardio-pulmonary dysfunction

Biswajit Chowdhury, Richard Hemming, Sabine Hombach-Klonisch, Bruno Flamion, and Barbara Triggs-Raine. ***J. Biol. Chem***. 288, 520-528, 2013.

Acknowledgements: Electron microscopy was performed by Sabine Hombach-Klonisch. Richard Hemming performed the analysis of HA size and assisted in mouse dissections.

This work was published as: **Chowdhury, B**., Hemming, R., Hombach-Klonisch, S., Flamion, B. and Triggs-Raine, B. (2013) Murine hyaluronidase 2 deficiency results in extracellular hyaluronan accumulation and severe cardiopulmonary dysfunction. J. Biol. Chem. **288**, 520-528. doi:10.1074/jbc.M112.393629; 10.1074/jbc.M112.393629

2.1 Abstract

Hyaluronidase (HYAL) 2 is a membrane-anchored protein that is proposed to hydrolyze hyaluronan (HA) to smaller fragments that are internalized for breakdown. Initial studies of a *Hyal2* knock-out (KO) mouse revealed a mild phenotype with high serum HA, supporting a role for HYAL2 in HA breakdown. We now describe a severe cardiac phenotype, deemed acute, in 54% of *Hyal2* KO mice on an outbred background; *Hyal2* KO mice without the severe cardiac phenotype were designated non-acute. Histological studies of the heart revealed that the valves of all *Hyal2* KO mice were expanded and the extracellular matrix was disorganized. HA was detected throughout the expanded valves, and electron microscopy confirmed that the accumulating material, presumed to be HA, was extracellular. Both acute and non-acute *Hyal2* KO mice also exhibited increased HA in the interstitial extracellular matrix of atrial cardiomyocytes compared with control mice. Consistent with the changes in heart structure, upper ventricular cardiomyocytes in acute *Hyal2* KO mice demonstrated significant hypertrophy compared with non-acute KO and control mice. When the lungs were examined, evidence of severe fibrosis was detected in the acute *Hyal2* KO mice but not in non-acute *Hyal2* KO or control mice. Total serum and heart HA levels, as well as size, were increased in acute and non-acute *Hyal2* KO mice compared with control mice. These findings indicate that HYAL2 is essential for the breakdown of extracellular HA. In its absence, extracellular HA accumulates and, in some cases, can lead to cardiopulmonary dysfunction. Alterations in HYAL2 function should be considered as a potential contributor to cardiac pathologies in humans.

2.2 Introduction

Hyaluronidase (HYAL) 2 is a glycophosphatidylinositol-linked protein and a member of the hyaluronoglucosaminidase family [59,87]. It is proposed to initiate the degradation of HA, an abundant GAG in the extracellular matrix of many vertebrate tissues including heart valves, vitreous of the eye, and synovial fluid. The viscoelastic properties of HA influence the properties of the ECM and are important for cell proliferation, differentiation and migration. A role for HA in embryogenesis has been established using HA synthase 2-deficient mice which die at embryonic day 9.5 due to loss of endocardial cushion swelling and a lack of epithelial to mesenchymal transition [126].

Regulation of HA levels is required for normal development, and to maintain normal tissue homeostasis. Degradation of HA by HYALs is important to maintaining these levels. Six HYAL-encoding genes have been identified which are grouped into two tightly linked triplets, one on human chromosome 3p21.3 (*HYAL1*, *HYAL2*, *HYAL3*) and a second on human chromosome 7q31.3 (*HYALP1*, *HYAL4*, *SPAM1*) [41]. With the exception of HYAL4 and HYALP1, all the HYALs are thought to be capable of degrading HA. A role for HYAL1 and HYAL2 in HA degradation in somatic cells has been proposed. In this model, HYAL2 initiates HA degradation into small fragments that are endocytosed and degraded in lysosomes by HYAL1 and exoglycosidases [39]. HYAL2 is a GPI-anchored protein [59] that could act at low pH at the cell surface [67]. It has been suggested that HYAL2 resides in lysosomes in some cell types [180]. Despite the proposed role for HYAL2 in HA degradation, only a deficiency of HYAL1 has been found to cause a human disorder. It causes mucopolysaccharidosis (MPS) IX, a lysosomal storage disorder characterized by joint abnormalities due to HA accumulation [46,51].

In the heart valves, GAGs are abundant and play important roles in both developing and mature valves [139,181]. It is not surprising that cardiovascular manifestations are a

prominent feature of many forms of MPS that result from GAG accumulation [170]. For example, mitral valve thickening and stenosis are found in Hurler and Scheie diseases, and these findings are also reflected in the corresponding mouse model [182]. Therefore, defects in ECM modifying enzymes are among the many causes of cardiovascular disease.

HA is one of the major GAGs in the heart valves. Surprisingly, no broad spectrum HA accumulation, including in the heart, was identified during the characterization of *Hyal1*-, *Hyal2*-, or *Hyal3*-deficient mice [52,63,183]. Previous studies of *Hyal2* KO mice revealed craniofacial abnormalities and chronic anemia, as well as unexplained pre-weaning lethality [63]. However, in addition to these features, on an outbred background (*C129/Ola;CD1;C57BL/6*), we have found a gross enlargement of either the left or right atrium in more than half of the *Hyal2* KO mice that survived to weaning. Since HA synthesis is known to be essential for normal heart development, we hypothesized that a failure to degrade HA in these mice had resulted in HA accumulation, leading to cardio-pulmonary dysfunction, and premature death.

2.3 Materials and methods

2.3.1 Generation of *Hyal2* KO Mice.

Hyal2 KO mice were generated as part of a previous study [63]. For the current study, *Hyal2* KO mice and littermate controls, either wild type (+/+) or heterozygous (+/-), on an outbred background (*C129/Ola;CD1;C57BL/6)* were derived through breeding of *Hyal2* heterozygotes. Mice were genotyped using PCR-based strategies on DNA samples isolated from ear punches. For the amplification of wild type *Hyal2* and the Neo-targeted *Hyal2* allele we used the forward and reverse primers (5'-actcagctgctggttcccta-3'; 5'-atagcactggcagcgaaagt-3'), and (5'-aaggaacatcagggaagatcat-3'; 5'-cggtgcccgagactaagtc-3'), respectively. All animal procedures were conducted under protocols approved by the University of Manitoba Animal Care Committee and following the guidelines of the Canadian Council on Animal Care.

2.3.2 Histology.

Mice were sacrificed by carbon dioxide inhalation and tissues for light microscopy were immediately collected and fixed overnight in either formalin or 10% buffered formalin (Protocol) containing 1% hexadecylpyridinium chloride monohydrate. Tissues for subsequent biochemical studies were stored at -80^{o}C. Fixed tissues were embedded in paraffin, and 5 μm sections were stained for morphological analysis using established methods for hematoxylin and eosin [184] or for GAG detection using alcian blue [184], with minor modifications in the time of incubation with the stain. Counter staining for alcian blue was performed with Nuclear Fast Red (ScyTek Laboratories) for 2.5 min. Heart and lung ECM was stained using Masson's trichrome stain (Sigma-Aldrich) according to the manufacturer's protocol. Slides were dehydrated, mounted and visualised using bright field microscopy. For the analysis of

hypertrophy in cardiomyocytes, slides were incubated for 30 min with 4 μg/ml wheat germ agglutinin (Alexa Fluor® 488 conjugate), mounted using Prolong Gold (Invitrogen) and visualised by fluorescence microscopy. The area of the cardiomyocytes, as defined by WGA, was measured using AxioVision 4.5 software. A minimum of 7 fields, containing an average of 8 cells per field, were examined for each animal.

2.3.3 Electron microscopy.

The valve and surrounding myocardium were collected by punch biopsy from a whole heart that was sliced using a Rodent Heart Slicer Matrix (Zivic Instruments). Tissues were fixed for 4 h at room temperature in 2% glutaraldehyde, 2% paraformaldehyde prepared in 100 mM sodium cacodylate buffer, pH 7.2, containing 10 mM calcium chloride ($CaCl_2$) and 0.7% ruthenium red. After fixation, tissues were washed with wash buffer (100 mM sodium cacodylate, 10 mM $CaCl_2$, 0.7% ruthenium red, 0.7% sucrose, pH 7.2.) for 5 min, 30 min and 1 h at room temperature. Tissues were post-fixed for 1 h in 100 mM sodium cacodylate containing 1% osmium tetroxide and 0.7% ruthenium red followed by three 10 min wash in ddH_2O. Tissues were dehydrated for 10 min each in 50% ethanol, 75% ethanol, 95% ethanol, 2 changes in 100% ethanol followed by 100% methanol, and 3 changes in propylene oxide. After dehydration, tissues were infiltrated by incubating in a mixture of propylene oxide and Araldite 502 Kit (mixture of araldite, DDSA and DMP-30 was 58.9%: 46%: 2%, w/v, Ted Pella Inc). The infiltration solution were prepared with propylene oxide and Araldite (3:1, 1:1, and 1:3) and incubated for 1 hr each. Slow hardening of the araldite was performed through 1 day incubations at each of room temperature, 45^{o}C and 60^{o}C.

2.3.4 Detection of HA, alpha smooth muscle actin (α-SMA), F4/80, and CD31.

HA was detected with biotinylated HA-binding protein (HABP; Calbiochem) as described previously [52], except without enzyme retrieval and using HABP (1.67 µg/ml for heart sections and 6.68 µg/ml for lung sections) in Tris-buffered saline (pH 7.5) overnight at 4^{o}C. Sections were incubated with avidin-conjugated horse radish peroxidase, detected with diaminobenzidine (DAB), and counter stained in Nuclear Fast Red. To verify the specificity of the HABP, sections were incubated overnight with 25 U/ml hyaluronidase from *Streptomyces hyalurolyticus* (Sigma) before the HABP detection.

For the detection of α-SMA, F4/80, and CD31, the sections were incubated overnight at 4^{o}C with mouse monoclonal anti-human smooth muscle actin (1:300, DaKO Denmark), rat monoclonal anti-mouse F4/80 (1:100, AbD Serotec), or rabbit polyclonal anti-CD31 (1:50, Abcam) antibodies respectively. Secondary antibodies, biotinylated rabbit anti-mouse (1:1000, Dako Denmark), or goat anti-rat (1:500, Invitrogen), were used to detect the primary complexes, and complex detection was as for HA, above. For F4/80 and CD31, antigen retrieval was performed by incubating the slides for 20 min at 95^{o}C in 10 mM sodium citrate (pH 6).

2.3.5 Analysis of HA concentration and sizes.

Blood was collected from mice immediately following euthanasia or from the saphenous vein of live mice at 6 and 12 weeks. Serum was collected from clotted blood by centrifugation at 3000 rpm for 10 min and stored at -80^{o}C. HA levels were quantified using an ELISA-like HA test plate (R&D System) according to the manufacturer's instructions. All

samples were analyzed in duplicate and the average value was used for subsequent comparisons.

Fluorophore assisted carbohydrate electrophoresis (FACE) was performed for quantification of HA and chondroitin sulphate levels in tissues [95]. Briefly, GAGs isolated from frozen heart tissue using 50 µg/µl proteinase K digestion and ethanol precipitation, were cleaved to disaccharide units by overnight incubation in hyaluronidase SD (Seikagaku Cat# 100741-1) or chondroitinase ABC (Sigma-Aldrich) in 200 mM ammonium acetate. The disaccharides were isolated, labelled with 2-aminoacridone, and quantified in comparison to known disaccharide standards as described previously [185]. The fluorescence was detected using the Fluor-S Max MultiImager (Bio-Rad) and quantified using Quantity One 4.6.9 software (Bio-Rad).

For sizing of HA, GAGs were prepared from tissue (10-15 mg) or serum (200-400 µl) as for FACE, except 5 mM deferoxamine was included in the proteinase K digestion, and a 4 h incubation at 37^{o}C with 10 U of DNAse I, and 50 µg of RNAse A was incorporated after inactivating the proteinase K by boiling. Instead of digesting the GAGs to disaccharides, they were enriched by precipitating with 1% hexadecylpyridinium chloride monohydrate, as described previously [186]. The pellet was then resuspended in 100 µl of 20 mM Tris pH 8.0, and Pronase was added to 0.2 mg/ml. Following overnight incubation, the GAGs were precipitated with 900 µl of 100% ethanol. The final pellet was resuspended in 15 µl of water; 3 µl of Orange G tracking dye was added and the sample was separated by electrophoresis on a 0.8% agarose gel prepared in Tris-acetate buffer (pH 8.3). The gel was stained overnight with 0.005% Stains-all prepared in 50% ethanol, destained with 10% ethanol until the bands were clearly visible, and photographed. Negative control samples to verify the identity of the HA were prepared by incubating the GAGs overnight with 2.5 U of Hyaluronidase SD before they were analyzed by electrophoresis.

2.3.6 Statistical analysis.

The genotype distributions were compared to expected Mendelian ratios using the chi-square test. For all other statistical analysis, data are presented as mean ± SEM (standard error mean). Means were compared by student's *t* test. $P \leq 0.05$ was considered statistically significant.

2.4 Results

2.4.1 Increased mortality in *Hyal2* KO mice.

We obtained viable *Hyal2* KO mice by inter-crossing *Hyal2* $^{+/-}$, although as reported previously [63], pre-weaning lethality was observed. In fact, only ~9% (70 of 789) of the offspring were *Hyal2* KOs at weaning instead of the expected Mendelian 25% ($\chi^2_{(2)}$= 109.86; p<0.001). Of the viable *Hyal2* KO mice, 54% were smaller in size than their littermates, and exhibited a rapid onset of lethargy, weight loss, dull coat, and shortness of breath requiring euthanasia at an average of 3.2 months of age. Upon dissection, the left or right atrium of these mice were grossly dilated (Figure 2.1). The remaining 46% of *Hyal2* KO mice developed a slower onset of lethargy, loss of weight, and poor grooming that required euthanasia at an average of 5.8 months of age. Severe atrial dilation was not found in these mice, or in control (*Hyal2* $^{+/+}$/*Hyal2* $^{+/-}$) littermates. However, one kidney was found to be missing in 1% of control mice and 43% (N=29) of *Hyal2* KO mice, suggesting this phenotype is increased by *Hyal2*-deficiency. The kidney phenotype was not further investigated as it was found to be independent of the atrial dilation. For the studies described herein, the *Hyal2* KO mice were divided into two categories; mice with atrial dilation were defined as 'acute' and those without atrial dilation were defined as 'non-acute'.

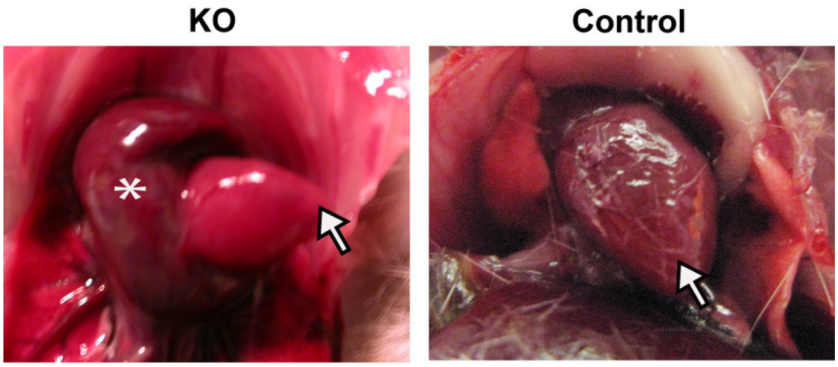

Figure 2.1. Atrial dilation in *Hyal2* KO mice

For orientation, an arrow indicates the apex of the *Hyal2* KO and control (+/+) hearts; an asterisk indicates the dilated atrium of the KO heart.

2.4.2 Heart valve expansion in *Hyal2* KO mice.

The atrial dilation in the acute *Hyal2* KO mice, together with the knowledge that HA is abundant in the heart valve, led us to look for valve abnormalities in the *Hyal2* KO mice. H & E staining revealed a profound expansion of the pulmonary, mitral, aortic, and tricuspid valves in all mice that were examined (n=9) compared to control littermates (n=7). Representative sections of the pulmonary and mitral valves are presented in Figure 2.2 A-D. To determine if there was any difference in the expansion of the valves in the acute and non-acute *Hyal2* KO mice, we compared the expansion/length of the valve leaflet/cups by determining the number of serial sections that included each valve. The valve thickness was significantly greater in *Hyal2* KO mice than controls, but there was no significant difference between the acute and non-acute *Hyal2* KO mice (Figure 2.2 E).

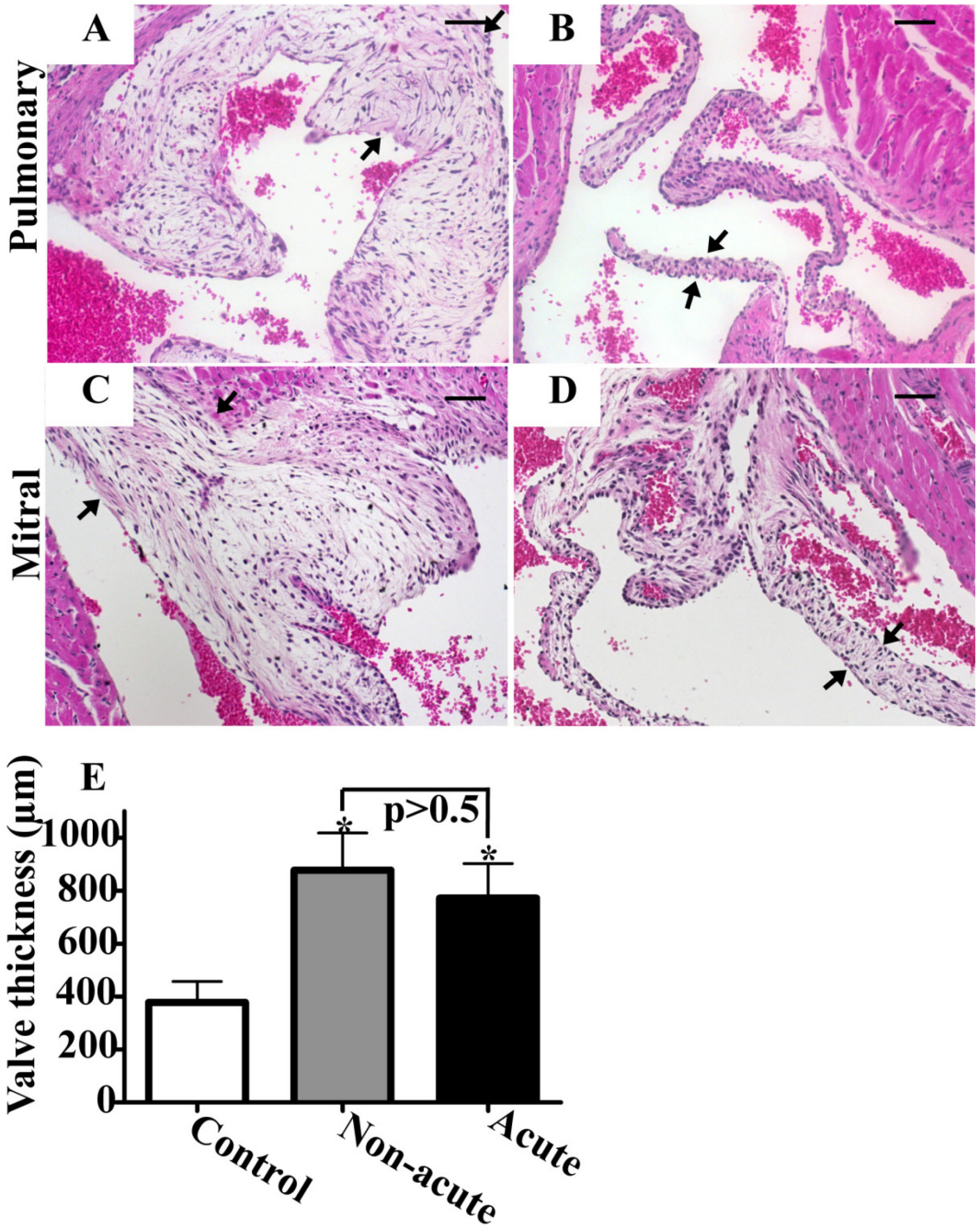

Figure 2.2. Histopathology of heart valves

(*A-D*) H & E stains of cross sections of the heart of *Hyal2* KO (*A* and *C*) and control (*B* and *D*) mice. Representative photographs of the pulmonary (*A* and *B*) and mitral (*C and D*) valves show the expansion in the *Hyal2* KO mice (arrows bound valve edges). (*E*) Comparison of the valve thickness in *Hyal2* KO and control (+/- and +/+) mice. Thickness was estimated by determining the total number of 5 µM serial cross sections that included any of the four heart valves. Graphed values represent the mean thickness ± SEM. Significant expansion of the valves in *Hyal2* KO mice compared to control littermates (n=4, * indicates $P < 0.05$) was found, but there was no significant difference between non-acute and acute *Hyal2* KO mice (n=4, $P = 0.60$). Calibration bars represent 50 µm.

2.4.3 Structure/organization of the valves in *Hyal2* KO mice.

To determine if HA was accumulating in the *Hyal2* KO mice, we used HABP to detect HA. Abundant HA was found throughout the valves (Figure 2.3 A-J), and given the expanded size of the valves in the *Hyal2* KO, this indicates HA was accumulating in the *Hyal2* KO valves.

To determine if the accumulating HA was altering the organization of the ECM of the valve, we examined ECM components using Masson's trichrome staining. Compared to normal valves (Figure 2.4 B), the ECM of valves from *Hyal2* KO mice were disorganized, with GAGs (non-stained material) deposited between the collagen fibres in the fibrosa and ventricularis/atrialis layers respectively, and resulting in an expanded spongiosa layer (Figure 2.4 A). Endothelial cells in the valve were identified by staining for the endothelial marker CD31. The CD31 positive cells (brown) appeared less frequent in the *Hyal2* KO valve, probably because these cells were stretched over the extended surface area of the expanded valve (Figure 2.4 C and D). These findings indicate that the accumulated HA in the ECM of *Hyal2* KO mice leads to the expansion, thickening, and disorganization of the valve leaflet/cups.

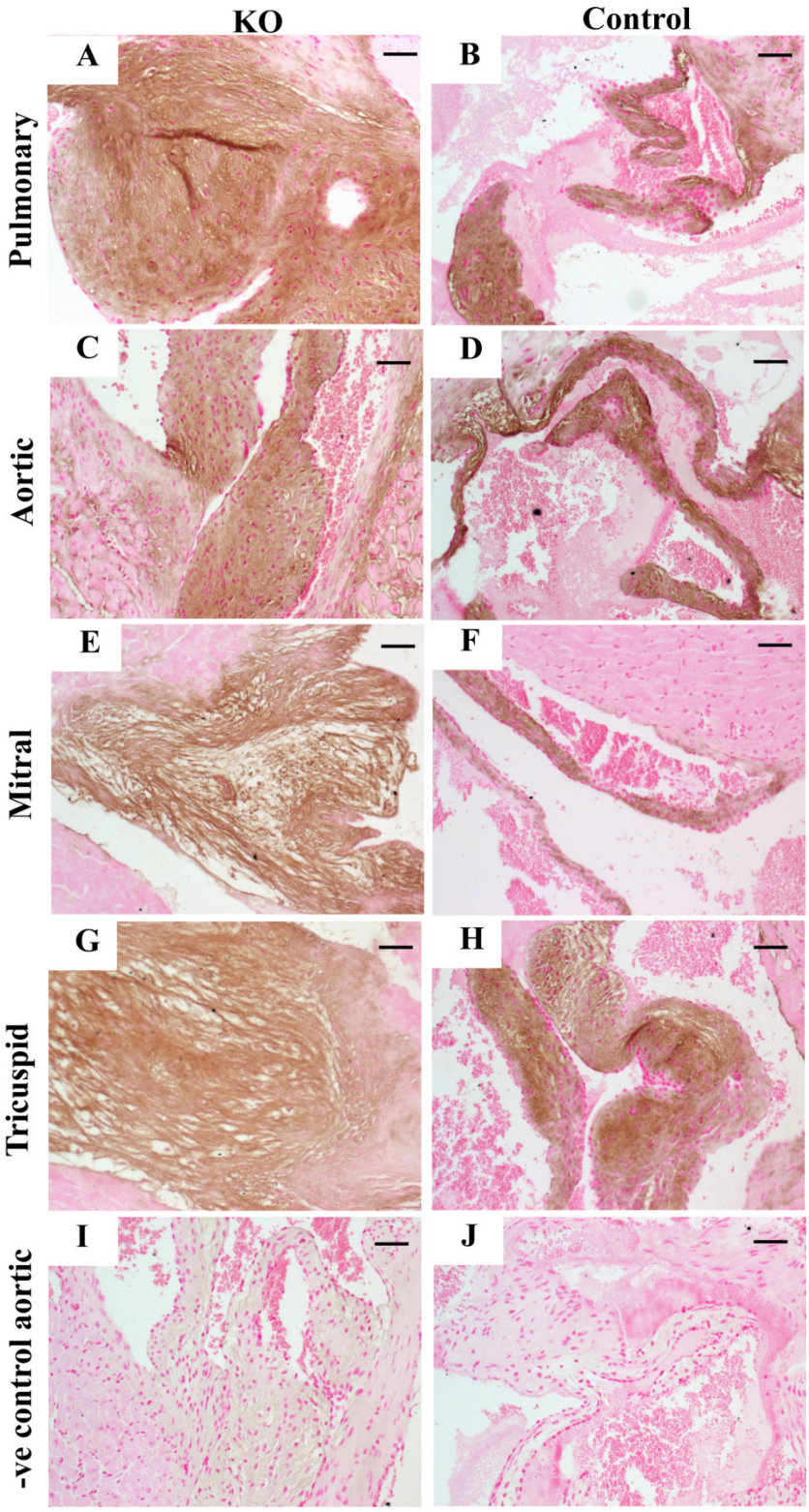

Figure 2.3. Analysis of HA in heart tissues

(*A-J*) Detection of HA in cross sections of the heart was performed using the HABP. Representative results for all four valves are shown. The intensity of HA staining (brown

colour) was similar throughout the *Hyal2* KO and control (+/-) valves. (*I-J*) Representative negative (-ve) controls for the HABP staining. Calibration bars represent 50 μm.

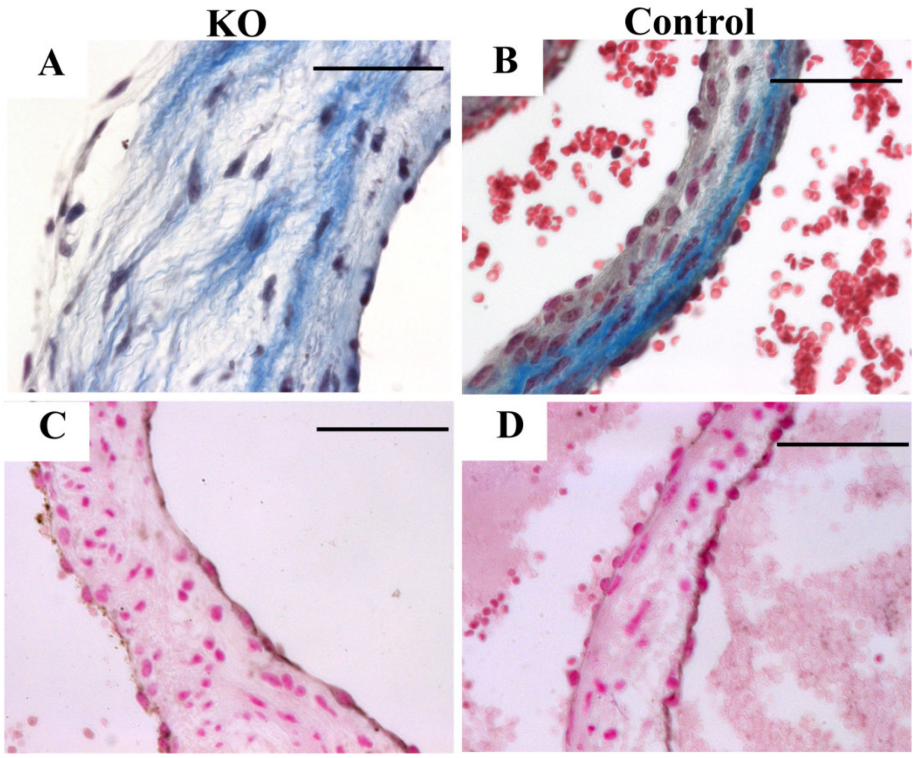

Figure 2.4. Analysis of valvular organization.

(A-B) Masson's trichrome staining of aortic valves show increased GAGs (unstained) separating the collagen fibres (light blue) in *Hyal2* KO (A) compared to the control (+/-) mice (*B*). (C-D) Anti-CD31 antibodies were used to detect endothelial cells (brown) on the valve surface in *Hyal2* KO and control (+/+) mice. CD31 positive cells were found to be closely spaced on the control valves (D), but are widely spaced on the *Hyal2* KO valves (C). Calibration bars represent 50 μm.

We also examined the structure of the atrial and ventricular myocardium of acute and non-acute *Hyal2* KO mice and controls for additional pathologies. Staining for total GAG with alcian blue revealed accumulation of interstitial GAGs between the atrial cardiac myocytes (Figure 2.5 A, C and E). This staining was more prominent in the acute *Hyal2* KO mice than the non-acute *Hyal2* KOs, and was always stronger in *Hyal2* KO mice than controls, indicating that GAGs were accumulating in the KO mice. In adjacent serial sections, HA was found to be abundant in the ECM of the acute mice compared to both non-acute and control mice (Figure 2.5 B, D and F), providing further evidence that HA is accumulating in the *Hyal2* KO mice.

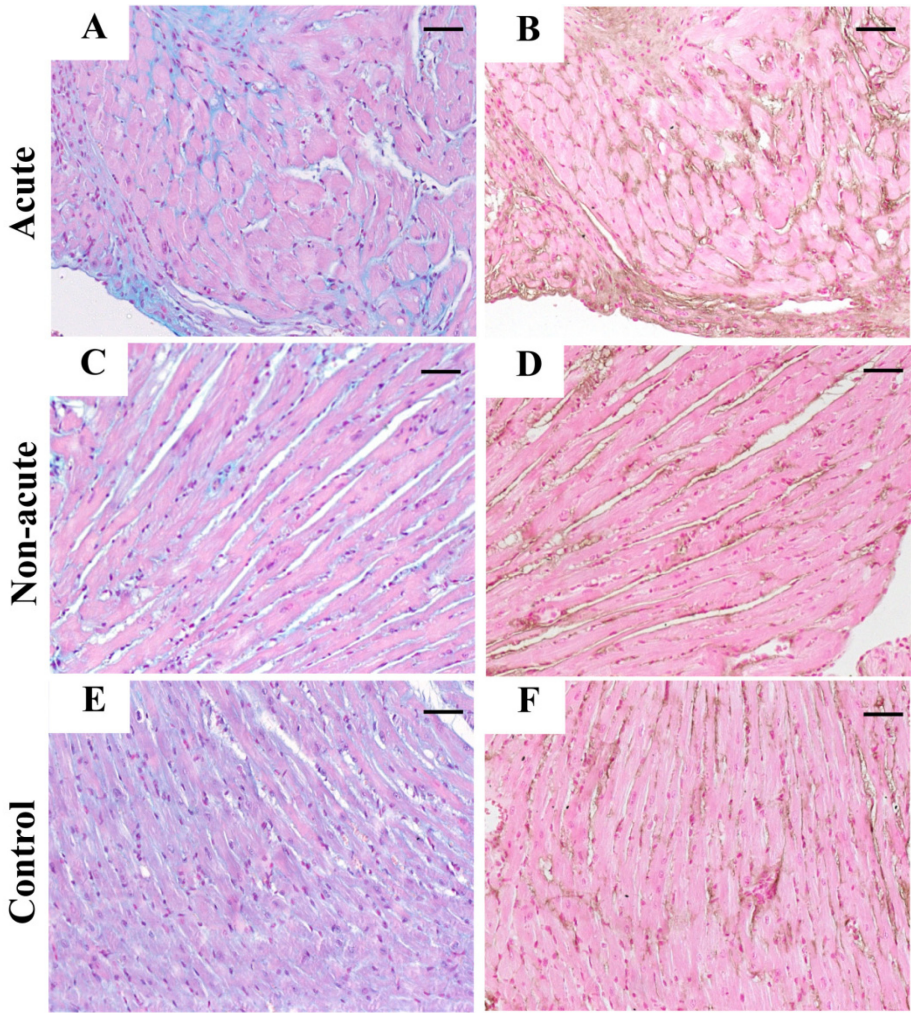

Figure 2.5. Analysis of GAGs in the myocardium.

Representative examples of alcian blue stained myocardium show increased intercellular GAG accumulation in the acute *Hyal2* KO (A) compared to the non-acute *Hyal2* KO (C) and control (E) mice. Enhanced HABP staining (brown) of consecutive serial slides showed the presence of more HA in the acute (B) than non-acute (D) and control (F) mice. Calibration bars represent 50 µm. The genotype of the control animals is +/+.

2.4.4 Cardiac hypertrophy in *Hyal2* KO mice.

To determine if there were additional abnormalities in the cardiac myocytes of *Hyal2* KO mice, sections were stained with fluorescently labelled wheat germ agglutinin, and the sizes of the cardiomyocytes were determined. Significant cardiac hypertrophy was found in the upper ventricular region, close to the base of the heart, of acute *Hyal2* KO mice as compared to controls (Figure 2.6 A), but this hypertrophy did not reach significance in the lower ventricular region of acute *Hyal2* KO mice (Figure 2.6 B), or in non-acute *Hyal2* KO mice (Figure 2.6 C and D).

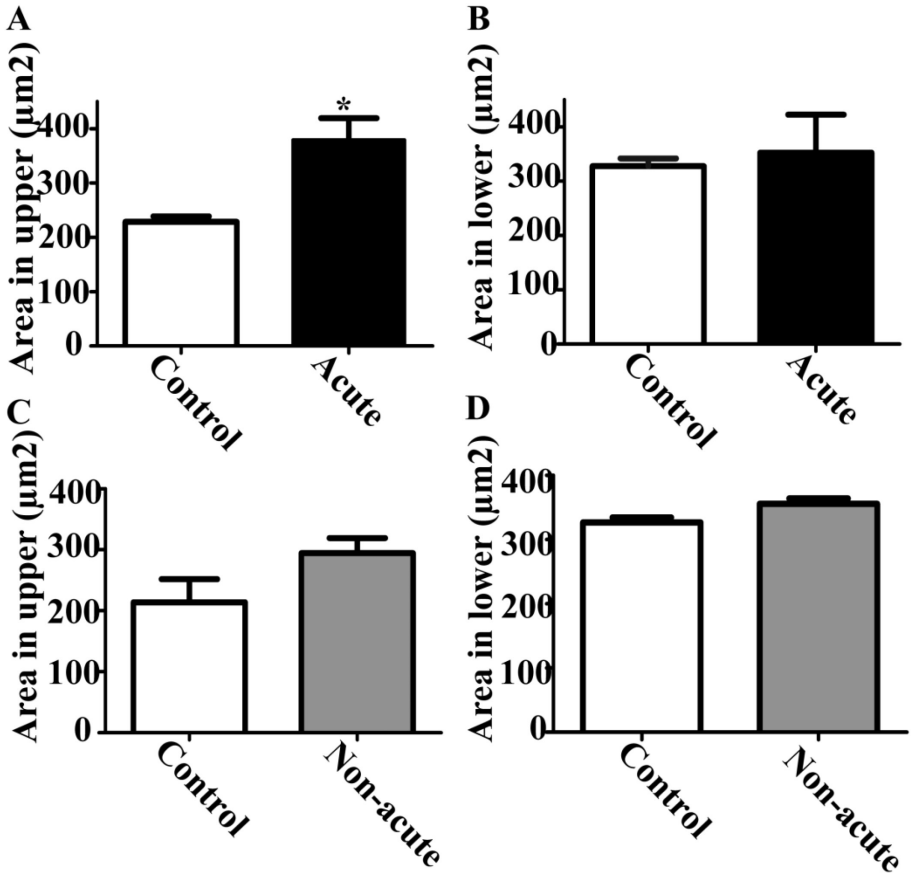

Figure 2.6. Cardiac hypertrophy in *Hyal2* KO mice.

(A) Cardiomyocytes of the upper ventricular myocardium showed significant hypertrophy in acute *Hyal2* KO mice compared to controls (n=3, *, $P < 0.05$.), whereas (B) lower ventricular myocardium showed no significant difference between acute *Hyal2* KO and control mice (n=3; p=0.74). Graphed values are expressed as mean ± SEM. The size of the cardiomyocytes of the upper ventricular (C) and lower ventricular (D) myocardium of non-acute *Hyal2* KO and control mice (n=3; p=0.14, 0.06) did not differ significantly. Graphed values represent the mean ± SEM. The control data presented in this figure is combined from mice with both +/+ and +/- genotypes.

2.4.5 Accumulation of ECM in *Hyal2* KO hearts.

To further characterize the changes in the *Hyal2* KO hearts, we performed transmission electron microscopy on the valves as well as ventricular and atrial myocardium. In the control valves (Figure 2.7 E), the ECM was densely packed with collagen fibrils, whereas in the *Hyal*2 KO valves (Figure 2.7 A) ECM separated the collagen fibrils. The accumulated material in the *Hyal2* KO valves was clearly extracellular, and was presumed to be HA. The atrial myocardium of *Hyal2* KO mice (Figure 2.7 B and C) contained cardiomyocytes which showed a disorganized arrangement of myofibrils and mitochondria and a substantial reduction in myofibrils. In contrast, the atrial cardiomyocytes of control mice showed a sarcoplasm with tightly packed myofibrils and mitochondria (Figure 2.7 F and G). Within the ventricular myocardium, we observed cardiomyocytes with a disorganized arrangement of myofibrils and mitochondria and a more loosely packed sarcoplasm (Figure 2.7 D) when compared to controls (Figure 2.7 H)

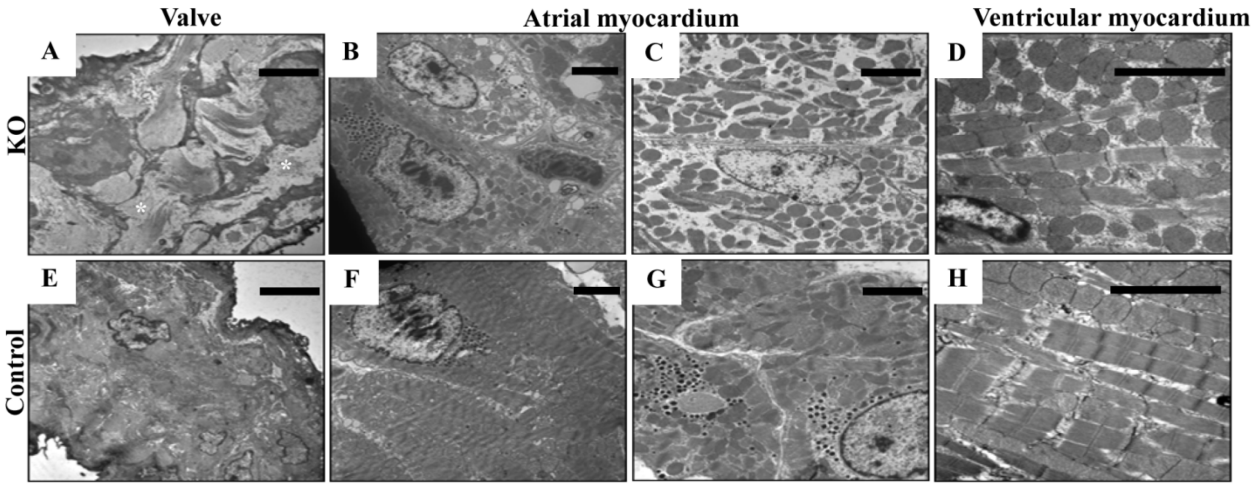

Figure 2.7. Subcellular structure of *Hyal2* KO heart tissues.

Representative transmission electron microscopy images are shown for *Hyal2* KO (A, B, C, and D) and for control (E, F, G, and H) mice. Compared to the organization of the ECM in the valve of control mice (*E*), the extracellular space in the *Hyal2* KO mouse valve (A) contains excessive GAG accumulation (*, white space) between the fibroblasts causing separation of the collagen fibrils (A). The atrial myocardium in *Hyal2* KO mice contained cardiomyocytes lacking an organized arrangement of myofibrils and mitochondria (B) and showing reduced myofibrils (C). In contrast, the atrial cardiomyocytes of control mice show tightly packed myofibrils and mitochondria (F and G). We observed a disorganized arrangement of myofibrils and mitochondria within a more spacey sarcoplasm in ventricular cardiomyocytes of *Hyal2* KO mice (D) compared to controls (H). All control mice (E-H) for this study were +/-. Scale bars represent 2 μm.

2.4.6 Histopathology of lungs in *Hyal2* KO mice.

To search for additional differences in acute, non-acute and control mice that might be related to atrial dilation, we examined the lungs. A dramatic difference between the acute and non-acute *Hyal2* KO lungs was identified. The alveoli were reduced and the alveolar septa thickened in the acute *Hyal2* KO mice compared to non-acute and control mice (Figure 2.8 A-C). Further, Masson's trichrome staining revealed that collagen levels were increased in the alveolar septae of the acute mice that was absent in both non-acute and control mice (Figure 2.8 D-F). Further investigation of the thickened alveolar septa using anti-α-SMA immunostaining revealed a strong signal for α-SMA in the alveolar interstitium of acute mice which was not detected in the lungs of the non-acute or control mice (Figure 2.8 G-I). Increased levels of HA were also detected in the lungs of acute and non-acute *Hyal2* KO compared to control mice (Figure 2.8 J-L) although the levels were much higher in the acutely affected animals. Therefore pathology typical of severe pulmonary fibrosis was present only in the acute *Hyal2* KO mice. Compared to control mice we observed numerous alveolar macrophages (foam cells) in the inter- and intra-alveolar spaces of acute, and to a lesser extent, non-acute *Hyal2* KO mice (Figure 2.8 A-B), suggesting the accumulation of HA led to the recruitment of macrophages to the lung parenchyma. To confirm that these infiltrating cells were macrophages, we used an antibody toward F4/80 (Figure 2.8 M-O).

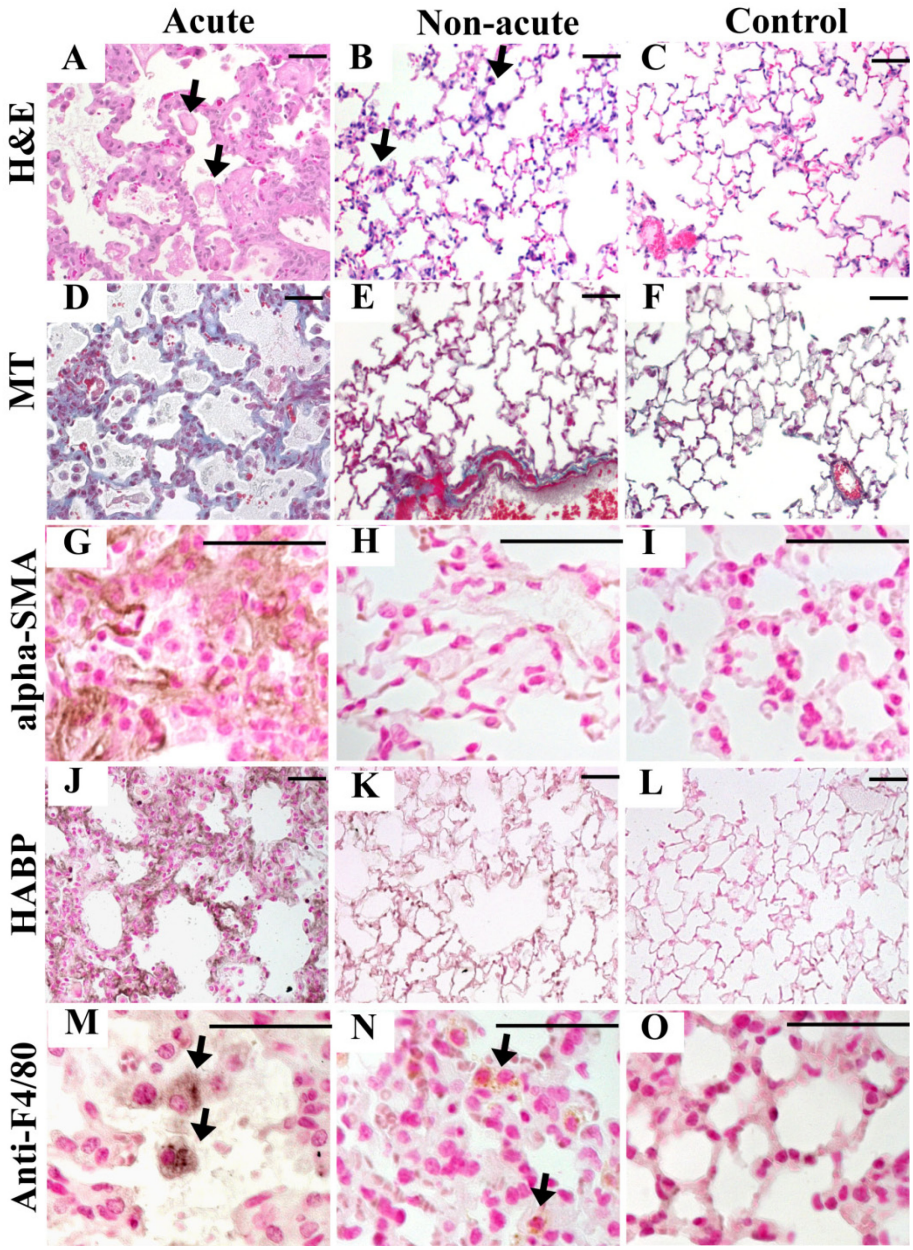

Figure 2.8. Histopathology of lungs.

(A-C) H&E staining of alveolar structure in acute (*A*), non-acute (B) and control (C) mice. Acute mice show dilated alveoli and thickened septae compared to the other two groups. (D-F) Masson's trichrome shows the accumulation of collagen (light blue) in acute (D) mice compared to non-acute (E) and control (F) mice. (G-I) Staining for α-SMA (brown) clearly shows the presence of α-SMA in the alveolar septae of acute (G) mice but not in non-acute (H) or control (I) mice. (J-L) Staining for HABP (dark brown) clearly shows the presence of more HA in the alveolar septae of acute (G) mice compared to non-acute (H) and control (I) mice. Alveolar macrophages (foam cells, arrows) were found in acute (M) and non-acute (N) mice compared to controls (O). Calibration bars represent 50 µm. Genotypes of control mice were (+/+) for C, F, L and (+/-) for I, O.

2.4.7 Increased HA levels and size in serum and heart of *Hyal2* KO mice.

A deficiency of HYAL2 had already been demonstrated to lead to increased serum HA [63]. As expected, we found the levels of HA to be approximately 19 fold higher in *Hyal2* KO mice compared to controls at 12 weeks (Figure 2.9 A). The levels of HA increased with age in the *Hyal2* KO mice reaching an average fold increase of 27 at the time of euthanasia (Figure 2.9 A). Interestingly, the levels of serum HA were elevated in both acute and non-acute *Hyal2* KO animals, indicating that differences in the levels of circulating HA are unlikely to be the cause of the more severe phenotype in the acute *Hyal2* KO animals.

We also quantified the levels of HA in the heart and lungs of *Hyal2* KO mice using FACE. Consistent with the detection of increased HA by IHC, elevated levels of HA were found in *Hyal2* KO hearts and lungs compared to controls (Figure 2.9 B and C). No significant difference between the levels of HA in non-acute and acute *Hyal2* KO mice was detected in the heart (Figure 2.7 B). The HA levels also appeared similar in the lungs of acute and non-acute *Hyal2* KOs, but our sample size was not large enough for statistical analysis. We also examined the chondroitin sulphate levels in the heart by FACE, and no significant difference between *Hyal2* KO (0.91 ± 0.17ng/mg) and control (0.77 ± 0.12 ng/mg) mice was found ($p=0.51$, $n=4$).

Given HYAL2's predicted role in initiating HA degradation by cleavage of high molecular mass HA to smaller fragments for internalization, we expected that the HA found in the tissues of *Hyal2* KO mice would have a larger molecular mass than that in control animals. In order to assess this, HA was partially purified from the serum and hearts of *Hyal2* KO and control mice and its size was analyzed by agarose gel electrophoresis. Accumulating HA was clearly evident in the heart (Figure 2.9 D) and serum (Figure 2.9 E) of *Hyal2* KO mice compared to controls. The size of the HA in *Hyal2* KOs was also increased compared to that in control tissues (Figure 2.9 D and E). The size of the isolated HA did not differ between

acute and non-acute *Hyal2* KO mice (data not shown). The material that we identified as HA in Figure 2.9 D and E, was readily digested with hyaluronidase SD, as shown in Figure 2.9 F, verifying its identity. Some of the lower molecular mass bands did not digest with hyaluronidase and are presumably represent other GAGs or contaminating proteins.

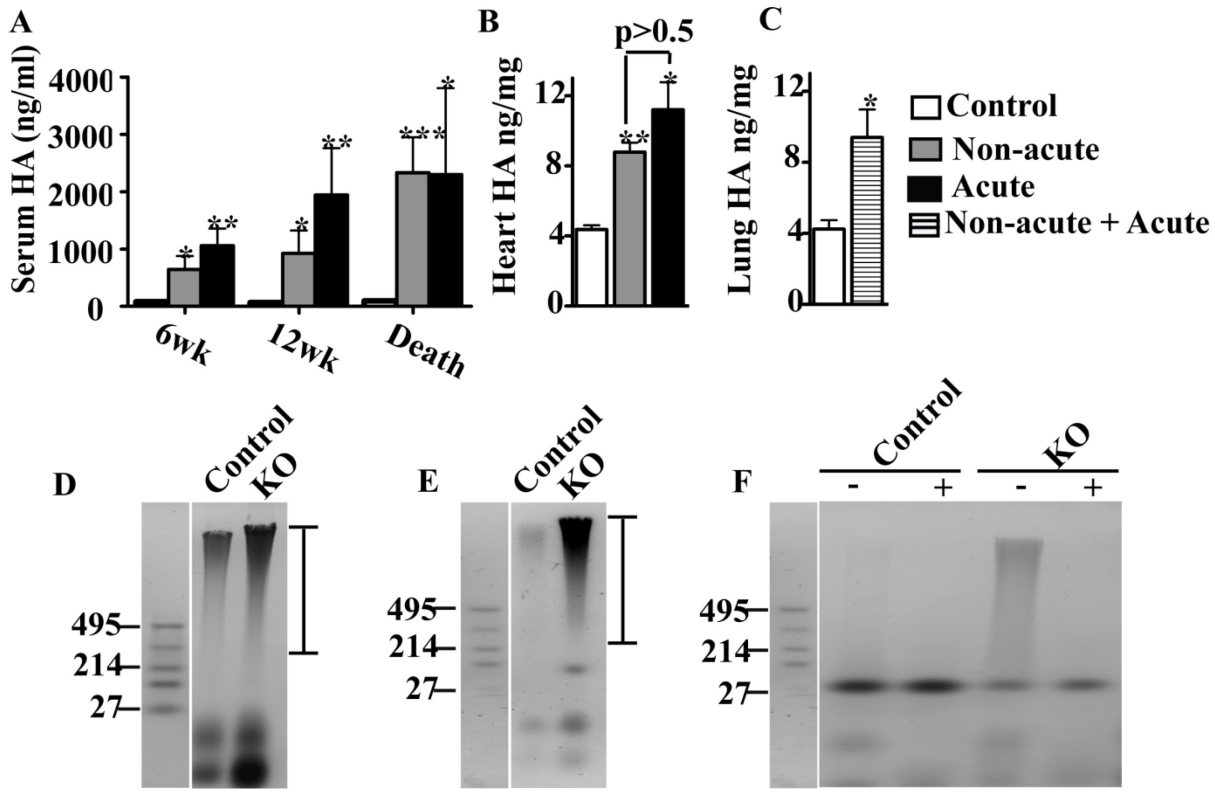

Figure 2.9. Serum and tissue HA content and size in *Hyal2* KO mice.

(A) Mean serum HA levels in control, as well as non-acute and acute *Hyal2* KO mice at 6 wk (control n=7, non-acute n= 5, acute n=4), 12 wk (control n=6, non-acute n=5, acute n=3), and at death (control n=15, non-acute n=11, acute n=7). The levels of HA in the serum are significantly increased in non-acute and acute *Hyal2* KO mice compared to controls. (B) Total HA content in the heart (n=3 in each group). The amount of HA is significantly increased in non-acute and acute *Hyal2* KO mice compared to controls but acute and non-acute mice do not differ from one another ($P = 0.22$). *(C)* Total HA content in the lung (n= 3 in each group). The amount of HA is significantly increased in the lung of *Hyal2* KO compared to control mice (P= 0.04). Graph values expressed as mean ± SEM. Student's *t*-test, $*P < 0.05$; $**P < 0.001$; $***P < 0.0001$. The control data presented in this figure were from both +/+ and +/- mice. HA size in the heart (D) and serum (E) of *Hyal2* KO and control mice was analyzed by agarose gel electrophoresis of GAGs isolated from these tissues. The size of HA standards (Select-HA™ LoLadder; Hyalose) in kDa are shown to the left of the panels. The dark-staining high molecular mass material, spanning the region indicated by the bar to the right of panels D and E*,* is HA. (F) To differentiate HA within the stained material on the agarose gel from other GAGs and contaminating proteins, GAGs isolated from the serum of control and *Hyal2* KO mice were not treated (-) or treated (+) with hyaluronidase and then analyzed by agarose gel electrophoresis. The high molecular mass material was removed by hyaluronidase treatment, identifying it as HA.

2.5 Discussion.

This study demonstrates that HYAL2 is essential for cardio-pulmonary function in mice. In its absence, extracellular HA accumulates in the serum and the interstitium of the heart muscle and lungs, heart valves thicken, and pulmonary fibrosis develops in some animals, leading to severe cardio-pulmonary dysfunction and premature death. This cardio-pulmonary failure follows an acute course (mean survival ~3 months) in some animals and a subacute course (mean survival < 6 months) in others. Acutely affected animals exhibited severe atrial dilation, cardiac hypertrophy, and pulmonary fibrosis that were absent from subacute animals. However, increasing plasma HA levels, heart valvulopathy, myocardial infiltration with GAGs and HA, and influx of pulmonary macrophages were present in all *Hyal2* KO mice, confirming a major role of HYAL2 in cardio-pulmonary function and possibly in overall HA turnover. Indeed, using the HABP, we have found increased HA levels in most tissues of both acute and non-acute *Hyal2* KO mice. Previous examinations of the *Hyal2* KO mice had revealed pre-weaning lethality, bone abnormalities, mild anemia, and elevated serum HA [63].

Whether or not the *Hyal2* KO mice develop the more severe acute phenotype is likely determined by other genetic loci. Indeed, the heart phenotype is infrequent on the *C57BL/6* background, and the frequency of pre-weaning lethality is lower in the *C57BL/6* (<10%) than the outbred background (16%). Taken together, these findings suggest that other loci can strongly influence the phenotype associated with HYAL2 deficiency.

The heart may be especially susceptible to the effects of HYAL2 deficiency because of the high levels of HA in the developing heart [126]. In contrast to HA synthase 2 KO mice, where a deficiency of HA synthesis prevents the formation of the endocardial cushion, as well as epithelial to mesenchymal transition [187,188], the heart and valves appear to develop normally in *Hyal2* KO mice. However, an apparent failure to remove excess HA in the

myocardium and valves after their formation, together with a possible ongoing failure of normal HA degradation, leads to postnatal cardio-pulmonary dysfunction.

Heart valvular pathology of the *Hyal2* KO mice was not limited to the pulmonary valve, indicating that HYAL2 is important in the homeostasis of valvular ECM in general. This finding is not surprising given that HA is a major GAG in heart valves and has viscoelastic properties that allow it to absorb shear force during the cardiac cycle [189]. The valvular ECM is expanded and disorganized in various MPSs that result from mutations in GAG degrading enzymes [182,190]. In addition, similar phenotypes result from defects in some ECM remodelling enzymes, including a deficiency in the ADAMTS 9 enzyme [179]. Abnormalities in HA levels in valves have also been associated with common disorders such as myxomatous valve disease [157,191,192]. Given the important role that HYAL2 can play in regulating HA levels, alterations in its level should be considered as a factor that could contribute to valve disease in humans. A complete deficiency of HYAL2 results in a severe phenotype, and therefore it is less likely that a complete deficiency of HYAL2 is compatible with human life.

Mice with HYAL2 deficiency also had excess ECM and accumulated HA in the atrial myocardium. In the acute *Hyal2* KO mice there were clearly increased levels of HA although when the level of HA in the total heart was determined, no significant difference between acute and non-acute *Hyal2* KOs were detected. It is possible that as the heart attempts to respond to the stress placed on it by abnormal valve function, additional ECM is synthesized, and HA then accumulates. Interestingly, we did not find HA accumulation in the ventricular myocardium, suggesting that *Hyal2* deficiency impacts the atrial more than the ventricular myocardium.

HA can make fluids highly viscous and higher plasma viscosity can increase circulatory resistance and induce or aggravate heart failure [193], possibly leading to cardiac hypertrophy and pulmonary edema. This in turn, could result in the accumulation of αSMA and collagen that is seen in the acutely affected *Hyal2* KO mice. However we have no pathological evidence as yet for such a chain of events. Although the contribution of elevated serum HA to the phenotype of *Hyal2* KO mice is unclear, it is interesting to compare the phenotype of the *Hyal2* mouse to the phenotype resulting from a deficiency of a major receptor of HA, HARE [116]. Interestingly, *Hare* KO mice have been reported to show high levels of serum HA, dilated cardiomyopathy, and premature mortality [118]. These findings provide further evidence that a disturbance in extracellular HA is responsible for the cardiac phenotype seen in *Hyal2* KO mice.

An alternative explanation for the observed lung pathology in acute mice is that a failure to degrade HA results in a primary defect in lung development [194]. The smaller size, cardiomyocyte pathology, and atrial dilation in acute *Hyal2* KOs could be secondary to impaired lung function. The numerous alveolar and interstitial macrophages in the lungs of *Hyal2* KO mice may indicate the attempt to reduce the interstitial deposits of HA and collagen. Such developmental delay could also cause high pre-weaning lethality in *Hyal2* KO mice.

Hyal2 is one of six hyaluronidase genes in humans and seven in mice [195]. It is a GPI-anchored protein with a neutral pH optimum, and a preference to cleave high molecular mass HA into 20 kDa fragments [87]. Most studies indicate that HYAL2 functions at the cell surface, and therefore has been proposed to degrade extracellular HA to smaller fragments that are internalized for further degradation [196]. Our findings support this model as the level of serum HA was extremely high whereas the level of circulating HA has not been shown to be elevated in mouse models with HYAL1 or HYAL3 deficiency. The larger size

of the HA that we detected in *Hyal2* KO tissues and serum also supports a role for HYAL2 in cleaving HA to smaller fragments for internalization. Further, electron microscopy indicates that the accumulating material in the *Hyal2* KO mice is extracellular whereas the material appears to be intracellular in humans that are deficient in HYAL1 [51]. The phenotype observed in *Hyal2* KO mice is much more severe than that in the *Hyal1* and *Hyal3* deficient mice [52,183] and more similar to that seen in other forms of MPS. This may be due to a redundancy in the intracellular pathway of HA degradation, but no other enzyme that can substitute for HYAL2 in extracellular degradation.

Finally, in 43% of the surviving *Hyal2* KO mice we found one kidney was missing. Interestingly, the kidney is another organ that has high levels of HA during development [196], so, like the heart, it may be more susceptible to defects due to HA accumulation. In the longer term, studies of *Hyal2* KO mice at different embryonic and pre-weaning stages will help to identify those tissues where HA degradation by HYAL2 is critical.

In conclusion, the present study illustrates the importance of HYAL2 in HA degradation in the heart and in normal cardio-pulmonary function. Localized extracellular accumulation of HA in the KO mice results in a storage disorder which is different from classic MPS disorders where the storage is typically both lysosomal and extracellular. Although a human condition resulting from alterations in HYAL2 activity has not yet been described, it will be interesting to examine the levels of HYAL2 and serum HA concentration in patients with unexplained heart valve abnormalities.

Chapter 3: Disruption of hyaluronan degradation due to hyaluronidase 2-deficiency causes increased mesenchymal cells, congenital heart defects and heart failure

Biswajit Chowdhury, Bo Xiang, Xiao-Qing Liu, Richard Hemming, Vernon W. Dolinsky, Barbara Triggs-Raine.

Acknowledgements: Ultrasound imaging was performed by Bo Xiang**.** Richard Hemming provided assistance during dissection and performed the western blot. Xiao-Qing Liu performed statistical analysis. Dr. Mike Jackson provided assistance during Micro-CT data analysis. Special thanks to Joy Armistead for generously providing E8.5- 12 mouse tissues.

3.1 Abstract

Hyaluronidase 2 (HYAL2) is a membrane-anchored protein proposed to initiate hyaluronan (HA) degradation. HA degradation in the developing heart is thought to be essential to inhibit epithelial to mesenchymal transition (EMT). To determine if changes in levels of HA and EMT in the developing *Hyal2* KO heart account for cardiac dysfunction in *Hyal2* KO mice, longitudinal analyses of heart structure and function were performed.

Echocardiography revealed atrial enlargement and diastolic dysfunction in all *Hyal2* KO mice, as well as cor triatrium in 50% of 4 week old mice. The *Hyal2* KO mice were divided into acute and chronic groups based on the severity of the cardiac dysfunction; the acute group died at ~12 wks of age, while the chronic group died at an average of 25 wks. All *Hyal2* KO hearts had increased HA, vimentin-positive cells, and fibrosis compared to controls. Analysis of hearts at embryonic day (E)14.5 and E18.5 confirmed that the levels of HA and number of vimentin positive cells were increased in *Hyal2* KO mice during development, and the EMT inhibitor, vascular endothelial growth factor, was decreased at E14.5. In control hearts, HYAL2 was broadly expressed and HA decreased with embryonic age.

This data demonstrates that disruption of normal HA catabolism causes increased HA levels and mesenchymal cells, presumably because EMT is not inhibited. Excess EMT is the likely cause of morphological abnormalities, including cor triatrium, which lead to progressive and severe diastolic dysfunction, resulting in heart failure.

3.2 Introduction

Congenital heart disease (CHD) can be detected in either childhood or adult life, and affects approximately 50 per 1000 live births [197]. The genetic causes of CHD are highly diverse, reflecting the complex molecular and cellular pathways that dictate normal heart development. Mutations affecting components of the cardiac extracellular matrix (ECM) are associated with a range of CHDs including Marfan syndrome, hypertrophic cardiomyopathy and dilated cardiomyopathy [198]. A deficiency in the synthesis of the ECM glycosaminoglycan, hyaluronan (HA), causes early embryonic death in mice due to defective heart development [126]. Recently, defective degradation of HA due to hyaluronidase 2 (HYAL2)-deficiency was also identified as a cause of cardiopulmonary dysfunction in mice [199]. To better understand how HYAL2-deficiency impacts heart development we have performed a longitudinal study of cardiac structure and function in *Hyal2* KO mice.

During embryogenesis, the heart is the first organ to develop. It is initially formed as a straight tube consisting of an outer layer of myocardium and an inner layer of endocardium. At approximately embryonic day (E) 9.5 in the mouse, the ECM between these layers expands to form the cardiac jelly. Extensive remodeling of the cardiac ECM and looping of the tube results in the formation of the atrioventricular canal, outflow tract and cardiac cushion [200]. EMT of epithelial cells within the cushions establishes the primordium that will develop into the valves and ventricular septum [139]. This primordium grows into thin fibrous valve leaflets/cups, that mature through ECM deposition and remodelling [201]. This process continues even after birth to form the mature heart.

HA and its binding protein, versican, are abundant components of the provisional matrix in the developing heart and the mature matrix of adult heart valves [126,202]. A critical role for HA during heart development has been demonstrated through the analysis of HA synthase 2 (HAS2)- deficient mouse embryos. These embryos died at E9.5 due to a

failure to form the HA-rich cardiac jelly needed to support transition of endothelial cells in the cardiac cushions into mesenchymal cells (endoEMT) to form the heart valves and septa [126]. Similar to *Has2*$^{-/-}$ mice, versican-deficient mice died at E10.5 due to abnormal cardiac cushion formation [202]. Studies of mouse cardiac explants revealed that exogenous high molecular mass HA promoted EMT whereas HA fragments inhibited EMT and activated the vascular endothelial growth factor (VEGF) pathway to form the four chambered heart [142]. Until now, *in vivo* studies of the role of hyaluronidase in normal EMT or in heart development have not been done.

Degradation of HA is presumed to be accomplished in somatic cells by HYAL1 and HYAL2 [39]. HYAL2 is anchored to the plasma membrane by a glycophosphatidylinositol linkage [59], and has weak activity toward high molecular mass extracellular HA to produce fragments of approximately ~ 20 kDa [39]. These shorter fragments are thought to bind a cell surface receptor for endocytosis, and be transported to the lysosome for degradation by HYAL1 and the exoglycosidases [43]. An important role for HYAL2 in HA degradation is demonstrated by the severe craniofacial abnormalities, pre-weaning lethality (only 9% survived at weaning), atrial enlargement (50%), cor-triatriatum (50%), and valve thickening (100%) present in *Hyal2* KO mice [63,199]. Further, histological analyses of hearts and lungs from *Hyal2* KO mice showed significant accumulation of HA that was not present in control mice [199]. However, the developmental basis of these changes, their effect on function, and whether the phenotypes progress with age was unknown.

In this study, we have characterized and compared the heart structure and function in *Hyal2* KO and control mice over time using echocardiography. Severe atrial dilation accompanied by diastolic dysfunction was found as early as 4 weeks of age in *Hyal2* KO mice, and progressed with age. Histological analyses revealed that the atrial dilation was the result of excess tissue, and did not correlate with the presence of cor triatrium. *Hyal2* KO

mice were found to have increased numbers of mesenchymal cells at early stages of embryonic development, suggesting increased EMT and decreased differentiation, presumably due to the presence of excess HA, that leads to cardiac dysfunction. These findings suggest that HA degradation by HYAL2 is required to attenuate EMT, and in the absence of HYAL2, excess mesenchymal cells are formed.

3.3. Materials and methods

3.3.1 Mice

Mice that are null for HYAL2, *Hyal2* KO mice, were generated as part of a previous study [63]. These mice were maintained on an outbred (*C57BL6; C129; CD1*) background on which 9% of *Hyal2* KO mice survive [199]. *Hyal2* KO and control mice ($Hyal2^{+/+}$) were generated through heterozygous intercrosses. Embryos for analysis of heart development were collected from timed-pregnant females at E18.5 and E14.5. PCR-based genotyping of DNA from tissue samples collected from offspring or embryos was performed as described previously [199]. All studies were performed using protocols approved by the University of Manitoba Animal Care Committee in accordance with the Canadian Council on Animal Care.

3.3.2 Ultrasound analyses of heart function

Cardiac imaging of *Hyal2* KO and control mice was performed using high frequency ultrasound with the Vevo 2100 system (Visual Sonics, Toronto, Canada) equipped with a 40 MHz transducer as described previously [203]. Mice were imaged at 4 wks of age, and then every 4 wks until 6 months of age, unless an earlier humane end point requiring euthanasia was reached. Euthanasia was performed by isoflurane overdose. During imaging, the body temperature of the mice was maintained at 37°C ± 0.5°C under mild anesthesia (sedated with 3% isofluorane and 1.0 L/min oxygen and maintained at 1-1.5% isofluorane and 1.0 L/min oxygen).

Structural and functional cardiac parameters in adult and embryonic hearts were assessed using three imaging formats: brightness (B)-mode, motion (M)-mode and Doppler imaging. B-mode was used to generate 2-D views of cardiac and associated vasculatures, while the M-mode was used to characterize ventricular functional parameters, and pulsed-

wave Doppler was used to determine velocity and direction of the blood flow in a localized region of the heart. Measurements were performed over four cardiac cycles. Each parameter used in the calculations for the study was measured in triplicate for each mouse at each time point. The data were analyzed by a trained and blinded research animal echocardiographer using the Cardiovascular Package from VisualSonics following a published approach [203].

3.3.3 Micro-computed tomography (micro-CT)

Hearts were fixed overnight in alcoholic Bouin's solution containing 1% phosphotungstic acid as described previously [204] and imaged at 9 μm using the Skyscan 1176 micro-CT scanner. The scanning parameters were set at 0.5 mm thick aluminium filter, X-ray source voltage 50 kV, and current 500 μA. The reconstructed 3D images were space-filled, rotated, and colourized using Bruker-Micro-CT CT-Analyser Version 1.13.

3.3.4 Histology

Hearts were harvested from adult *Hyal2* KO mice at 6 months of age unless a humane end point was reached earlier. Each control heart was collected at the same time as an experimental (*Hyal2* KO) heart. Embryonic hearts were collected from E14.5 or E18.5 mice. Control embryos at E8.5, 11.5 and 12.5 were obtained as part of a previous study [205]. Morphology was examined by hematoxylin and eosin (H & E) staining and HA was detected using the HA binding protein (HABP) following established procedures [199]. ECM components were visualized with Masson's trichrome (Sigma) following the manufacturer's instructions.

Immunohistochemistry (IHC) was performed as described previously [199], except that antigen retrieval was in 0.1% sodium acetate pH 6.0 for 20 min. Rabbit polyclonal anti-vimentin (Abcam ab45939, 1:700), anti-VEGFA (Proteintech 19003; 1:1000) and anti-HYAL2 (Abcam 1:200) were detected by incubation with biotinylated goat anti-rabbit (Vector Labs, 1:500) for 1h. Antibody complexes were visualized with Impact diaminobenzadine (Vector Labs), counterstained with nuclear fast red for 2.5 min, rehydrated, and mounted with Permount (Fisher Scientific). Sections were visualised with a Zeiss bright field microscope and analysed with Axiovision software. The number of vimentin positive cells in the atrium and ventricle were calculated using Image J software Fiji 1.46 [206]. Three fields containing on average of 25 cells per field were counted for each mouse.

3.3.5 Immunoblot analysis

Immunoblots were performed as described previously [54]. Briefly, mouse heart extracts were prepared by sonication in PBS and 30 μg of protein were separated by electrophoresis on a 7.5% sodium dodecyl sulfate–polyacrylamide gel. Blots with anti-vimentin (1/1000) or anti-β-actin (1/5000) were performed as described previously[54].

3.3.6 Statistical analysis

Data presented in this article are presented as mean±SEM. Statistical analysis were performed using GraphPad Prism 6. Student *t*-test were used to determine the significant level between the groups and differences were considered as significant when $p< 0.05$. For the cardiac functional analysis, for each phenotype with repeated measures, comparisons were conducted using PROC MIXED from SAS v9.3 (SAS Institute Inc., Cary, NC).

3.4 Results

3.4.1 Atrial enlargement in *Hyal2* KO mice

To understand the developmental origins of the cardiac phenotype of *Hyal2* KO mice, we examined whether cardiac dysfunction and atrial enlargement (dashed lines, Figure 3.1 A-C) previously detected at spontaneous death or at a humane end point in *Hyal2* KO mice [199], was progressive in nature. We conducted a longitudinal analysis of cardiac structure and function at 4 wk intervals beginning at 4 wks of age by using high-frequency ultrasound. At 4 wks of age, all *Hyal2* KO mice exhibited significant atrial enlargement (Figure 3.1 A-C, and G); in 50% of the *Hyal2* KO mice, the size of the atrium was already 1.3 fold larger that of control mice by 4 wks. These mice reached a humane end point at an average of 9 wks, 15 wks earlier than their less severely affected *Hyal2* KO littermates. The severe atrial enlargement in 50% of mice was consistent with our previous study where 54% of mice were found to have severe atrial enlargement at death [199]. Based on these findings, the severely affected *Hyal2* KO mice, or acute group, were analyzed independently of the less severely affected or chronic group of *Hyal2* KO mice.

Ultrasound imaging revealed that the enlargement of the atria in *Hyal2* KO mice was accompanied by increased tissue density (Figure 3.1 D-F). In the acute group of *Hyal2* KO mice with severe enlargement, excess tissue blocked the view of the atrium (Figure 3.1 D) that was normally clearly visible (Figure 3.1 E-F). No progressive change in the size of the atrium was detected in the *Hyal2* KO mice (Figure 3.1 G). We were unable to measure the ventricular diameter using ultrasound imaging because the apex of the heart could not be reproducibly visualized in the images. However, there were no instances where the ventricles were grossly distended like the atria of *Hyal2* KO mice.

3.4.2 Valve thickening in *Hyal2* KO mice

In a previous study, we demonstrated that all four valves of the heart were increased in thickness in adult *Hyal2* KO mice [199]. However, it was not clear whether increased valve thickness was present at birth, or if the valves increased in thickness over time. B-Mode images revealed significantly thickened valves were already present at 4 wks of age in *Hyal2* KO mice, and that the degree of thickening did not change significantly with age (Figure 3.1 H,I). No significant difference was found in the valve thickness of acute and chronic *Hyal2* KO mice. B-mode imaging allowed the measurement of only the aortic and mitral valves, which we used as a proxy for valve thickness in general (Figure 3.2).

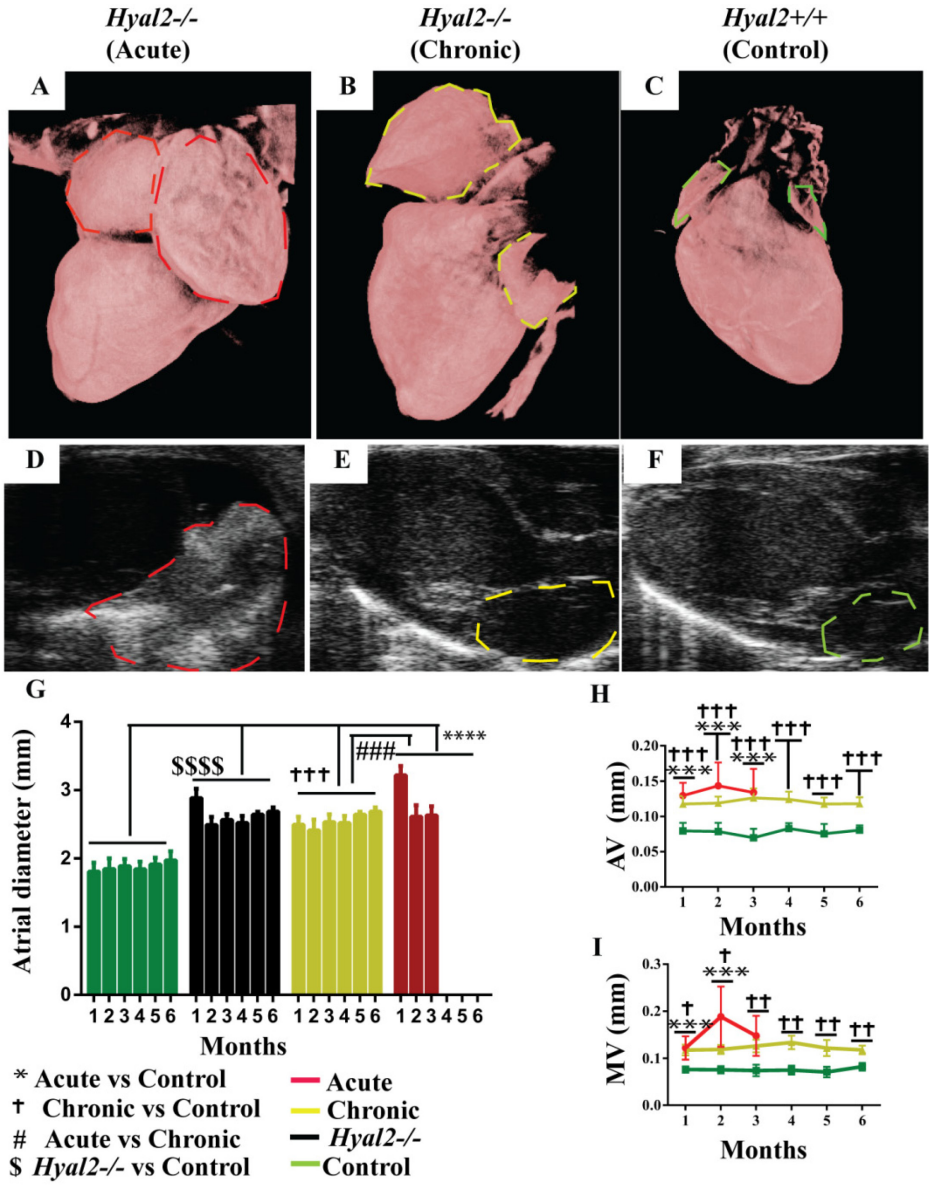

Figure 3.1. Structural abnormalities in *Hyal2* KO mouse hearts.

(A-C) High-resolution micro-CT images of *Hyal2* KO and control hearts. Micro-CT images were reconstructed in 3D and colorized to enhance structural visualization. *Hyal2* KO mice with a grossly enlarged atrium (A) were deemed acute while those with a mildly enlarged atrium (B) were deemed as chronic. A heart from a control mouse is shown in (C). (D-F) Ultrasound images of *Hyal2* KO and control hearts. B-mode images of the heart showed an enlarged and dense left atrium (dashed lines) in the acute *Hyal2* KO mice compared to chronic *Hyal2* KO and control mice. The increased density is indicated in the image by the stronger white signal. (G) Atrium diameter in *Hyal2* KO and control mice. The diameter of the atrium was significantly larger in both acute and chronic *Hyal2* KO mice compared to controls. (H) Atrial valve (AV) and (I) Mitral valve (MV) thickness was significantly increased in acute and chronic *Hyal2* KO mice compared to controls. *,† or # $P<0.05$; ** or †† $P<0.001$; ***, ††† or ### $P<0.0001$. The number of animals used were: for atrial enlargement control and chronic (n=6); acute (at 1 month n=7; 2 months n=4, 3 months n=3),

for AV thickness control and chronic (n=6); acute (at 1 month n=7; 2 months n=4, 3 months n=3), for MV thickness control and chronic (n=6), acute (at 1 month n=6; 2 months n=4, 3 months n=3).

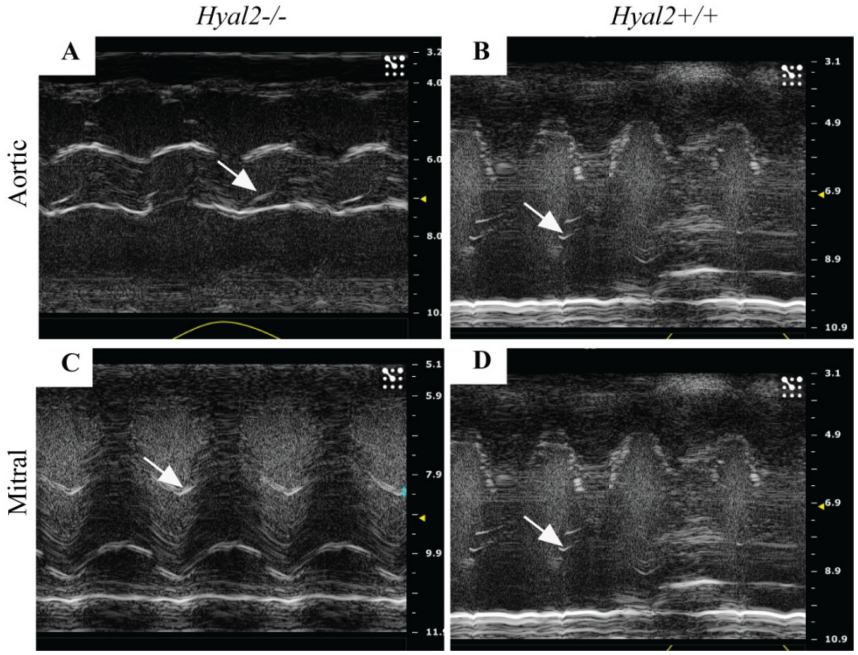

Figure 3.2. Valve thickening in *Hyal2* KO and control mice.

B-mode image of high-frequency ultrasound exhibiting thickened aortic and mitral valves in the *Hyal2* KO mouse (arrow, A,C) compared to the control (arrow, B, D). This is a representative image from n=14 pairs of mice.

3.4.3 Heart function in *Hyal2* KO mice

To determine how the enlarged atria and thickened valves affected cardiac function in *Hyal2* KO (acute and chronic) and control mice [199], we analysed several parameters using echocardiography. The peak velocities of early (E) to late atrial (A) filling of the left ventricle were inverted in *Hyal2* KO as compared to control mice (Figure 3.3), and resulted in a significantly reduced E/A ratio in all *Hyal2* KO mice compared to controls (Figure 3.4 A). In the acutely affected *Hyal2* KO mice, the E/A ratio was significantly lower by three months than that in the chronic group of *Hyal2* KO mice. Another measure of left ventricular diastolic function, the isovolumetric relaxation time (IVRT) was significantly increased in all *Hyal2* KO mice at all time points (Figure 3.4 B). The reduced E/A ratio and prolonged IVRT show there is an increased interval between mitral valve closure and aortic valve opening, indicating severe diastolic dysfunction in both acute and chronic *Hyal2* KO compared to controls, although the acute *Hyal2* KO mice were more severely affected at earlier ages.

To evaluate systolic function, the ejection fraction (EF) and fractional shortening (FS) of acute and chronic groups of *Hyal2* KO mice and controls were compared. No significant difference was observed among the groups (Figure 3.4 C,D). Left ventricular (LV) corrected mass was assessed to determine if hypertrophy detected by histological studies in *Hyal2* KO mice was present at the level of the whole heart [199]. Consistent with these earlier findings, both acute and chronic groups of *Hyal2* KO mice showed progressively increased LV mass compared to control mice (Figure 3.4 E). In the first 12 wks, acute *Hyal2* KO mice had reduced LV mass compared to control and chronic *Hyal2* KO mice (Figure 4.4 E).

Global cardiac function, represented by the myocardial performance index (MPI), was impaired in all *Hyal2* KO mice compared to control littermates, reflecting reduced overall cardiac performance (Figure 3.4 F). Reduced cardiac output (CO) was also evident in the acute *Hyal2* KO mice compared to chronic *Hyal2* KO mice and controls (Figure 3.4G).

Together, our data suggests that severe diastolic dysfunction accompanied by reduced cardiac output contributes to the development of heart failure in the acute group of *Hyal2* KO mice within the first 3 months of life. In the chronic group of *Hyal2* KO mice, progressive diastolic dysfunction without reduced CO, developed over time leading to heart failure at an average age of 6 months.

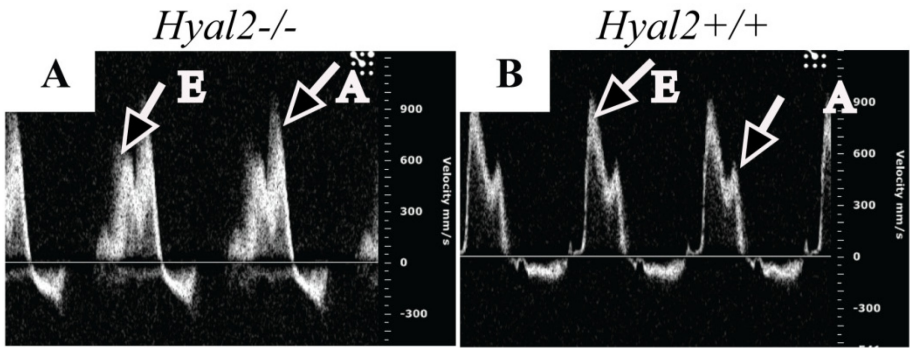

Figure 3.3. E/A ratio in *Hyal2* KO and control mice.

M-mode image of mitral early (E) and late atrial (A) flow was calculated to evaluate the E/A ratio of *Hyal2* KO and controls. *Hyal2* KO (A) showed reduced E and increased A in comparison to that of the control mouse (B).

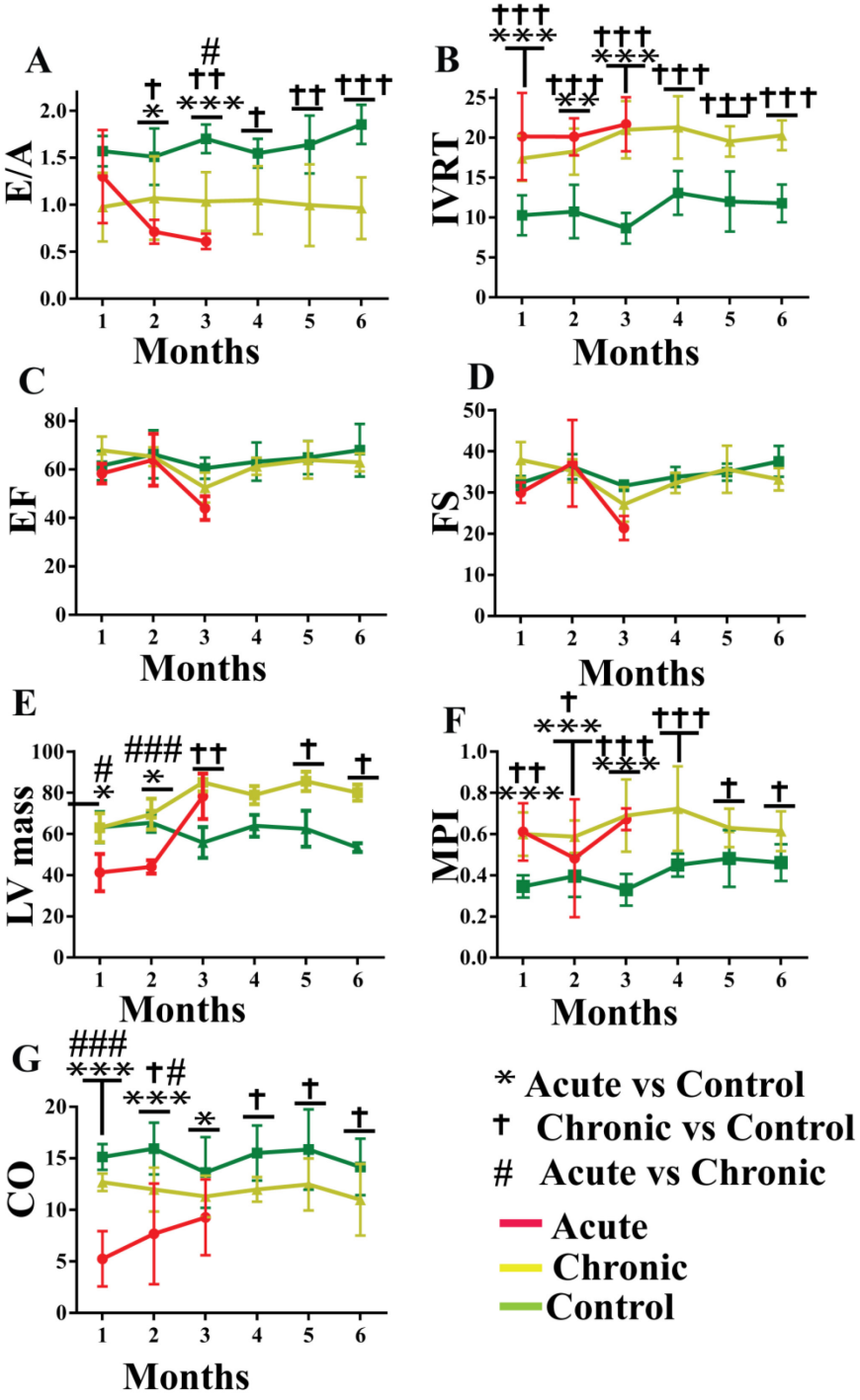

Figure 3.4. Cardiac function in *Hyal2* KO and control mice.

Pulse wave Doppler images were used to measure E/A (A) and IVRT (B). (A-B) Acute and chronic *Hyal2* KO mice showed significant impairment at all ages compared to controls. There was no significant difference between acute and chronic *Hyal2* KO mice except at 4 wks where the IVRT of the acute group was significantly prolonged compared to the chronic group. (C-D) M-mode images were used to measure systolic parameters including ejection

fraction (EF) and fractional shortening (FS). No significant difference in the EF or FS was found between *Hyal2* KO and control mice, although the function was trending downward in the acute *Hyal2 KO*mice at the last measurement before a humane end point was reached. (E) Left ventricular (LV) mass. LV mass increased progressively in both the acute and chronic groups of *Hyal2* KO mice compared to controls. (F) The myocardial performance index (MPI) was increased significantly at all ages in acute and chronic groups of *Hyal2* KO mice compared to controls. (G) Cardiac output (CO) in the most significantly impaired in the acute group of *Hyal2* KO mice compared to controls, although the chronic group of *Hyal2* KO mice also showed CO at most ages. *,† or # $P<0.05$; ** or †† $P<0.001$; ***, ††† or ### $P<0.0001$, n=3 to 7 per group at all ages.

3.4.4 Cor triatrium in *Hyal2* KO mice

Half of the *Hyal2* KO (n=7 of 14) mice, including those with or without significant atrial enlargement (acute and chronic), had cor triatrium (Figure 3.5 A,B). High-resolution ultrasound revealed two septal walls in the middle of the enlarged left or right atrium of these mice. Further, pulse wave Doppler imaging showed a turbulent blood flow through these walls, suggesting that the orifice was central and that normal blood flow was impeded at the orifice (data not shown). To further characterize the cor triatrium, histological analyses were performed. Consistent with the ultrasound findings, valve-like structures were detected with H & E staining in the middle of the atrium of *Hyal2* KO mice that were absent in controls (Figure 3.5 C-F). These valves stained strongly for HA (Figure 3.3 G), similar to normal valves in other parts of the heart.

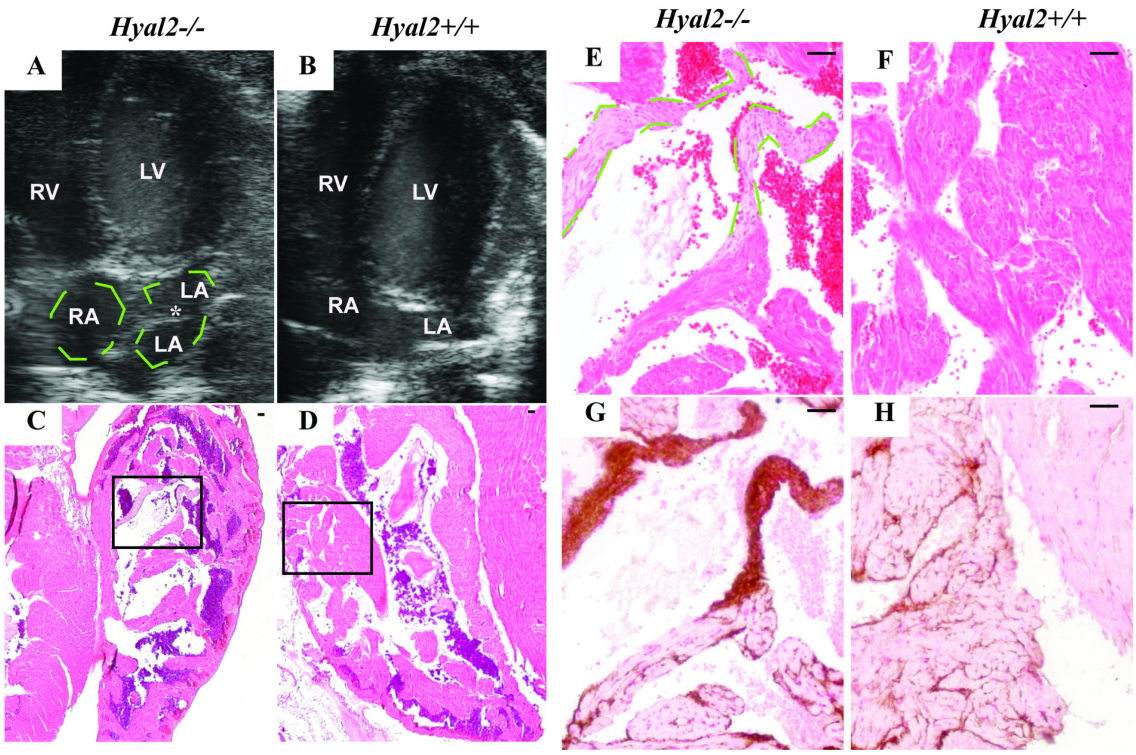

Figure 3.5. Apical 4-chamber view of *Hyal2* KO and control hearts.

High resolution (40 MHz) ultrasound was used to image the hearts at 4 wks of age. (A, B) Images from a *Hyal2* KO (A) and control (B) mouse show the presence of a dividing septum (*) in the left atrium of the *Hyal2* KO mouse that results in cor triatrium (green dashed line). (C-D) Images of H & E stained transverse sections of *Hyal2* KO (C) and control (D) atria show the presence of valve-like tissue (black box) in the *Hyal2* KO atrium but not in the control atrium. (E-F) An enlarged view of the area in the box in C and D. A green dashed line outlines the valve-like structure in the *Hyal2* KO atrium. (G-H) Detection of HA in the atrium of *Hyal2* KO and control mice showed the strong HA staining in the valve-like structure in the *Hyal2* KO atrium that is absent in the control atrium. These images are representative of 3 pairs of mice that were studied. Scale bar = 50 µm.

3.4.5 Increased tissue density in *Hyal2* KO mice

To better understand the basis for the increased tissue density observed by ultrasound imaging, we performed histological analyses on transverse sections of hearts from *Hyal2* KO and control mice. H & E staining revealed enlarged atria in all *Hyal2* KO mice compared to controls, consistent with the ultrasound findings (Figure 3.6 A-C, n=7 pairs). Further, in hearts from the acutely affected *Hyal2* KO mice, masses of tissue (*, potentially tumours) were apparent in the atria that were absent in chronic *Hyal2* KO and control mice (Figure 3.6 A, n=4 pairs). To determine if this abnormality was associated with HA accumulation, HABP staining was performed. Abundant HA was evident in the atrium and ventricle of acute and chronic groups of *Hyal2* KO mice compared to controls (Figure 3.6 D-F). However, the increased HA staining was only detected in the periphery of the tumour, and not in the central region, which appeared to be comprised of cardiomyocytes (Figure 3.6 D, open arrow). Additionally, HABP staining revealed excess valve like tissues in other regions of the heart from both acute and chronic groups of *Hyal2* KO mice in compared to controls (arrows in Figure 3.6 E). Masson's trichrome staining demonstrated fibrosis in the atrium and ventricle of *Hyal2* KO mice (acute and chronic, green arrows) compared to controls (Figure 3.6 G-I).

The excess fibrous tissues suggested there may be large numbers of fibroblasts secreting ECM. To assess this, we used the mesenchymal marker, vimentin. Abundant vimentin positive cells in the atrium and ventricles were detected. In a representative image of the atrium, excess vimentin positive cells were obvious in the *Hyal2* KO mice compared to controls (Figure 3.6 J-L). Semi-quantitative analysis of vimentin positive cells in the atrium showed increased numbers of mesenchymal cells in both acute and chronic groups of *Hyal2* KO mice compared to controls (Figure 3.6 M), although the number of mesenchymal cells was significantly higher in the acute compared to the chronic *Hyal2* KO mice. Similarly, mesenchymal cells in the ventricle region were also assessed and revealed abundant vimentin

positive cells in the *Hyal2* KO compared to controls (Figure 3.7). In this case, the number of vimentin-positive mesenchymal cells was higher in the chronic *Hyal2* KO mice than the acute *Hyal2* KO and control mice (Figure 3.7 M). Expression analysis in the adult heart (including atrium and ventricle) revealed increased levels of vimentin in the *Hyal2* KO mice compared to controls, consistent with the immunohistochemistry results (Figure 3.6 N,O). The increased number of mesenchymal cells, and the presence of abnormal heart structures are consistent with a developmental defect in the *Hyal2* KO mice.

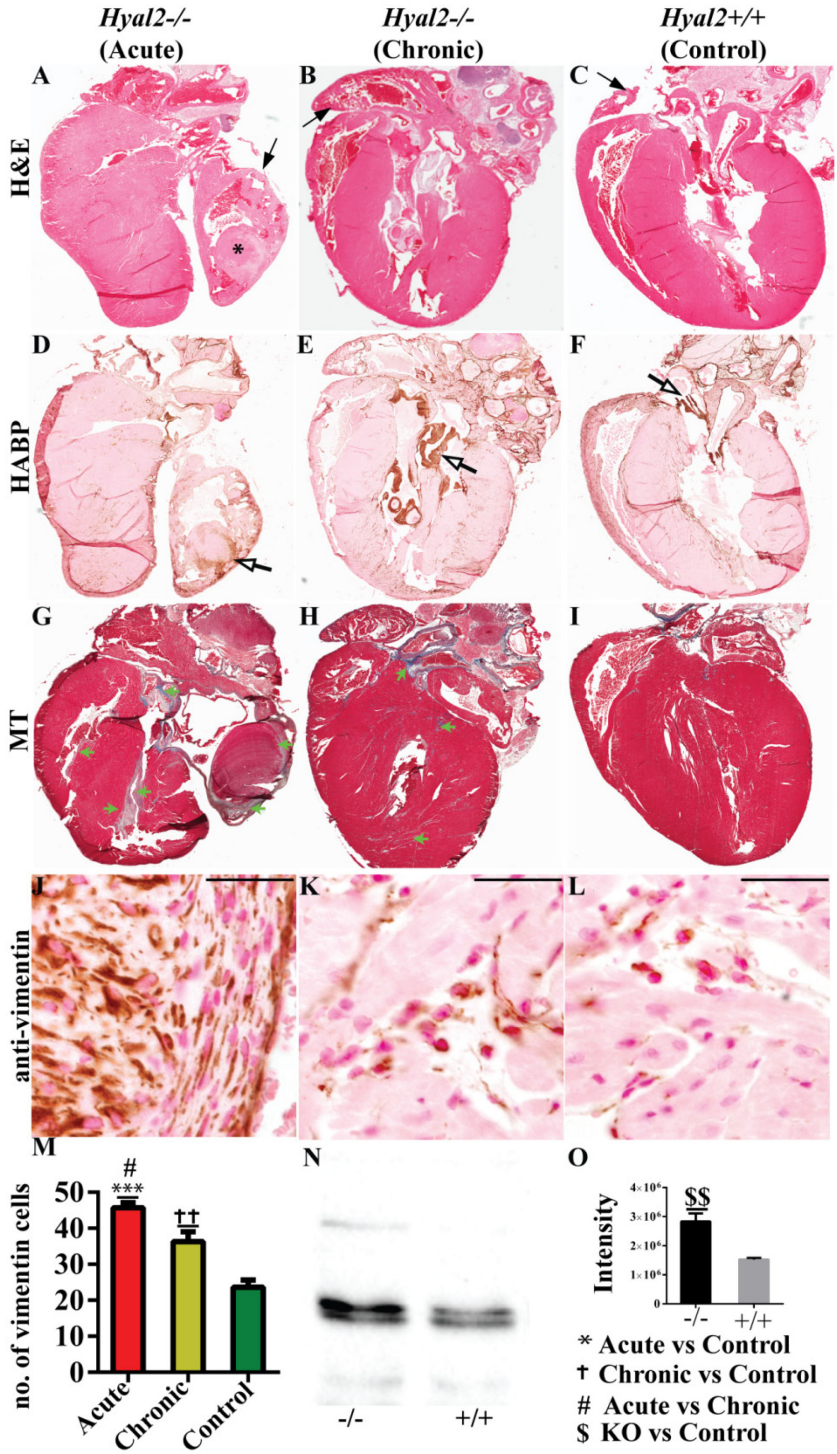

Figure 3.6. Histological analysis of *Hyal2* KO and control hearts.

Transverse sections of hearts from *Hyal2* KO (acute and chronic) and control mice were compared for differences in morphology and structure. (A-C) Images of H & E stained sections revealed an enlarged atrium (arrow) in both the acute (A) and chronic (B) groups of *Hyal2* KO mice compared to control mice (C). An * indicates an extra tissue mass in the atrium of the acute *Hyal2* KO mouse. (D-F) Images of HA distribution the *Hyal2* KO and control hearts. HA was detected as a brown precipitate using the HA binding protein. There

is intense brown staining in several regions of the *Hyal2* KO hearts (open arrows in D, E) while the intense brown staining is limited to the valves in the control hearts (open arrow in F). (G-I) Masson's Trichrome staining of *Hyal2* KO and control hearts. Masson's trichrome stains the ECM components collagen and elastin as blue and GAGs remain unstained. Excess ECM indicating fibrosis (green arrows) is widespread in the *Hyal2* KO hearts compared to the control heart (I). (J-L) Detection of mesenchymal cells in *Hyal2* KO and control hearts. Anti-vimentin (brown) indicates the presence of mesenchymal cells. There are increased numbers of vimentin positive cells in both the acute and chronic *Hyal2* KO atria (J,K) compared to the control atrium (L). (M) Semi-quantitative analysis of vimentin positive cells in *Hyal2* KO and control atria. Significantly increased numbers of vimentin-positive cells are present in *Hyal2* KO atria compared to control atria, and significantly more in the acute *Hyal2* KO than in control *Hyal2* KO atria. (N,O) Vimentin protein levels in *Hyal2* KO and controls hearts (atrium and ventricle). (N) Western blot analysis showed increased expression of vimentin in the *Hyal2* KO heart compared to controls. (O) Quantification of vimentin levels in N. The chemiluminescent images from western blot analysis of vimentin from *Hyal2* KO and control hearts (n=4) were quantified using a BioRad ChemiDoc. The columns represent the average level of vimentin ± SEM (n=4). Significance was determined using the student's T test. Scale bar = 50 μm. The images in this figure are representative of those from 7 pairs of *Hyal2* KO and control mice.

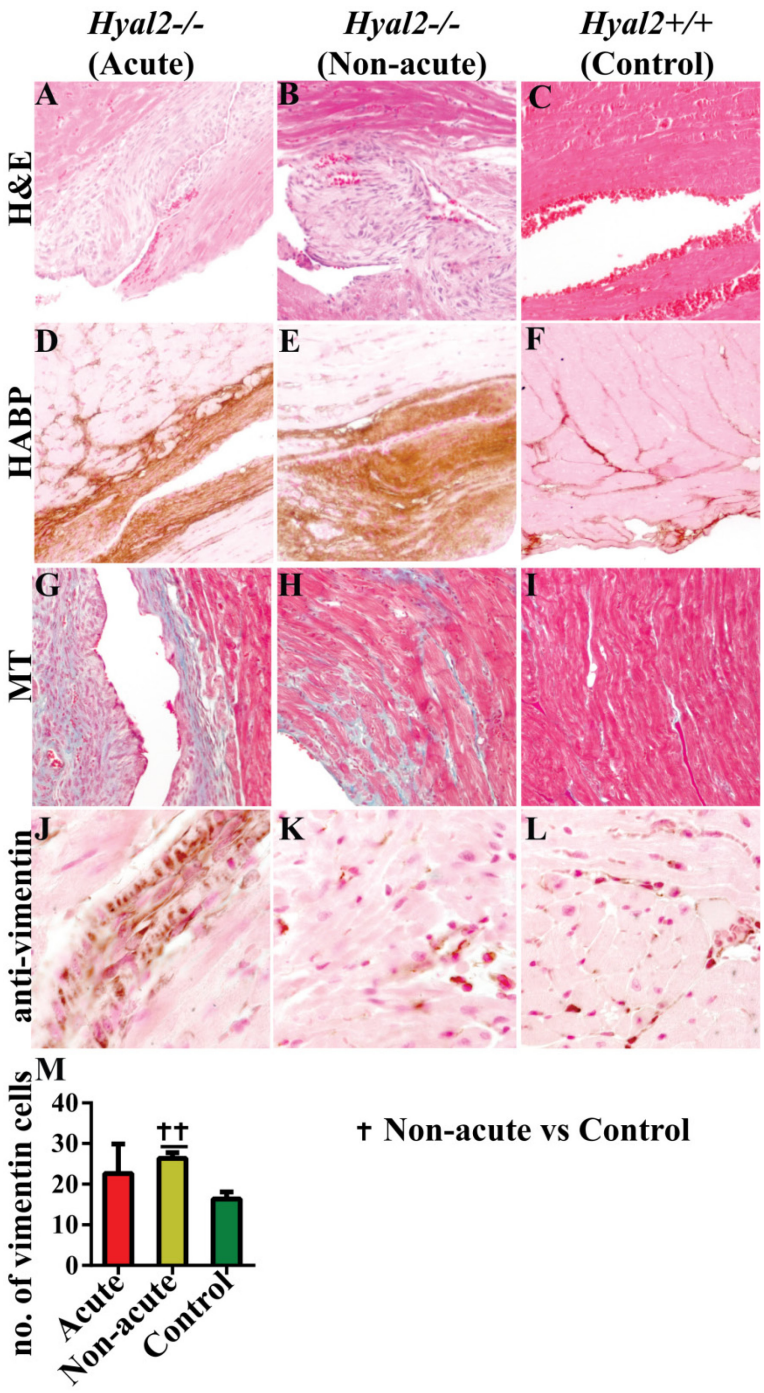

Figure 3.7. Histological analysis of the ventricle of *Hyal2* KO and control hearts.

Transverse sections of hearts from *Hyal2* KO (acute and chronic) and control mice were stained for different cellular components. (A-C) H & E staining of the heart revealed fibrous tissues in the ventricle region of the acute (A) and chronic (B) *Hyal2* KO compared to control mice (C). (D-F) Detection of HA in *Hyal2* KO and control ventricles using the HA binding protein. HA (brown) was abundant in the ventricle of the *Hyal2* KO acute and chronic groups (D-E) compared to the control (F). (G-I) Masson's trichrome staining of the ventricle of *Hyal2* KO and control mice. The atrium of *Hyal2* KO (G,H) show increased collagen (light blue) and accumulation of GAGs (white) compared to controls (I). (J-L)

Detection of mesenchymal cells in *Hyal2* KO and control heart. Vimentin was detected using anti-vimentin (ab45939) and detected as a brown colour. Increased numbers of vimentin positive (brown color) cells are evident in the *Hyal2* KO heart (J,K) compared to control (L). Scale bar = 50 μm.

3.4.6 Morphological analysis of embryonic heart in *Hyal2* KO and control mice

To determine if the structural abnormalities in the adult heart of the *Hyal2* KO mice have developmental origins, we analysed *Hyal2* KO and control hearts at E18.5, a point well after the four chambered heart had formed. H&E staining revealed an enlarged atrium (arrow in Figure 3.8 A) and the presence of fibrous tissues in the intraventricular septum, atrium and ventricle in *Hyal2* KO mice (open arrow in Figure 3.8 A, n=8) compared to controls (Figure 3.8 B, n=3). Further, detection of HA with the HABP confirmed the presence of excess HA in the *Hyal2* KO atrium compared to controls (Figure 3.8 C-D, n=3). To determine the type of cells in the fibrous tissues in the embryonic heart, we used antibodies toward vimentin. Abundant vimentin positive cells in the atria and ventricles demonstrated the presence of excess mesenchymal cells in *Hyal2* KO embryos compared to controls (Figure 3.8 E-F; n=3).

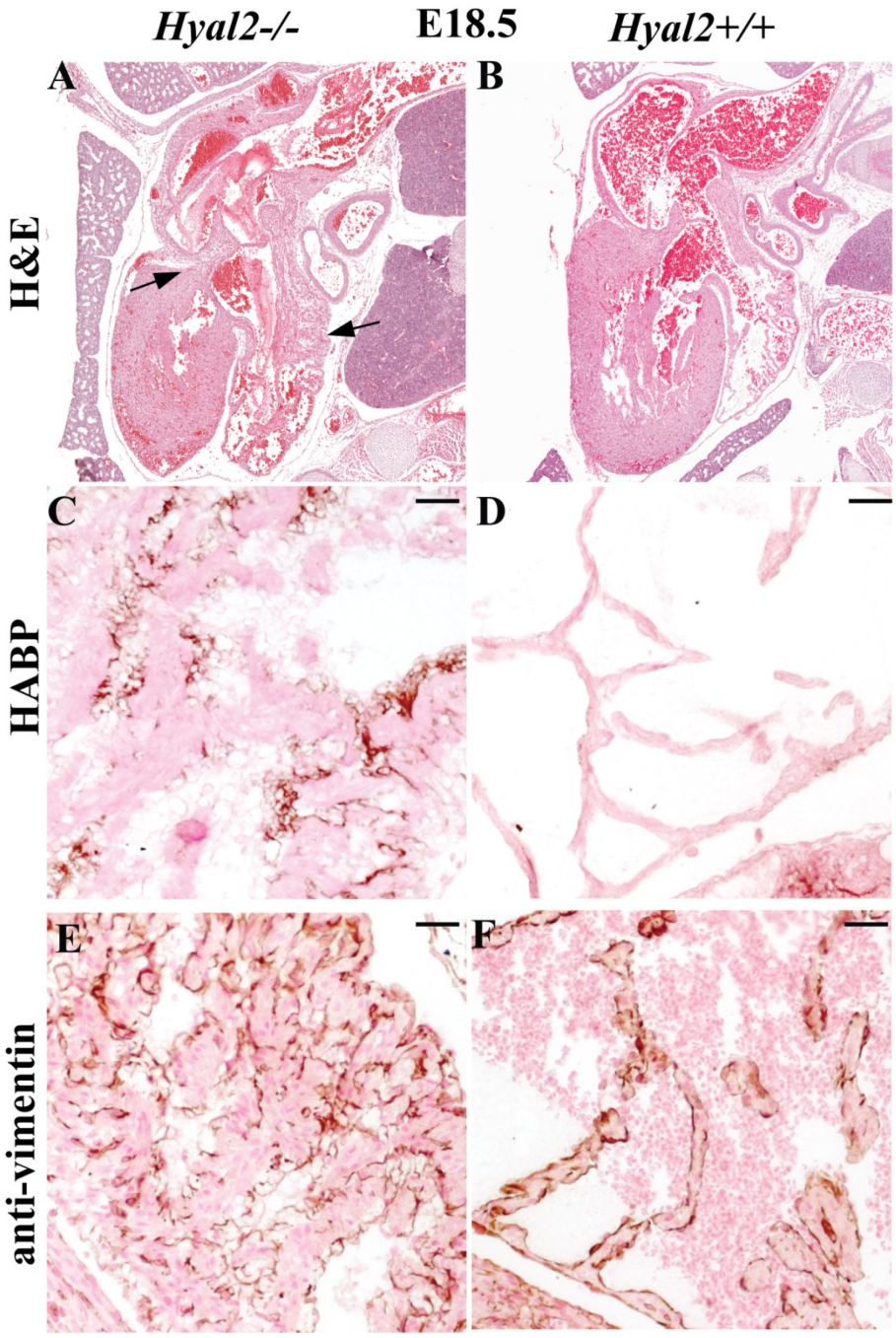

Figure 3.8. Histological analysis of *Hyal2* KO and controls hearts at E18.5.

Paraffin sections from E18.5 embryos were either stained or used for immunohistochemistry. (A-B) Images of H & E stained embryo sections revealed an enlarged atrium (left arrow) and the presence of fibrosis (open arrow) in the *Hyal2* KO heart (A) compared to the control (B) heart. (*Hyal2*$^{-/-}$, n=8; control, n=6). (C-D) Images showing HA (brown) in the atria, show increased HA in the *Hyal2* KO atrium (C) compared to the control atrium (D; n=3). (E-F) Detection of vimentin positive cells (brown) revealed an excess in the *Hyal2* KO atrium (E) compared to the control (F; n=3). Scale bar = 50 µm.

3.4.7 Abnormal EMT in *Hyal2* KO mice

Previous *ex vivo* studies of mouse cardiac explant at E9.5 showed that high molecular mass HA promoted EMT, and HA fragments inhibited EMT and activated the vascular endothelial growth factor pathway [142]. To study this *in vivo*, we first analysed the distribution of HYAL2 and HA in embryonic tissues of wild type mice at E8.5, 11.5 and 12.5. HYAL2 was detected primarily in the *bulbus cordis* (open arrow), endocardial cushion and wall of the ventricular chamber (arrow) of the developing heart (Figure 3.9 B,E,H). To verify the specificity of the HYAL2 signal, detection was performed on slides that had not been incubated with the primary antibody (Figure 3.9 A,D,G). HA was found to be most abundant in the E9.5 developing heart, and progressively decreased during development (Figure 3.9 C,F,I). These findings are consistent with HYAL2 having a role in the degradation of HA during cardiac development [142].

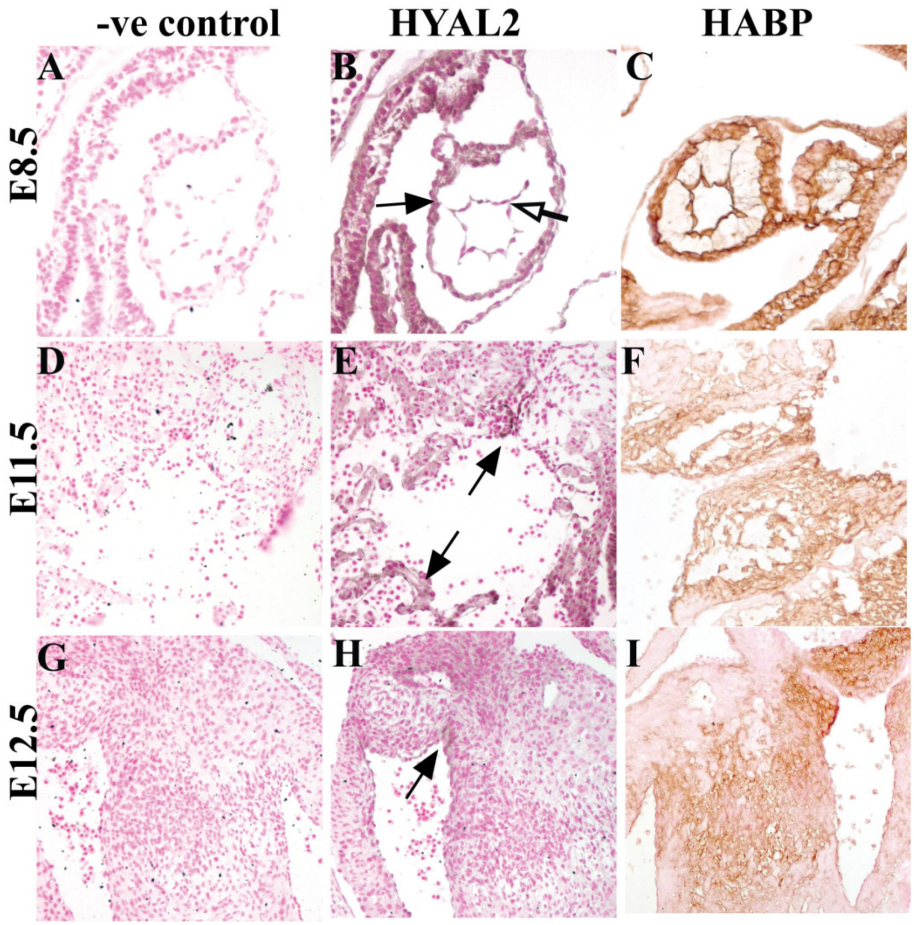

Figure 3.9. HYAL2 and HA distribution in wild type embryos.

Sections of the embryonic heart at E8.5, 11.5 and 12.5 from a previous study were used for the detection of HYAL2 and HA using histochemical approaches. (A) HYAL2 (brown) in the wall of the bulbus cordis (open arrow) and endocardial lining of the truncal region (arrow) of the E9.5 heart. (E) HYAL2 in the endocardial cushions (arrow) of the outflow tract and the trabeculated wall of the ventricular chamber of the E11.5 heart. (H) HYAL2 in the endocardial cushions and the aortic-pulmonary spiral septum at E12.5. (A,D,G) HYAL2 is not detected in sections where no primary antibody was used. (C, F, I) HABP staining in the heart shows a progressive decrease in HA with increasing embryo age.

Examination of the hearts at E14.5 showed the presence of fibrous tissues and HA in the intraventricular septum, atrium and ventricle in *Hyal2* KO mice (n=3) compared to controls (n=3) (Figure 3.10 A-D). Consistent with increased EMT in the *Hyal2* KO heart, there were increased numbers of vimentin-positive cells (Figure 3.10 C-D), and decreased levels of VEGF (Figure 3.10 G-H). Therefore, our data suggest that disruption of normal HA catabolism in the heart results in increased EMT.

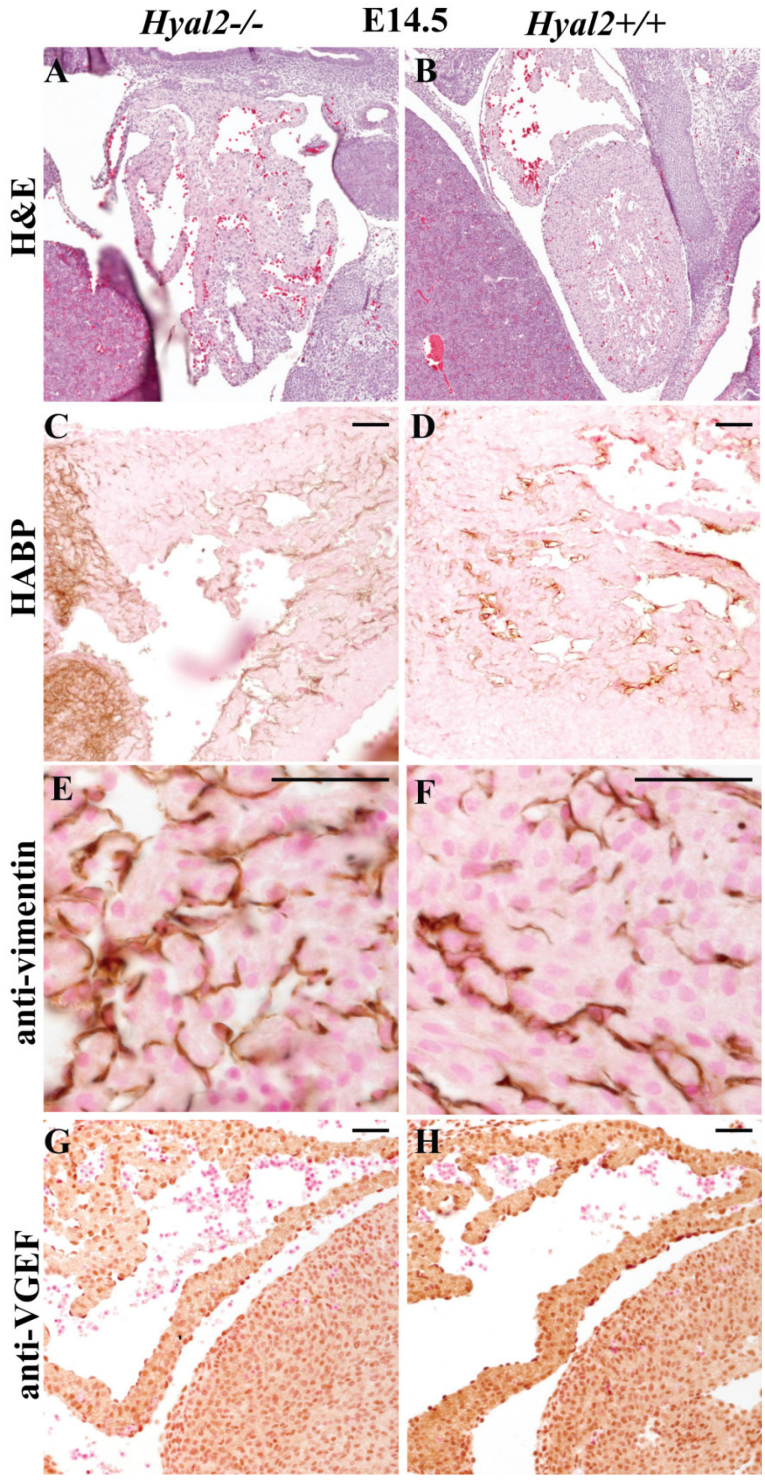

Figure 3.10. Histological analysis of *Hyal2* KO and control hearts at E14.5.

(A-B) Images of H & E stained sections show excess tissue in the ventricle in *Hyal2* KO (A) compared to control (B) hearts. (C-D) Detection of HA (brown) showed increased HA in the *Hyal2* KO ventricle (C) compared to the control (D). (E-F) Vimentin-positive cells were found to be more abundant in the *Hyal2* KO heart compared to the control (F). (G-H) VEGF (brown) appeared to be more abundant in the *Hyal2* KO (G) than in control (H) heart. n=3, Scale bar = 50 µm.

3.5 Discussion

HA is an abundant component of the provisional matrix of the developing embryo [207]. Previously, the importance of HA in the developing heart was clearly demonstrated by the early embryonic death of HAS2-deficient embryos [126]. Without HA, EMT in the cardiac cushions of *Has2*$^{-/-}$ embryos was not supported to form the heart valves and septum. A failure to degrade HA also resulted in cardiac abnormalities in *Hyal2* KO mice [199]. Herein we show that HYAL2 deficiency is associated with increased HA and mesenchymal cells, presumably due to excess EMT. These mice exhibited abnormal heart structures including cor triatriatum and atrial tumours. Fibrosis in the hearts of the *Hyal2* KO mice was associated with early diastolic dysfunction that progressed to heart failure with preserved ejection fraction.

Normal heart development appears to require a regulated level of HA. Heart defects in HYAL2-deficient mice suggest that increased HA during development poses a risk for abnormal heart development. The embryonic lethality of HAS2-deficiency indicates that HA is essential and too little HA also causes abnormal cardiac development [126]. In humans, a single case of partial HAS2-deficiency, due to a Glu to Val substitution at position 499, was associated with a ventricular septal defect [208]. Defects due to complete HAS2 deficiency are likely not to be compatible with live birth. Whether complete HYAL2 deficiency might also lead to lethality during development is unclear as a small proportion of *Hyal2* KO mice die at approximately E15.5. Although the cause of embryonic death in *Hyal2* KO mice is currently unknown, further studies are needed to determine whether cardiac abnormalities are the cause.

The cardiac defects that we have identified in *Hyal2* KO mice are uncommon. No other molecular cause of cor triatriatum or atrial tumours have to our knowledge been described. There are several other examples of excess EMT leading to valve thickening. For example in

Noonan syndrome, mutations in PTPN11 encoding the protein tyrosine phosphatase SHP2, leads to increased activation of the RAS/ERK pathway [209]. In mice deficient in EPHRIN-A1, aortic and mitral valves are thickened and there are increased numbers of mesenchymal cells, consistent with increased EMT [210]. More studies are needed to understand how HA accumulation and specifically HYAL2 deficiency impacts these pathways.

The studies herein focused on the characterization of the cardiovascular defect in *Hyal2* KO mice, although craniofacial dysmorphism, and a missing kidney, also affect a proportion of *Hyal2* KO mice [199]. An important role for HA in the development of each of these organs/tissues is suggested by these findings. Indeed, HA levels are elevated during embryonic development in each of these tissues [207]. The early lethality of HAS2-deficient embryos prevented determination of whether HA was required for the development of these organs. However, it is possible that similar to the heart, excess EMT in these other tissues leads to excess mesenchymal cells, and possibly a failure in normal differentiation, resulting in abnormal organogenesis.

A specific role for hyaluronidase in organ development was first proposed by Bernanke and Orkin, who reported that hyaluronidase activity was increased in the cardiac cushion and muscles of the developing chick [141]. A role for hyaluronidase was also suggested by *in vitro* studies by Rodgers *et al*., who showed that high molecular mass HA promoted EMT in cardiac explants whereas low molecular mass HA inhibited EMT and promoted VEGF expression [142]. Our studies provide *in vivo* evidence that HYAL2 is required for normal cardiac development. The absence of HYAL2 results in the accumulation of high molecular mass HA and excess mesenchymal (vimentin-positive) cells. Taken together, this suggests that HYAL2 is normally required to remove HA to inhibit EMT and promote differentiation.

Several studies show that left ventricular hypertrophy [211], interstitial fibrosis [212], and thickened valves [213] are the principal causes of diastolic dysfunction of the

heart.Thickening of the heart valves and walls, as well as restricted blood flow and regurgitation through the affected valves (data not shown) were present in all *Hyal2* KO mice. Together with abnormally placed valve tissues, these phenotypes are the probable cause of diastolic dysfunction. Interestingly, these mice exhibited a preserved ejection fraction, making it a model for heart failture with preserved ejection fraction [214]. In the acute group of *Hyal2* KO mice, the presence of abnormal "tumour-like" tissue in the atria also severely impacted cardiac function, leading these mice to an earlier and more severe diastolic dysfunction and eventually heart failure. In the chronic group of *Hyal2* KO mice, the increased fibrosis in the ventricles could be accentuated by compensatory changes for the ongoing diastolic dysfunction in the heart. In both cases, the eventual outcome was cardiac failure, although the 6 month end point prevented us from reaching heart failure requiring euthanasia in some chronic *Hyal2* KO mice.

In this and a previous study [199], *Hyal2* KO mice clearly fell into two groups differing in the severity of their heart phenotype. In the previous study, the acute group exhibited severe atrial dilation leading to death at ~ 3.2 months of age while the chronic (non-acute) group died at ~ 5.8 months of age [199]. In this current study, the acutely affected mice died earlier than in our previous study, and death often occurred soon after an ultrasound evaluation. Ultrasound evaluation revealed that atrial dilation, valve hypertrophy, and diastolic dysfunction were already present at 4 wks of age. Although overall cardiac function decreased until death, the structural parameters did not change significantly. The excess tissue growth found in the hearts of the acute mice is consistent with the finding of increased numbers of mesenchymal cells and extracellular matrix that results in the rapid onset of diastolic dysfunction. Several studies have shown that the increased IVRT and atrial size [215] are an indicator of left ventricular diastolic dysfunction, independent of atrial pressure [216], heart failure [217] or heart rate [218] and in the presence of preserved systolic

function. The basis for the differences in the severity of the phenotype in acute and chronic groups of *Hyal2* KO mice is probably due to a genetic determinant segregating in the outbred background. Modifying genes that influence the severity of a cardiac phenotype are extremely common [219] and future studies are required to determine the modifying genes that are involved in the acute and chronic phenotypes of the *Hyal2* KO mice.

The impact of interstitial fibrosis on cardiac function is seen in other disorders of extracellular matrix molecules. Normally, the ECM provides support for the contractile forces produced by the cardiac myocytes, and disruption of ECM homeostasis can result in impaired force transmission causing dilation or hypertrophy. For example, in the ADAMTS 9 and 5 KO mice, accumulation of versican in the heart disrupts the ECM homeostasis and cause cardiac disease pathology [179,220]. In addition, accumulation of glycosaminoglycans in the heart valves resulted in valve thickening. This thickened valve changed the atrial and ventricular volume overload and contributed to atrial dilation, ventricular hypertrophy and ultimately diastolic dysfunction in many MPS [170].

These studies of the cardiac phenotype in *Hyal2* KO mice clearly demonstrate an important role for HYAL2 and HA degradation in heart development. The presence of increased numbers of mesenchymal cells, and decreased VEGF expression in *Hyal2* KO embryos strongly suggests that HYAL2 is needed to inhibit EMT and that in its absence excess EMT leads to congenital malformations. Further studies are needed to clearly demonstrate the impact of HYAL2 deficiency on EMT and to determine whether it is the presence of excess high molecular mass HA or the absence of low molecular mass HA that results in the phenotypic changes.

Chapter 4: Hyaluronidase 2 (HYAL2) is expressed in endothelial cells, as well as some specialized epithelial cells, and is required for normal hyaluronan catabolism

Biswajit Chowdhury, Richard Hemming, Sana Faiyaz, and Barbara Triggs-Raine

Acknowledgements: Western blot analysis and a portion of HYAL2 localization studies were performed by Richard Hemming. Barbara Triggs-Raine generated the proposed model of HYAL2 function in HA catabolism

This work has been accepted as: **Chowdhury, B.**, Hemming, R., Faiyaz, S., and Triggs-Raine, B. (2015) Hyaluronidase 2 (HYAL2) is expressed in endothelial cells, as well as some specialized epithelial cells, and is required for normal hyaluronan catabolism. Journal of Histochemistry and Cell Biology 2015

4.1 Abstract

Hyaluronidase 2 (HYAL2) is a membrane-anchored protein that is proposed to initiate the degradation of hyaluronan (HA) in the extracellular matrix. The distribution of HYAL2 in tissues, and of HA in tissues lacking HYAL2, is largely unexplored despite the importance of HA metabolism in several disease processes. Herein we use immunoblot and histochemical analyses to detect HYAL2 and HA in mouse tissues, as well as agarose gel electrophoresis to examine the size of HA. HYAL2 was detected in all tissues that were examined, including the brain. It was localized to the surface and cytoplasm of endothelial cells, as well as specialized epithelial cells in several tissues, including the skin. Accumulated HA, often of higher molecular mass than that in control tissues, was detected in tissues from *Hyal2* KO mice. The accumulating HA was located near to where HYAL2 is normally found, although in some tissues, it was distant from the site of HYAL2 localization. Overall, HYAL2 was highest in tissues that remove HA from the circulation (liver, lymph node and spleen), but the levels of HA accumulation in *Hyal2* KO mice were highest in tissues that catabolize locally synthesized HA. Our results support HYAL2's role as an extracellular enzyme that initiates HA breakdown in somatic tissues. However, our findings also suggest that HYAL2 contributes to HA degradation through other routes, perhaps as a soluble or secreted form.

4.2 Introduction

Hyaluronan (HA) is a non-sulfated GAG that is present in the ECM of most vertebrate tissues, and particularly abundant in loose connective tissues such as the skin and synovial fluid [19,221,222]. HA levels are increased during proliferative processes, including development, wound healing and metastasis [121,223]. The size of HA is thought to be important in regulating these processes; for example during development, high molecular mass (HMM) HA (>1000 kDa) promotes EMT whereas low molecular mass (LMM) HA (~3-100 kDa) inhibits EMT and promotes differentiation [142]. Hyaluronidases are considered to be key regulators of HA size and abundance. In humans, six HYAL-related genes have been identified; they form two tightly linked triplets on human chromosomes 3p21.3 (*HYAL1*, *HYAL2*, *HYAL3*) and 7q31.3 (*HYALP1*, *HYAL4*, *PH20*) [43]. Of these, only *HYAL1* and *HYAL2* are broadly expressed in somatic tissues [41] and encode products with demonstrated HA-degrading activity [45,58]. With the exception of a single study where HYAL2 was localized to lung epithelium [61], the distribution of the HYAL2 protein has not been examined in tissues.

A model of HA catabolism has been proposed in which HYAL2 initiates the extracellular degradation of HMM-HA into smaller fragments which are endocytosed and degraded in lysosomes by HYAL1 and exoglycosidases [43]. Consistent with HYAL1's role in this model, its deficiency causes a lysosomal storage disorder called MPS IX, which is characterized by lysosomal HA storage and joint abnormalities [46,52]. The proposed model is further supported by the identification of HYAL2 as a membrane-localized glycosylphosphatidylinositol (GPI)-linked protein [59] with weak activity toward HMM-HA [58]. The accumulation of extracellular HMM-HA in the heart, lungs and serum of *Hyal2* KO mice also provided *in vivo* evidence for HYAL2's proposed role in the initiation of HA degradation [63,199].

HA has a high rate of constitutive turnover, with ~1/3 of the 15 g of HA estimated to be present in a 70 kg person turned over daily [224]. Approximately 30% of HA is degraded "locally", in the tissue where it was synthesized [19]. The remaining HA enters the circulation, where 50 to 90% is removed by the lymphatic system, and the residual approximately10% of HA enters the blood and is removed primarily by the liver and spleen [35,36]. The rate of HA degradation is tissue dependent; for example, turnover is slow in avascular tissues such as heart valves and cartilage [225] whereas turnover is rapid in the skin [226]. Uptake is receptor dependent, and may involve several cell surface receptor proteins including CD44, LYVE-1, and HARE which bind with HA and promote endocytosis [114,227,228]. Interestingly, only *Hare* KO mice have elevated levels of serum HA [229], indicating HARE played a key role in the uptake of circulating HA. Elevated HA in the valves, lungs, and serum of *Hyal2* KO mice [199] suggested a role for HYAL2 in the turnover of both locally synthesized and circulating HA.

We have examined the distribution and localization of HYAL2 in a broad range of mouse tissues involved in both local and circulating HA degradation. HYAL2 was detected in all tissues examined, including the brain. It was primarily localized to the surface and cytoplasm of endothelial cells as well as specialized epithelial cells in some tissues. In the absence of HYAL2, accumulating HMM-HA was clearly evident in all mouse tissues, although the extent of accumulation varied.

4.3 Materials and Methods

4.3.1 Experimental animals

Mice with a *Hyal2* null allele were generated in a previous study by removing exons 2-4 of *Hyal2* [63]. For this study, $Hyal2^{+/-}$ mice on an outbred (C129/Ola;CD1;C57BL6) background [199] were intercrossed to generate *Hyal2* KO and control ($Hyal2^{+/+}$ or $Hyal2^{+/-}$) mice. Mouse genotypes were determined by PCR amplification as described previously [199]. Mice were euthanized by isoflurane inhalation and immediately dissected. A wide range of tissues (lymph node, liver, spleen, femur, kidney, heart, lung, muscle, skin, brain, small intestine, ovary, and testes) from *Hyal2* KO, as well as age and sex matched control mice, were collected. Mouse embryonic fibroblasts (MEFs) were generated from $Hyal2^{+/+}$ and *Hyal2* KO embryos collected from timed-pregnant female mice following previously described methods [54]. All animal procedures were conducted in compliance with the Canadian Council on Animal Care guidelines and approved by University of Manitoba Animal Care Committee.

Tissues were fixed overnight in 10% buffered formalin containing 1% hexadecylpyridinium chloride (CPC), or immediately frozen at -80^{o}C. Fixed tissues were decalcified for 7 days in Immunocal (Decal Chemical Corp) where appropriate, and embedded in paraffin. Sections (5 μm) were prepared for histological analysis.

4.3.2 Immunodetection of HYAL2

HYAL2 was detected by immunoblot analysis as described previously [54]. Mouse tissue or cell extracts were prepared by brief sonication in PBS containing protease inhibitors (Sigma) and 30 μg of protein lysate was separated by sodium dodecyl sulfate–polyacrylamide gel electrophoresis (SDS-PAGE) on 7.5% gels. HYAL2 was detected by overnight

incubation at 4°C with an anti-HYAL2 (rabbit polyclonal ab60608 (Abcam) 1/1,000) antibody. Immune complexes were detected with horseradish peroxidase (HRP)-conjugated secondary antibody (donkey anti-rabbit (Jackson Labs); 1/15,000), followed by incubation with a chemiluminescent substrate for HRP (Millipore).

4.3.3 Immunohistochemistry and immunofluorescence

Tissue sections were deparaffinized in xylene and rehydrated with graded alcohols. Antigen retrieval was performed by incubation in 10 mM sodium citrate pH 6 for 20 min at 95°C. Sections were treated for 10 min with 3% hydrogen peroxide, followed by 1 h blocking with 3% bovine serum albumin in TBST. Endogenous biotin in tissues was blocked with an Avidin-Biotin blocking kit as recommended by the manufacturer (Vector Labs). Sections were then incubated overnight with anti-HYAL2 (1:200) or anti-CD31 (1: 50; AbD Serotec) antibody. Primary complexes were detected with biotinylated goat anti-rabbit (1:500; Vector laboratories) or goat anti-rat (1:1000; Invitrogen) antibodies. After a 1 h incubation using an ABC kit (Vector laboratories) to amplify the signal, complexes were detected using either DAB or NovaRed peroxidase (Vector Laboratories) substrates. Counterstaining was for 2.5 min with either hematoxylin or Nuclear Fast Red (ScyTek Laboratories). For immunofluorescence, primary complexes were detected using a Cy3-conjugated anti-rabbit secondary antibody. Slides were dehydrated, mounted and visualised using bright field or fluorescence microscopy.

HA was detected in tissue sections using HA binding protein (HABP) staining as described previously [199]. To monitor the specificity of the HABP, sections were treated overnight in sodium acetate (pH 6.0) containing 500 U/ml of hyaluronidase from *Streptomyces hyalurolyticus* (Sigma).

4.3.4 Analysis of HA size and abundance

Total GAGs were isolated from equal dry weights of *Hyal2*$^{+/+}$ or *Hyal2* KO frozen tissues by digestion with proteinase K, followed by treatment with DNase 1 and RNase A as previously described [199]. The samples were extracted with 3 volumes of acetone and stored at -20^{o}C for 2 h. Precipitates were collected by centrifugation, resuspended in water, and reprecipitated with 3 volumes of 100% ethanol at -20^{o}C. The pellet was again collected by centrifugation, resuspended in water and precipitated with 2% CPC (1:1 volume). For sizing, GAGs were then precipitated with ethanol and the pellet was dissolved in 15 µl of water. Samples were separated on 0.8% agarose gels, and stained with 0.005% stains-all overnight at room temperature. Gels were de-stained with 10% ethanol and visualized using the Chemidoc^{TM} imaging system (Bio-Rad). The size of the HA was determined using the 1 Kb DNA ladder (Invitrogen) as a molecular mass marker. For quantification, the GAGs were analyzed by FACE as described previously [95,199].

4.4 Results

4.4.1 HYAL2 expression in mouse tissues

As a first step in examining the distribution of the HYAL2 protein in a broad range of adult mouse tissues, we performed immunoblot analysis. Protein lysates were analysed from tissues that contain abundant HA in the extracellular matrix (brain, heart, kidney, lung muscle, testes, ovary and skin) as well as the lymph nodes, liver and spleen which were known from previous studies to be involved in the uptake and degradation of circulating HA [35,36]. To verify the specificity of the detected bands, the signals obtained from wild type (*Hyal2*$^{+/+}$) tissues were compared to those obtained from mice lacking HYAL2 (*Hyal2* KO). A signal at ~57 kDa, similar to the 60 kDa previously observed in mouse tissues [58], was detected in all *Hyal2*$^{+/+}$ tissues, and absent in the *Hyal2* KO tissues (Figure 4.1 A, B). This size is larger than the 53.6 kDa predicted from its amino acid sequence (NP_034619.2 calculated using http://web.expasy.org/compute_pi/), presumably due to glycosylation. Additional bands detected in some tissues were unrelated to HYAL2 as they were present in both *Hyal2* KO and *Hyal2*$^{+/+}$ tissues. These results demonstrated that HYAL2 is ubiquitously expressed in adult mouse tissues, with the lowest levels found in the brain and muscle (Figure 4.1 A) and the highest levels found in tissues responsible for circulating HA catabolism (Figure 4.1 B).

The levels of HYAL2 in embryonic development were analyzed in MEFs derived from *Hyal2*$^{+/+}$ and *Hyal2* KO embryos. Abundant HYAL2 was detected in *Hyal2*$^{+/+}$ but not *Hyal2* KO fibroblasts (Figure 4.1 C).

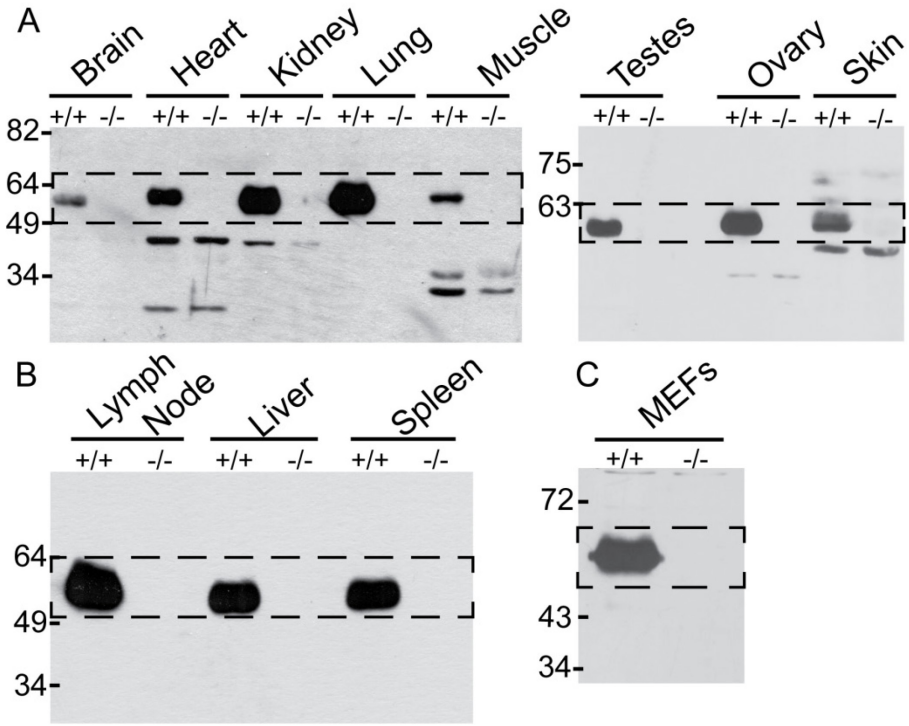

Figure 4.1. Immunoblot analysis of HYAL2 in mouse tissues.

Cell lysates (30 µg protein) prepared from *Hyal2*$^{+/+}$ and *Hyal2* KO tissues or MEFs were separated by SDS-PAGE, transferred to nitrocellulose and detected with ani-HYAL2. (A) Tissues involved in local HA degradation, (B) Tissues involved in circulating HA degradation, and (C) MEFs. Boxes surround HYAL2 which is absent in *Hyal2* KO tissues. Cross-reacting bands are identified by their presence in both *Hyal2* KO and *Hyal2*$^{+/+}$ tissues. Molecular mass markers are shown to the left of the gels in kDa.

4.4.2 Distribution of HYAL2 in mouse tissues

To investigate how HYAL2 was distributed within mouse tissues and organs, we performed immunohistochemistry on many of the tissues demonstrated by immunoblot to express HYAL2, as well as bone marrow and small intestine. Bone marrow has previously been shown to be involved in circulating HA catabolism [35], and small intestine was included because of the high level of endogenous HA in this tissue [230]. As in the immunoblots, tissues from *Hyal2* KO mice served as a negative control to identify any signals that were not HYAL2-related. Overall, the HYAL2 protein was detected in either endothelium or specialised cuboidal epithelium (Table 4.1).

Table 4.1. Tissue distribution of mouse HYAL2 in the wild type tissues

Tissue	Distribution pattern
Liver	Strong signal in hepatic sinusoidal endothelial cells
Spleen	Red pulp and marginal sinus endothelium, no signal found in white pulp sinus
Lymph node	lymphatic vessels endothelium and sinusoidal endothelium of cortical, medullary and subcapsular sinus
Bone marrow	Endothelial cells of bone marrow sinusoids
Heart	Endothelial cells of heart valves, blood vessels and endocardium
Lung	Endothelial cells of blood vessels, epithelial cells of the alveoli
Kidney	Single layer of epithelial cells in renal tubules, absent in cortex and renal papilla
Muscle	Endothelial cells of blood vessels
Small intestine	Endothelial cells of blood vessels and epithelial cells of the intestinal crypt
Skin	Epithelial cells of the sebaceous gland and endothelial of blood vessels in connective tissue
Brain	Ependymal/epithelial cells of the choroid plexus

Oviduct	Endothelium of blood vessels in muscularis and ciliated epithelial cells of the oviduct

HYAL2 distribution in tissues involved in circulating HA degradation

HYAL2 was found to be highly expressed in the major organs involved in circulating HA degradation, the lymph node, spleen, and liver (Figure 4.2 A-F), and weakly expressed in the bone marrow (Figure 4.2 G, H). In the lymph node and spleen, HYAL2 was found in endothelial cells lining the sinuses of the cortical, subcapsular and medullary sinuses of the lymph node (Figure 4.2 B), and the sinusoidal endothelium of the red pulp and marginal sinus of the spleen (Figure 4.2 D). No signal was detected in the white pulp of the spleen (not shown). In the liver, HYAL2 was strongly expressed in endothelial cells lining the hepatic sinus and blood vessels (Figure 4.2 F). HYAL2 was also detected in the endothelial cells of bone marrow sinusoids (Figure 4.2 H). HYAL2 was not detected in equivalent regions of the various tissues from *Hyal2* KO mice (Figure 4.2 A, C, E, G), demonstrating the specificity of the antibody for HYAL2. Consistent with HYAL2 being primarily localized to endothelial cells in these tissues, a similar pattern was detected using the endothelial cell marker CD31 (Figure 4.2 I-L).

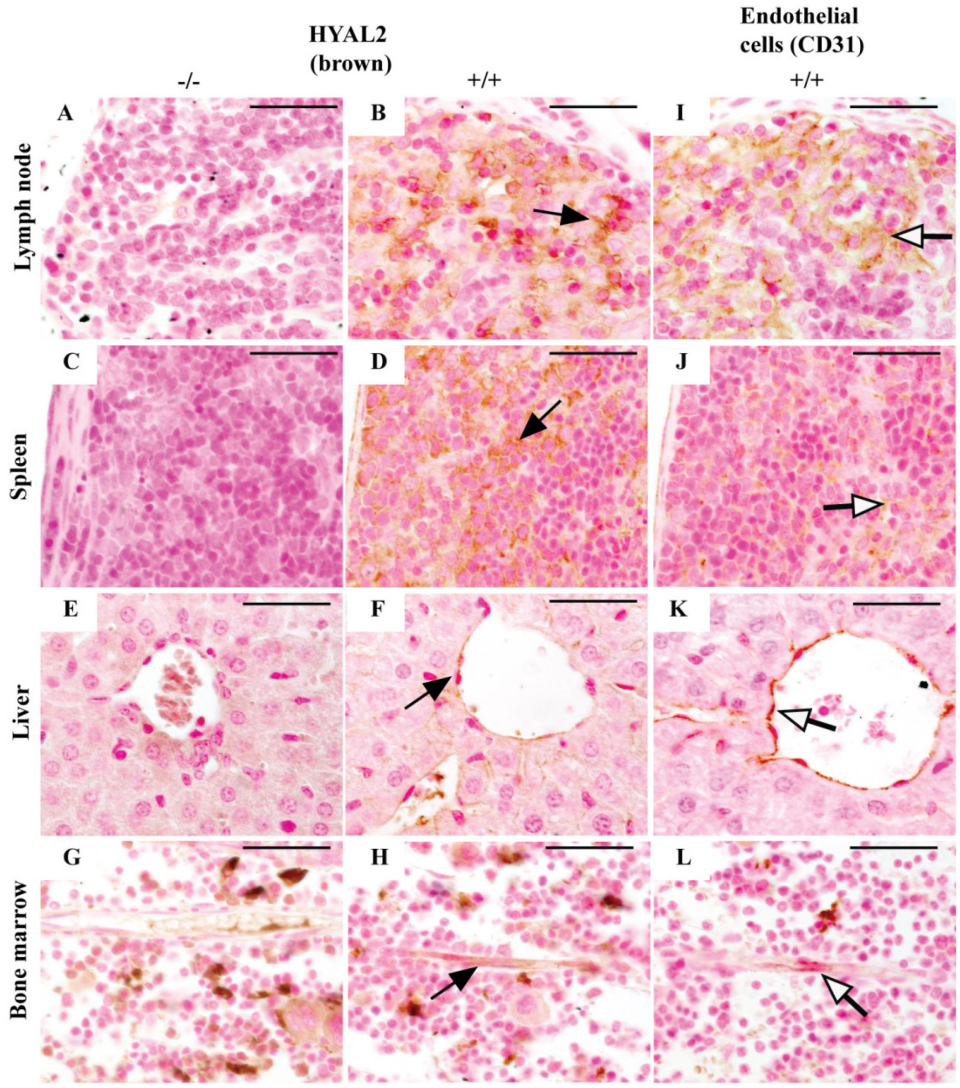

Figure 4.2. HYAL2 distribution in organs involved in circulating HA degradation.

HYAL2 and CD31 were detected in paraffin sections of tissues from *Hyal2*$^{+/+}$ mice using anti-HYAL2 or anti-CD31, respectively, followed be a biotinylated secondary antibody. The complexes were detected with DAB, resulting in positive signals that are brown. Positive staining in the sinusoidal endothelial cells is indicated by arrows in panels B, D, F, and H. As expected, no signal was detected in the *Hyal2* KO tissues in panels A, C, E, G. CD31 was used as a marker of endothelial cells (open head arrows in I, J, K and L) to verify its similar distribution to HYAL2. These sections are representative images chosen from the analysis of tissues from three (lymph node, liver, bone marrow) or four (spleen) pairs of mice. Scale bars represent 50 µm.

HYAL2 distribution in tissues involved in local HA degradation

The distribution of HYAL2 was examined in organs and tissues with abundant endogenous HA including heart, lung, kidney, muscle, skin, brain, small intestine, and ovary/oviduct (Figure 4.3). HYAL2 was localized to endothelium lining the blood vessels in all of these tissues (Figure 4.3**)** as well as to the endothelium lining the heart valves (Figure 4.3 B). HYAL2 was also detected in epithelial cells lining the alveoli of the lungs (Figure 4.3 D), cuboidal epithelial cells of the renal collecting tubules (Figure 4.3 F), the surface of secretory epithelial cells of the sebaceous glands of the skin and surrounding secretory vesicles within the cytoplasm of these cells (Figure 4.3 J). In the brain, HYAL2 was detected on the outer surface, and in the cytoplasm of ciliated cuboidal epithelial cells making up the choroid plexus (Figure 4.3 L). HYAL2 was detected on the surface and surrounding secretory vesicles in the cytoplasm of epithelial cells of the intestinal crypt (Figure 4.3 N), and in the ciliated epithelium of the oviduct (Figure 4.3 P). The specificity of our detection for HYAL2 was verified by comparing the signals to that obtained in equivalent regions of tissues collected from *Hyal2* KO mice that had been treated in the same way (Figure 4.4). Our results show that HYAL2 is expressed in both endothelial and specialized epithelial cells from a broad range of tissues.

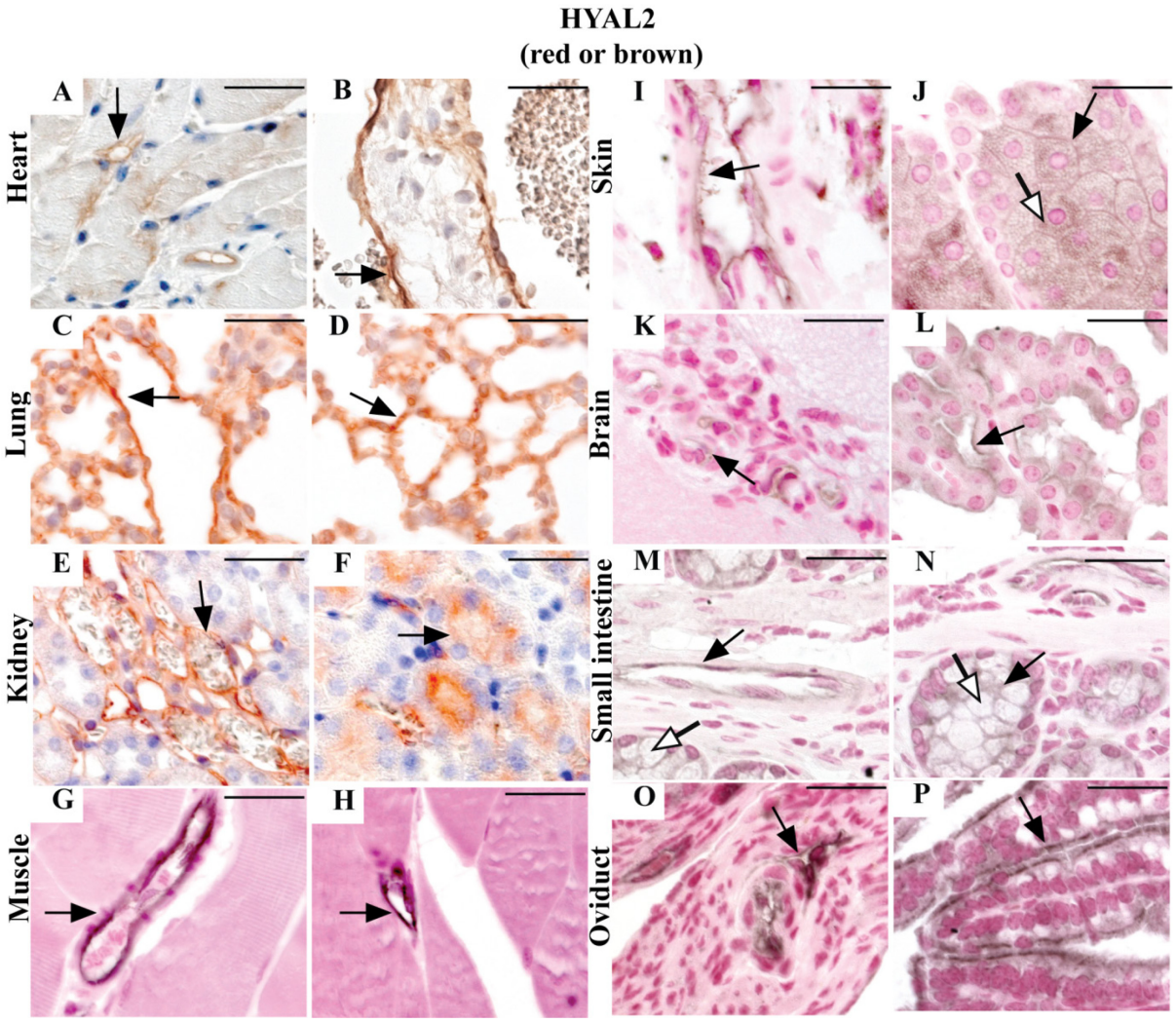

Figure 4.3. HYAL2 distribution in organs/tissues involved in local HA degradation.

HYAL2 was detected in paraffin sections of tissues from *Hyal2*$^{+/+}$ mice as described in Figure 2. Tissue sections from *Hyal2* KO mice that have been treated similarly are shown in Figure 5.4**.** Arrows indicate positive staining for HYAL2 in the endothelial cells of blood vessels of the heart (A), lung (C), kidney (E) and muscle (G, H), skin (I), brain (K), small intestine (M) and oviduct (O). Arrows also indicate positive staining for HYAL2 in the endothelial cells of heart valves (B), epithelial cells lining alveoli in the lungs (D), cuboidal epithelia lining the collecting ducts of the kidney (F), secretory epithelia of sebaceous glands of the skin (J), ependymal cells of the brain (L), epithelial cells of the intestinal crypt (N), and ciliated epithelial cells of the oviduct (P). Open arrows indicate the cuboidal epithelium that contains vesicles surrounded by HYAL2. These images are representative of those from 3-5 pairs of *Hyal2* KO and *Hyal2*$^{+/+}$ mice for each tissue. Scale bars represent 50 µm.

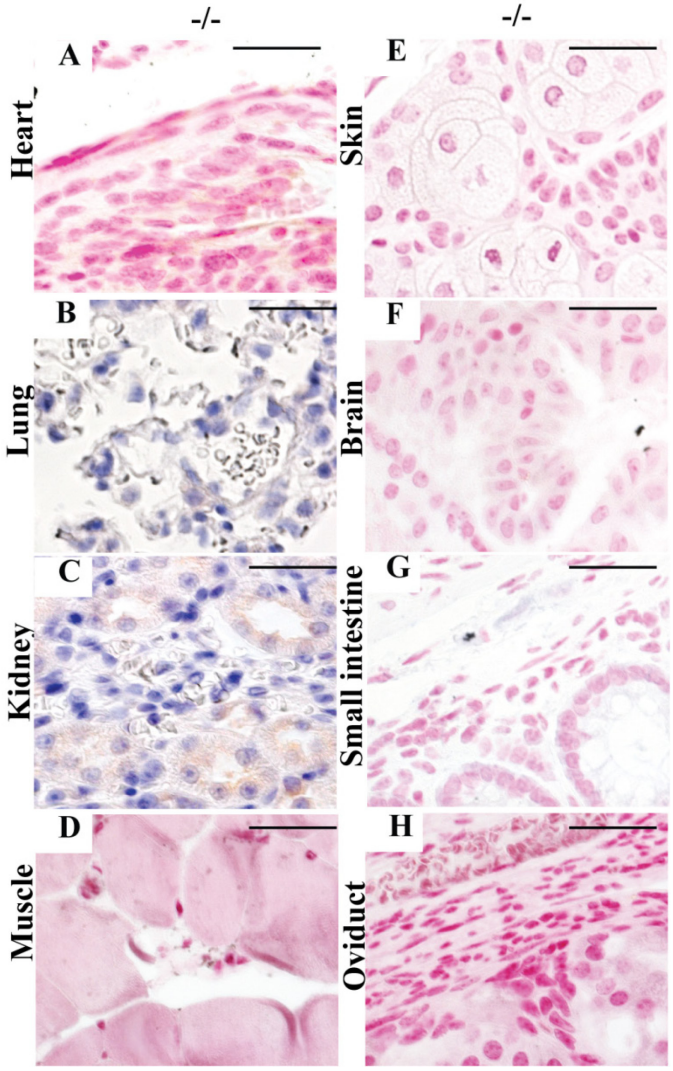

Figure 4.4. Absence of HYAL2 in the Hyal2 KO organs/tissues.

Paraffin sections of heart (A), lung (B), kidney (C), muscle (D), skin (E), brain (F), small intestine (G) and oviduct (H) were treated as wild type tissues using anti-HYAL2. As expected, no signal is detected in the *Hyal2 KO* organ/tissues indicating the antibody is specific for HYAL2.

In the cells of most tissues, HYAL2 appeared to be localized to both the cell surface and cytoplasm as illustrated in this fluorescent image of HYAL2 in lung epithelia and endothelium (Figure 4.5), spleen and lymph node endothelium (Figure 4.6).

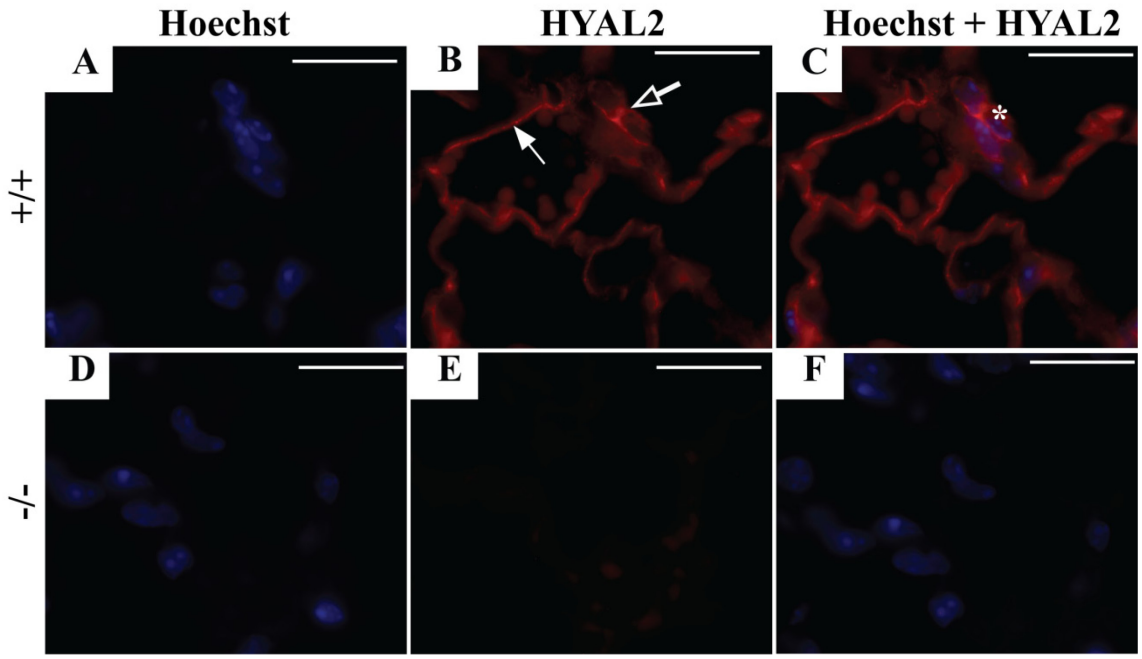

Figure 4.5. Subcellular localization of HYAL2 in the lung.

HYAL2 was detected in paraffin sections from *Hyal2*$^{+/+}$ and *Hyal2* KO mice using anti-HYAL2 followed by a Cy3-conjugated anti-rabbit antibody (Sigma). HYAL2 was detected in both the cytoplasm, and on the surface of endothelial cells (arrow) and on the surface (open-headed arrow) and in the cytoplasm (asterisk) of epithelial cells of the blood vessels in the lungs. Note the presence of red blood cells in the lumen of the vessel which clearly identifies it as a blood vessel. Scale bars represent 50 μm.

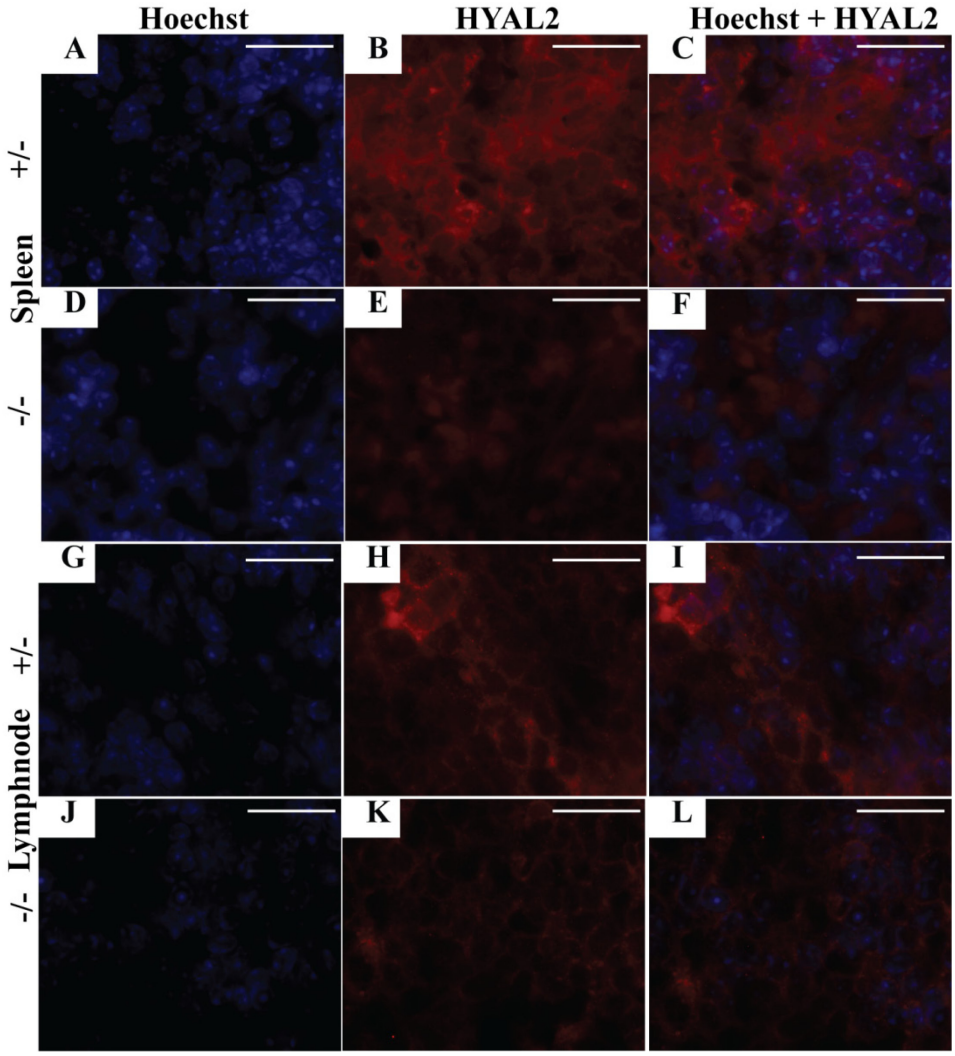

Figure 4.6. Subcellular localization of HYAL2 in the spleen and lymphnode.

HYAL2 was detected in paraffin sections from *Hyal2*$^{+/-}$ and *Hyal2* KO mice using anti-HYAL2 followed by a Cy3-conjugated anti-rabbit antibody (Sigma). HYAL2 was detected on the surface of endothelial cells of spleen and lymphnode (red). As expected no signal was detected in the KO tissues. Scale bars represent 50 μm.

4.4.3 Distribution of HA in *Hyal2*$^{+/+}$ and *Hyal2* KO tissues

In order to determine how the absence of HYAL2 impacted the levels and distribution of HA in mouse tissues, we detected HA using the HABP. In general, more HA was detected in *Hyal2* KO tissues than in controls (Figures 4.7- 4.8), although the level of HA accumulation was found to be tissue-specific. To confirm the specificity of the HABP for HA detection, the level of HA was always compared to slides from similar regions that had been pre-treated with *Streptomyces hyalurolyticas*, which would be expected to degrade most of the HA in tissues (Figure 4.9).

Accumulation of HA in Hyal2 KO tissues involved in circulating HA degradation

HA was detected around the sinusoidal cells of the lymph node, liver and spleen, where HYAL2 is normally expressed (Figure 4.7 A-F). The level of HA was clearly more abundant in the lymph node of the *Hyal2* KO mice, where it accumulated in the cortical and subcellular sinus (Figure 4.7 A, B). No HA was detected in the medulla of *Hyal2* KO or *Hyal2*$^{+/+}$ lymph nodes (not shown). In the spleen, HA was found in medullary sinus of *Hyal2* KO mice, but not controls (Figure 4.7 C, D). A very small increase in HA was detected around the sinusoidal endothelial cells of *Hyal2* KO liver compared to controls (Figure 4.7 E, F). It is worthy to note that HA was not detected in the bone marrow of either *Hyal2* KO or control mice (Figure 4.7 G, H).

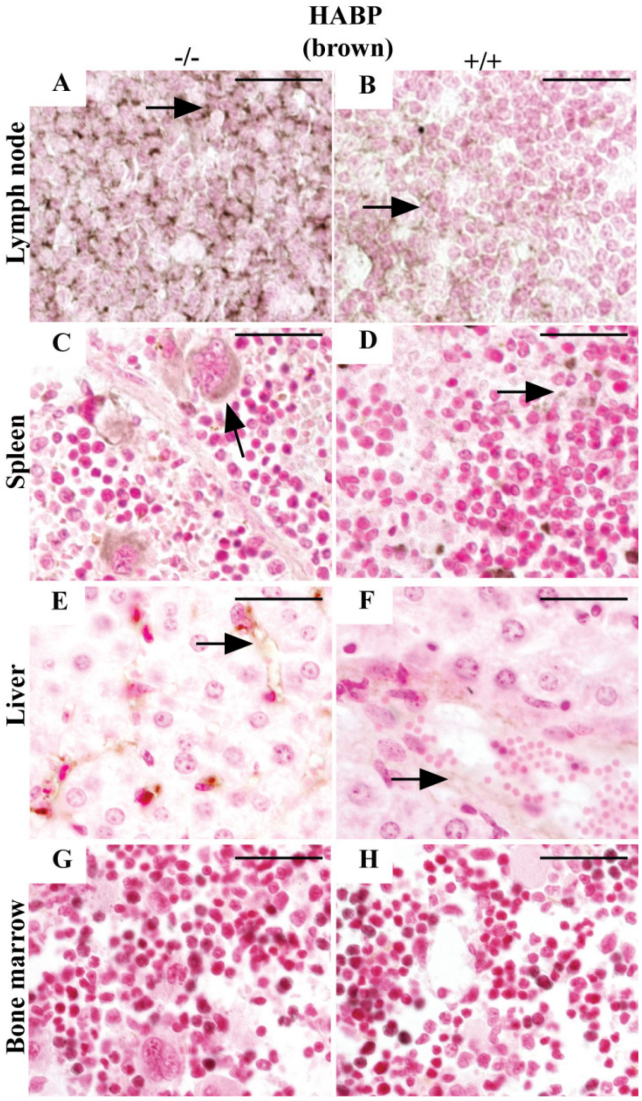

Figure 4.7. Detection of HA in tissues responsible for circulating HA degradation.

HA was detected in paraffin sections of *Hyal2*$^{+/+}$ and *Hyal2* KO mice using a biotin-conjugated form of the HABP. Detection of the signal was with the HRP substrate, DAB, resulting in a brown staining. An increase in HA staining was detected in the sinusoids of the lymph node (A), spleen (C) and liver (E) of *Hyal2* KO mice compared to controls (B, D, F). No HA was detected in the bone marrow (G, H). These images are representative of those from 3-4 pairs of *Hyal2*$^{+/+}$ and *Hyal2* KO mice. Scale bars represent 50 µm.

Accumulation of HA in Hyal2 KO *tissues with abundant endogenous HA*

Extracellular accumulation of HA was clearly evident in *Hyal2* KO tissues that are involved in local HA degradation (Figure 4.8). HA was abundant in the normal heart valves of *Hyal2*$^{+/+}$ mice (Figure 4.8 B), as well as throughout the grossly expanded valves of *Hyal2* KO mice (Figure 4.8 A). The level of HA detected in the alveolar sacs of the lungs was also much higher in *Hyal2* KO than *Hyal2*$^{+/+}$ mice (Figure 4.8 C, D). In the kidney, increased HA was detected only in the renal medulla of *Hyal2* KO mice, and was localized to the interstitium (Figure 4.8 E, F). There was only a small increase in the level of HA in the interstitial space of *Hyal2* KO muscle cells compared to controls (Figure 4.8 G, H). HA levels were clearly elevated in the connective tissue of skin, brain, small intestine, and oviduct (Figure 4.8 I, K, M, O) of *Hyal2* KO mice compared to controls. Although HA was accumulating to a greater extent in *Hyal2* KO tissues involved in local HA degradation than that those involved in circulating HA degradation, the accumulating HA was not restricted to the location of HYAL2. In skin HYAL2 was most abundant in the sebaceous glands of the skin, yet no HA accumulated in the sebaceous glands but did accumulate in the connective tissue outside of the gland. In the heart valve, HYAL2 is expressed on the endothelial surface, but HA accumulated throughout the valve. Similarly, in the brain, HA accumulation was evident throughout the brain although HYAL2 was only detected in the choroid plexus and blood vessels.

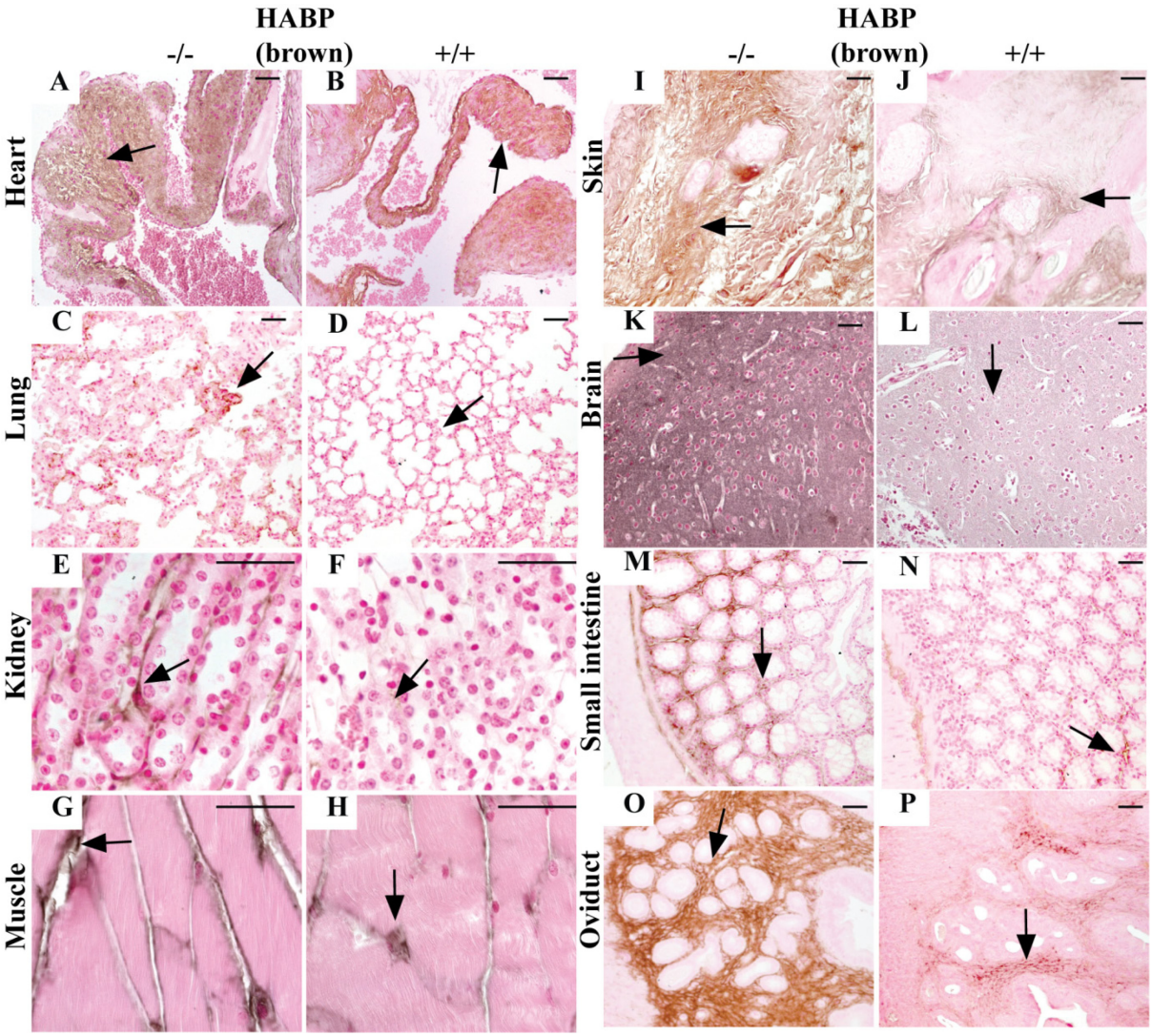

Figure 4.8. Detection of HA in tissues involved in local HA degradation.

HA (brown) was detected in paraffin sections of *Hyal2*$^{+/+}$ and *Hyal2* KO mice as described in Figure 5. HA was abundant in *Hyal2* KO (A) and *Hyal2*$^{+/+}$ (B) heart valves, although the heart valves of the *Hyal2* KO mice were clearly thickened. The intensity of the HA staining in *Hyal2* KO mice was also increased in the alveolar sacs (C), renal medulla (E) and connective tissue of the muscle (G) skin (I), brain (K), small intestine (M), and oviduct (O) compared to controls (D, F, H, J, L, N, P). These images are representative of those from 3-5 pairs of *Hyal2*$^{+/+}$ and *Hyal2* KO mice. Scale bars represent 50 μm.

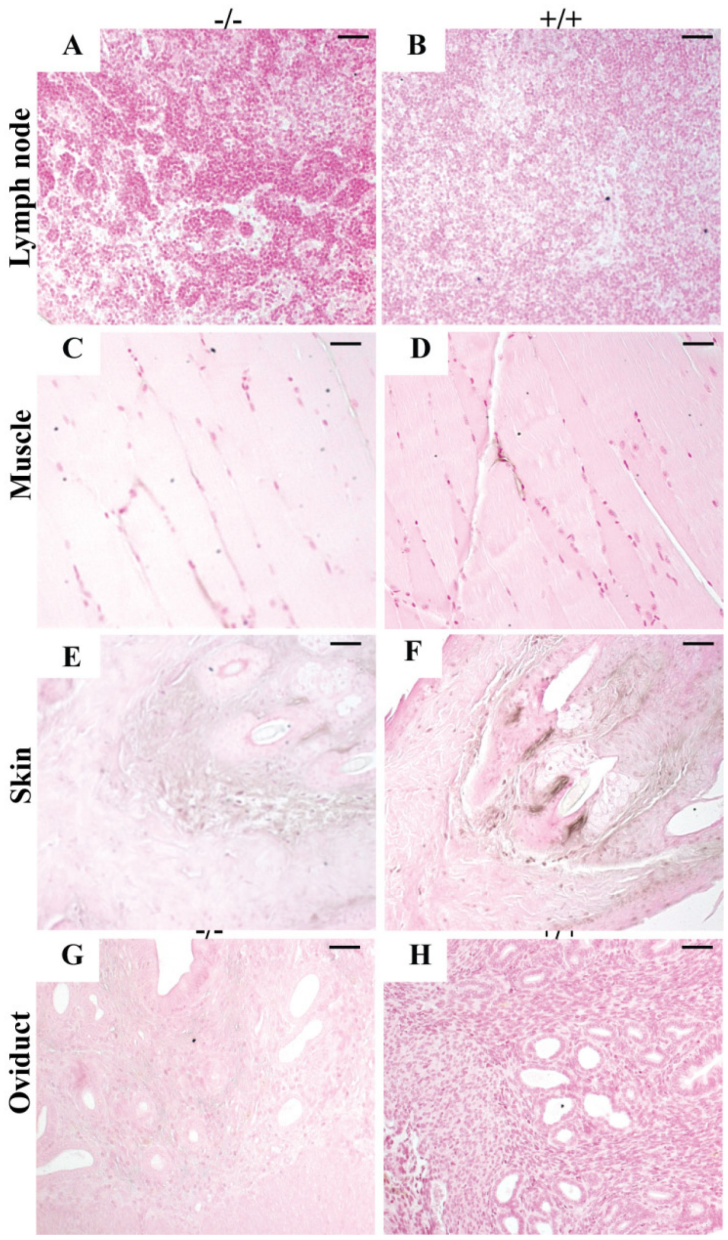

Figure 4.9. Experimental controls for HABP detection.

Paraffin sections of selected tissues including lymph node (A, B), muscle (C, D), skin (E, F) and oviduct (G, H) of *Hyal2* KO and *Hyal2*$^{+/+}$ were treated with 500 U/ml *Streptomyces hyalurolyticus* (Sigma) prior to incubation with biotinylated HABP. The absence of a signal (brown) for HA in the tissues after treatment with hyaluronidase indicates the HABP specifically detects HA in the *Hyal2* KO and *Hyal2*$^{+/+}$ organ/tissues.

4.4.4 Analysis of HA size in tissues from *Hyal2 KO* and *Hyal2*$^{+/+}$ mice

For the evaluation of the size of accumulating HA in tissues, GAGs were purified from the lymph node, liver, spleen, brain, heart, lung, kidney, muscle, and skin of *Hyal2* KO and *Hyal2*$^{+/+}$ mice, and separated on low percentage agarose gels. HA was detected as a dark staining material that was removed by hyaluronidase digestion (Figure 4.9). Consistent with the histochemical-based detection of HA, the levels of HA were clearly elevated in all but the muscle of *Hyal2* KO tissues (Figure 4.10). In the tissues responsible for circulating HA degradation, the levels were clearly more elevated in the lymph node, consistent with the histochemical detection of HA (Figure 4.10 A). The levels of accumulation in *Hyal2* KO mice were much higher in tissues involved in local HA degradation, most notably the brain, heart, lung and skin (Figure 4.10 B). The size of the accumulated HA was also higher in *Hyal2* KO tissues in general (Figure 4.10), but this was most notable for the lymph node, heart, and skin where the level of accumulation appeared to be highest (Figure 4.10 A, B). In order to verify the increased HA observed by both IHC and agarose gel electrophoresis, quantitative studies using FACE were undertaken on a subset of *Hyal2* KO and control tissues. The levels of HA were significantly elevated in the three tissues that were examined, heart, kidney and lung (Figure 4.11).

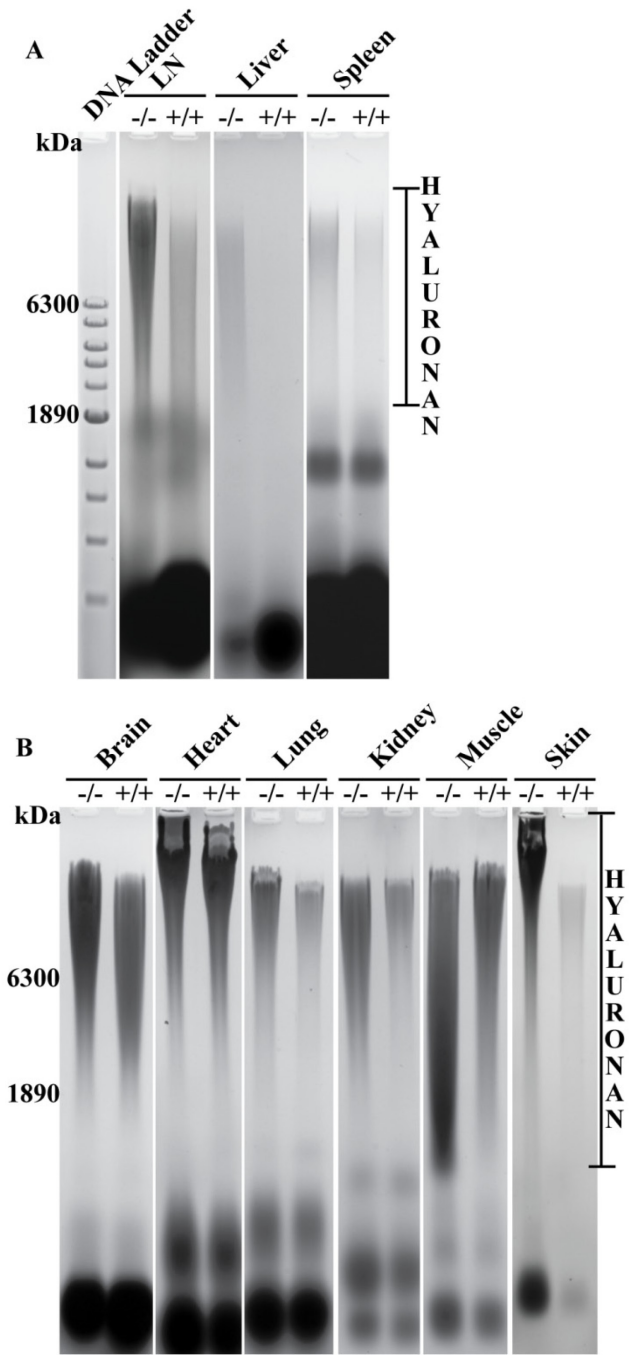

Figure 4.10. Analysis of HA size in *Hyal2* KO and *Hyal2*$^{+/+}$ mouse tissues.

Total GAGs from equal weights of *Hyal2*$^{+/+}$ and *Hyal2* KO tissues were isolated and analyzed by agarose gel electrophoresis followed by detection with Stains-all. The size of DNA or HA standards in kDa are shown to the left of each gel. The dark-staining material, spanning the region indicated by the bars to the right of images is HA. (A) HA in tissues involved in circulating HA degradation, and (B) HA in tissues involved in local HA degradation. To determine/verify which components of the dark-staining material isolated from *Hyal2*$^{+/+}$ or *Hyal2* KO tissues were HA, GAGs isolated from the heart were separated with no treatment (-) or after treatment (+) with *Streptomyces* hyaluronidase. (C)

Experimental control for differentiation of HA and other GAGs. The bands that were not digested at the bottom of the gel are likely to correspond to GAGs other than HA.

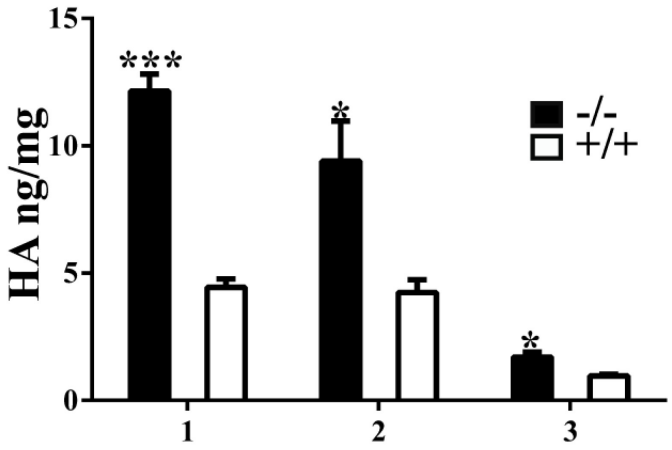

Figure 4.11. Quantification of HA in *Hyal2*$^{+/+}$ and *Hyal2* KO tissues.

The HA present in GAGS isolated from equal weights of heart (1), kidney (2) and lung (3) tissue were analysed by FACE. The graphed values represent the average amount of HA in the tissue, and the error bars represent SEM (n=3). The level of HA was significantly elevated in all *Hyal2* KO tissues (* $p<0.05$; ***$p< 0.0001$). Significance was evaluated using the student *t*-test.

4.5 Discussion

This study provides the first description of the distribution and localization of the HYAL2 protein within a broad range of tissues, and demonstrates an important role for HYAL2 in somatic cell degradation of HA. HYAL2 was detected in the endothelial cells lining blood vessels in all organs or tissues that were examined, although the level of expression was variable. In addition, HYAL2 was found in specialized epithelia of the lung, kidney, skin, brain, small intestine and oviduct. To gain a better understanding of how HYAL2 functions in these tissues, the levels of HA were also examined in tissues from *Hyal2* KO mice. HA levels were increased in almost all organs/tissues of *Hyal2* KO mice, although the levels of accumulation were much higher in those tissues responsible for local HA degradation than those responsible for circulating HA degradation (lymph node, liver, spleen and bone marrow). The size of the accumulating HA was also increased in some *Hyal2* KO tissues, supporting a role for HYAL2 in the cleavage of HMM-HA.

HYAL2's contribution to HA degradation has been controversial. Although initially identified as an acid-active hyaluronidase with weak activity toward HMM-HA [58], HYAL2 was later found to be a GPI-anchored membrane protein that functioned as a receptor for the jaagsiekte sheep retrovirus which is the cause of a form of lung cancer in sheep [60]. Since its initial characterization, most *in vitro* studies have failed to demonstrate HA-degrading activity associated with HYAL2. However, overexpression of HYAL2 in cultured cells increased the breakdown of exogenously added HA [55], reduced the thickness of the pericellular coat [69], and decreased the level of extracellular HMM-HA [85]. Further, a deficiency of HYAL2 in mice resulted in the accumulation of HA in the blood, heart, and lungs [63,199]. Our demonstration in the current study of broadly accumulating, extracellular, HMM-HA in *Hyal2* KO mouse tissues provides strong evidence that HYAL2 contributes directly to HA degradation.

The broad expression, cell surface localization, and weak hyaluronidase activity associated with HYAL2 formed the basis of a proposed model for HA degradation in which HYAL2 initiates the breakdown of extracellular HA in somatic tissues to produce fragments that are internalized via a receptor [43]. The HA receptor was proposed to be CD44 as HYAL2 has been demonstrated to interact with CD44 [55,66,69], as well as with the Na^+-H^+ exchanger NHE1 in one study [67]. NHE1 was proposed to acidify the local environment to allow HYAL2 to function. The resulting fragments were proposed to be internalized and further degraded in the lysosome through the action of HYAL1 and the exoglycosidases β-hexosaminidase and β-glucuronidase [95]. We have now proposed a revised model which incorporates some of the findings in this and other studies, as outlined in more detail below.

Our revised model (Figure 4.12) incorporates both the cell surface and intracellular localization of HYAL2 that we found in a number of different cell types within the tissues of mice. Notably, we observed that HYAL2 surrounded secretory vesicles in the sebaceous glands of skin and epithelial cells of the intestinal crypt, consistent with its regulated secreted to the cell surface. Others have also identified HYAL2 as an intracellular [180] and cell surface [59,60,66,69] protein. In addition, HYAL2 was recently shown to be translocated to the membrane surface upon platelet activation [62]. Although it is possible that some of the HYAL2 detected in the cytoplasm is in transit to the membrane, it is clear that the trafficking of HYAL2 is more complex than originally envisioned.

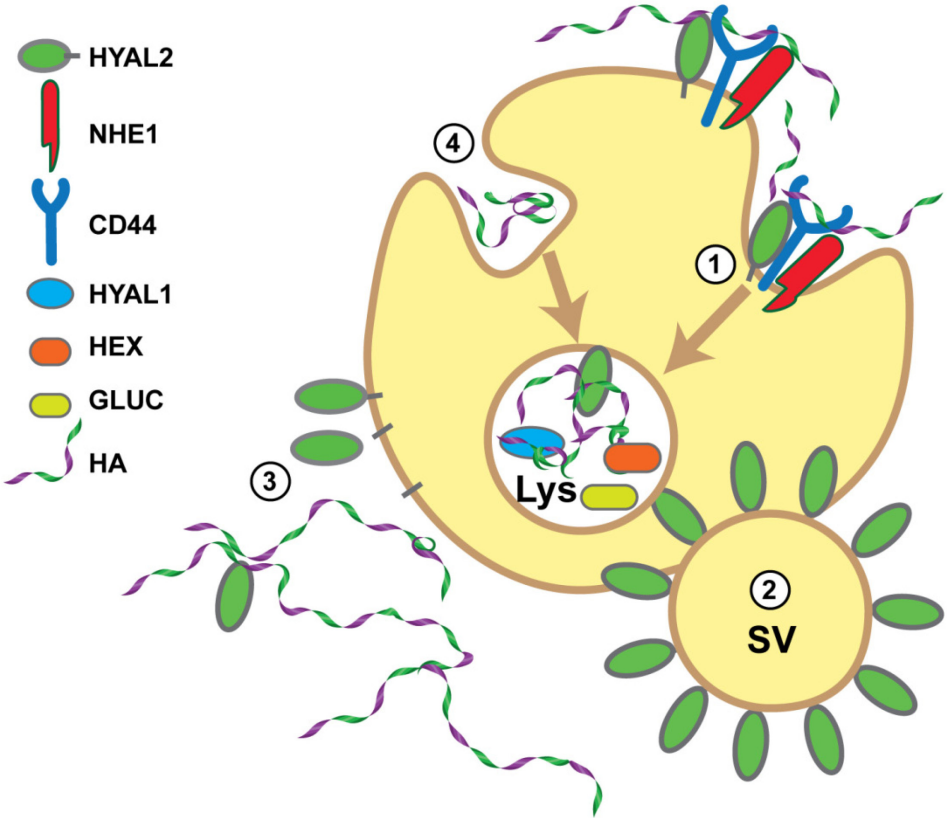

Figure 4.12. Proposed model of HA degradation.

HA degradation occurs through more than one pathway, each indicated by a different number, 1-4, in this model. In pathway **1**, cell surface HYAL2 initiates the hydrolysis of HA in partnership with a receptor, possibly CD44. NHE1 acidifies the local region to allow HYAL2 cleavage. The resulting HA fragments are endocytosed and transported to the lysosome (Lys) where they are degraded through the action of the endoglycosidase HYAL1 and the exoglycosidases, β-hexosaminidase (HEX) and β-glucuronidase (GLUC). In pathway **2**, secretory vesicles (SV) within specialized epithelial cells are surrounded by HYAL2. Upon secretion, these vesicles will degrade extracellular HA. In pathway **3**, cell surface HYAL2 is shed from the surface or released through by a lipase or protease to form a soluble form of HYAL2. This enzyme can enter the blood stream or diffuse from the surface to degrade HA distal from the site of HYAL2 expression. In pathway **4**, HA is internalized by a non-HYAL2 dependent route and transported to the lysosome for degradation.

The studies herein show that accumulating extracellular HA in many *Hyal2* KO tissues is in close proximity to the endothelial surface where HYAL2 is expressed in *Hyal2*$^{+/+}$ tissues. However, accumulated HA was also present in regions of tissues distant from where HYAL2 is detected in *Hyal2*$^{+/+}$ tissues. For example, HA accumulated in the connective tissue of the skin of *Hyal2* KO mice, but not in the sebaceous glands where HYAL2 is most highly expressed in *Hyal2*$^{+/+}$ skin. Thus, HYAL2 must be able to access HA distal to where it is detected. This may be through the secretion of HYAL2 or the cleavage of HYAL2 from its GPI anchor as depicted in our model (Figure 4.12). A recent study of HYAL2 in chondrocytes demonstrated a soluble form of HYAL2 [66]. It is possible that HYAL2 is normally present in the region of HA accumulation, but is not detected. Many GPI-anchored proteins change structure after removal of their anchor and are no longer detectable with the same antibody [231]. Clearly, additional studies are needed to determine if HYAL2 resembles PH-20, the sperm hyaluronidase which has functional membrane-anchored and soluble forms [232], or if there are other explanations for the accumulation of HA distal to the site of HYAL2 expression.

The increased size of the accumulating HA in several tissues of *Hyal2* KO mice provides strong evidence that HYAL2 is actively involved in the degradation of HA. HYAL2's preference for HMM-HA was demonstrated in previous studies [58,66], and supported by our studies. In this study, the increased size of HA was most remarkable in the skin and heart where the levels of endogenous HMM-HA are high in *Hyal2*$^{+/+}$ tissues. The basis of this specificity for HMM-HA is not clear although it is possible that it somehow relates to the structure or binding proteins associated with the HA. It is interesting that HYAL2 was previously demonstrated to cleave HA cables which are rich in the HA-binding protein inter-alpha-trypsin inhibitor [233].

Overall, the extent of HA accumulation in *Hyal2* KO tissues was directly correlated with the level of endogenous HA within the extracellular matrix of these tissues. The marked accumulation of HA in the skin, lung, heart valve, and small intestine where endogenous HA levels are very high indicates that HYAL2 has an important role in local degradation of HA. We found that HA accumulation in *Hyal2* KO mice was greater in tissues responsible for local HA degradation such as the skin and heart valves, than in organs (lymph nodes and liver) responsible for circulating HA clearance. Consistent with these findings, recent studies in the mouse of *in vivo* uptake of injected HA indicated that the majority of HA catabolism occurs locally [234]. This indicates a role for HYAL2 in the catabolism of locally synthesized HA.

Although the highest levels of accumulating HA were in tissues where local degradation takes place, the highest levels of HYAL2 protein were detected in the tissues that play a key role in the clearance of circulating HA, the sinusoidal endothelium of the lymph node, liver and spleen. Among these tissues, the levels of accumulating HA were highest in the lymph nodes of *Hyal2* KO mice, suggesting the HYAL2 contributes significantly to HA degradation in this tissue. Indeed, HA exiting the lymph nodes was previously shown to have a smaller average size than that entering the lymph nodes [235] suggesting partial degradation between entry and exit of the lymph node, possibly due to HYAL2. We noted that the distribution of HYAL2 resembled that of HARE [116] which has been identified as the major receptor in the clearance of circulating HA [236]. It is interesting that increased levels of circulating HA are only found in mice deficient in HYAL2 or HARE, and not in mice deficient in the other HA receptors, including the combined deficiency of LYVE-1 and CD44 [113]. These findings suggest an important role for both HARE and HYAL2 in the clearance of circulating HA although a direct interaction between these proteins has not been

reported. It is possible that HYAL2 must degrade HMM-HA before it can be internalized, therefore leading to the accumulation of HA in the circulation and lymph node tissues.

Although the levels of HA accumulation in *Hyal2* KO mice were significant, they were not as high as one would expect from HA's broad distribution and rapid turnover rate (estimated at 5 g per day in an adult human). Additional mechanisms of clearance for circulating and locally catabolized HA that are independent of HYAL2 must exist (Figure 4.12). One possible route of degradation is via KIAA1199 which binds HA and promotes its uptake/degradation in skin [92]. It is possible that HYAL2's activity is regulated and that it only contributes to HA turnover under specific conditions such as during development or wound healing, or if the HA is assembled with specific binding proteins.

Human HYAL2 mRNA and mouse HYAL2 protein were shown in previous studies to be highly expressed in most tissues, but absent in the brain [41,58]. In our study, we demonstrated low, but readily detectable expression of HYAL2 in the adult mouse brain and localized it to epithelial cells of the choroid plexus, known as ependymal cells. The choroid plexus lines the fluid filled cavities of the brain and is responsible for producing and cleaning the cerebrospinal fluid. This would be consistent with HYAL2 having a role in the degradation of HA in the cerebral final fluid. Interestingly, the HARE receptor, which is involved in the internalization of circulating HA, is also expressed in the ependymal cells of the choroid plexus [116].

The molecular characteristics of HA influence the nature of the ECM and are important for many cellular processes such as cell proliferation, migration and differentiation [121]. This is evident during development as HA regulates the development of several organs, including the heart [126], limb [129], kidney [130], ear [131], palate [132] and neural tube [133]. The physiological and biological properties of HA are size dependent. For

example, HMM-HA is responsible for the formation of heart chambers and epithelial to mesenchymal transition (EMT) of the cardiac cushion whereas LMM HA is thought to be important in partitioning the heart chambers by attenuating EMT through a vascular endothelial growth factor (VEGF) mediated pathway [142]. Accumulation of more HA in *Hyal2* KO heart, lungs, kidney, and muscle suggests that HYAL2 is involved in HA turnover and that the regulation of HA size might have an effect on the balance of ECM in these organs, and therefore impact development. Indeed it is not surprising that *Hyal2* KO mice have significant pre-weaning lethality [63,199].

Our studies demonstrate that HYAL2 is a broadly expressed protein that contributes to both circulating and local HA catabolism. Based on our results, we propose a revised model for HYAL2's contribution to HA degradation. We suggest that cell surface HYAL2 is primarily involved in local HA degradation in tissues like oviduct and lungs. In some regions of tissues where HYAL2 is not detected, but HA accumulates in its absence, we suggest that HYAL2 may be active in a soluble form that has been released from its GPI anchor, or on the surface of a secretory vesicle. Finally, our results support the existence of a non-HYAL2 dependent pathway that contributes to both local and circulating HA degradation. Whether the distribution of HYAL2 is the same during development or wound healing remains to be determined and this could have some impact on the distribution of accumulating HA in the *Hyal2* KO mice. Further studies of HYAL2 trafficking, and how its deficiency leads to pre-weaning lethality in *Hyal2* KO mice will no doubt provide new information about HA degradation and HYAL2's role in normal development.

Chapter 5: Conclusions and Future Directions

HYAL2 is a GPI-linked enzyme which is proposed to initiate the degradation of HA, a major component of the vertebrate ECM [59]. HA plays a significant role during development and in maintaining tissue homeostasis after birth. The role of HA in organ development has been characterized through the analysis of HAS2 KO mice; KO mice died at E9.5 due to the absence of EMT in the cardiac cushions [126]. HYAL1 and HYAL2 are thought to be the primary enzymes involved in somatic HA degradation. However, the deficiency of HYAL1 in mice and patients resulted in a very mild pathology suggesting HYAL2 might substitute for the loss of HYAL1 in HA catabolism [51,52]. Initial studies of HYAL2 KO mice revealed craniofacial abnormalities, and mild anemia that did not entirely support a key role for HYAL2 in HA catabolism [63]. However, further study of *Hyal2* KO mice demonstrated additional phenotypes, including atrial enlargement (54% of KOs) and severe pre-weaning lethality, that encouraged us to study the HYAL2 KO mice further.

This work started with the characterization of the cardiac phenotype in HYAL2 KO mice (Chapter 2). We demonstrated that HYAL2 is essential for normal cardiopulmonary function in mice. In its absence, extracellular HA accumulated in the heart valves, myocardium, serum and lungs that led to severe cardiopulmonary dysfunction and premature death. The cardiac failure in *Hyal2* KO mice followed an acute course (average lifespan ~3 months) in some animals and a chronic course (average lifespan ~6 months) in others. Increased levels of HA in the heart valves and myocardium was associated with disorganization of the valve ECM and upper ventricular hypertrophy in *Hyal2* KO mice. Analysis of serum HA in HYAL2 mice revealed progressively increasing levels of HA with age that reached an average 27 fold increase at the time of euthanasia in KO mice compared to controls. However, serum HA levels did not differ significantly between acute and chronic mice. Analysis of the lungs of *Hyal2* KO mice demonstrated severe pulmonary fibrosis due to

increased levels of HA in the acute mice compared to chronic and control mice. Further, assessment of HA size in the KO hearts and serum revealed the accumulating HA was HMM-HA, supporting the proposed model of HA degradation where HYAL2 initiates degradation of HMM-HA. Taken together, we concluded that HYAL2 is essential for the breakdown of extracellular HMM-HA and in the absence of HYAL2, extracellular HA accumulates in tissues and can lead cardiopulmonary dysfunction.

The structural abnormalities in the hearts of HYAL2 KO mice were thought to have a developmental origin. In Chapter 3, we describe the further characterization of the morphological and functional abnormalities of the cardiac phenotype. Severe atrial dilation was detected in acutely affected HYAL2 KO mice as early as 4 weeks of age. Histological analyses revealed that the atrial dilation was the result of excess tissue in the atrium. Functional analyses has shown progressive diastolic dysfunction in all HYAL2 KO mice. The severity of the dysfunction correlated with the severity of the atrial enlargement, but did not correlate with the presence of cor triatrium. Histological analysis of adult heart tissue demonstrated fibrosis due to increased levels of HA in the atrium and ventricle of HYAL2 KO hearts compared to controls. The cell type in the fibromuscular tissues was identified to be mesenchymal. Further, study of early embryonic mouse hearts revealed increased numbers of mesenchymal cells, suggesting increased EMT and decreased differentiation, presumably due to the presence of excess HA. The excess tissue growth in acute mice was clearly associated with increased cardiac dysfunction that led to euthanasia between 1-3 months of age. Our findings suggest that HA degradation by HYAL2 is required to attenuate EMT, and in the absence of HYAL2, excess mesenchymal cells are formed.

HA accumulation in the *Hyal2* KO heart, lungs and serum suggested that HYAL2 might be important in HA catabolism in a broad range of tissues, but its distribution had not been previously studied. In Chapter 4, we analyze a broad range of mouse tissues, and show that HYAL2 is mainly distributed to the surface and cytoplasm of endothelial cells, as well as specialized epithelial cells in several tissues, including the skin. The current study has also demonstrated detectable expression of HYAL2 in the adult mouse brain and localized it to ependymal cells. To gain a better understanding of how HYAL2 functions in those tissues, the levels of HA were also examined in tissues from *Hyal2* KO and control mice. HA levels were increased in almost all organs/tissues of *Hyal2* KO mice, although the levels of accumulation were much higher in those tissues responsible for local HA degradation than those responsible for circulating HA degradation (lymph node, liver, spleen and bone marrow), indicating a role for HYAL2 in local HA catabolism. Interestingly, accumulating HA in some tissues/organs was distant from where HYAL2 was localized whereas in others, HA localized in the surrounding matrix close to HYAL2. The accumulating HA in the tissues was found to be HMM-HA. Our results support HYAL2's role as an extracellular enzyme that initiates HA breakdown in somatic tissues. However, our findings also suggest that HYAL2 contributes to HA degradation through other routes, perhaps as a soluble or secreted form.

In summary, this work demonstrated that HYAL2 has an important role in the degradation of HMM-HA and heart development (Figure 5.1). *Hyal2* KO mice were unable to remove HMM-HA during heart development, resulting in increased EMT in HYAL2 Kos compared to controls. Accumulation of HMM-HA disrupted the homeostasis of other matrix components and led to abnormal cardiac development and organ dysfunction. The characterization of HYAL2 distribution and accumulation of HA in its absence in adult mouse tissues demonstrated that HYAL2 plays an important role in HMM-HA degradation in

a broad range of tissues. It seems likely that the proposed model in Fig. 5.1 for the role of HYAL2 in regulating normal EMT might also impact development in other tissues.

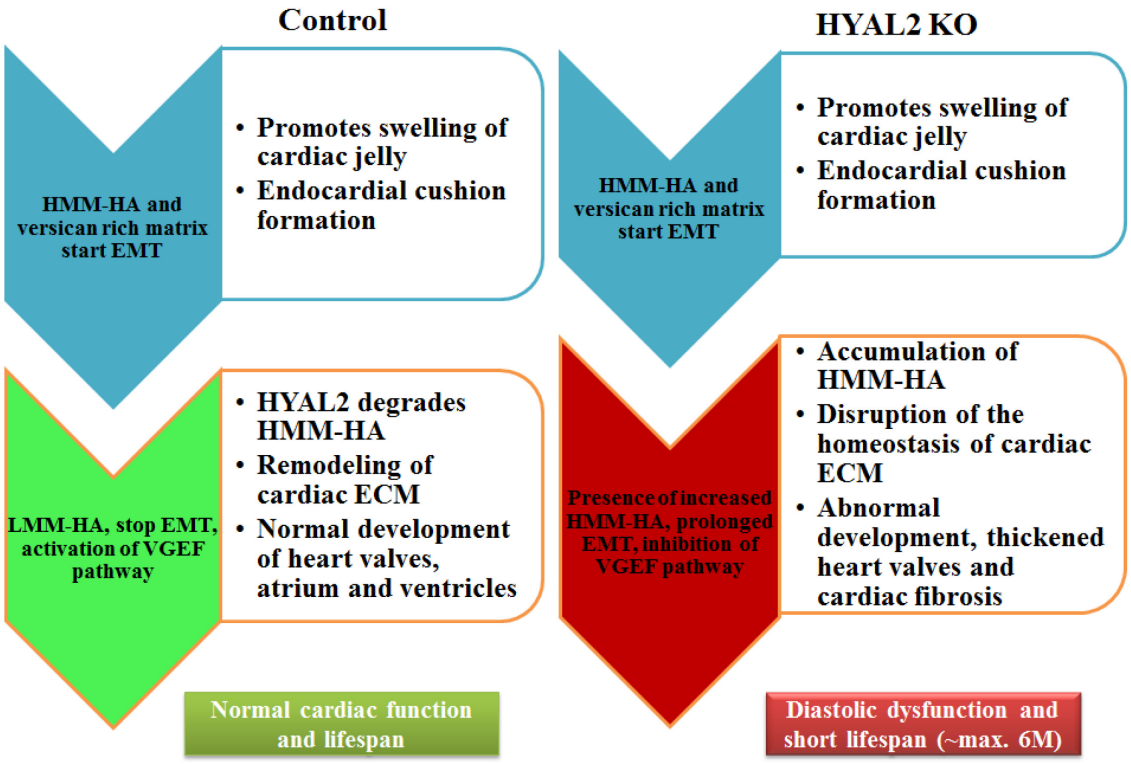

Figure 5.1. Model for the impact of HYAL2 deficiency on cardiac development.

During embryonic development, HMM-HA synthesis promotes swelling of the cardiac jelly and EMT within the endocardial cushions (EC). Following EMT, degradation of HMM-HA is required to inhibit EMT and activate the VGEF pathway Which promotes the production of the valves and septa of the developing heart. In HYAL2 KO mice, the absence of HYAL2 prevents the removal of HMM-HA and the generation of LMM-HA. As a result, EMT continues to be promoted and the activation of the VEGF pathway is reduced. This results in a disruption in normal heart development, thickened valves, and cardiac fibrosis. As a result, HYAL2 KO mice exhibited pre-weaning lethality and developed diastolic dysfunction that leads to a short lifespan in surviving KOs.

The heterogeneity of the phenotypes in the HYAL2 KO mice indicated the presence of other genetic loci that can modify the phenotype in some KO mice. It would be interesting to identify the genetic modifier within this outbred background on which we are working. The turnover of HA is regulated by different proteins including HASs, HYALs and cell surface receptors. Therefore, as a first approach to identifying the modifier, it would be interesting to look at the expression levels of these proteins in acute versus chronically affected HYAL2 KO mice. Ultimately, if this were not successful, a genome-wide sequencing approach of mice with the two phenotypes compared to controls could be taken to identify the responsible gene(s). A similar approach could also be used for the identification of a modifier of the kidney phenotype, which also exhibited variable penetrance.

A kidney was found to be missing in 43% of HYAL2 KO mice. Since the kidney phenotype was found to be independent of the atrial dilation, we focused our study on the characterization of the cardiac phenotype in HYAL2 KO mice. However, in our studies of the adult kidney, we have found accumulation of HA in the medullary region and further biochemical analysis confirmed the accumulating HA was HMM in the KOs compared to controls. However, no studies have been performed to describe how HYAL2 contributes to kidney development/pathology. Several *in vitro* and expression studies have been reported that HA and HYALs might play a significant contribution to kidney development and disease [237,238]. During the development of the chick embryonic kidney (day 11-18), reduced levels of HA and increased HYALs were demonstrated [237]. Therefore, a detailed molecular and histochemical analysis of the developing kidney in Hyal2 KO and control mice would be important in determining HYAL2's role. Further high-frequency ultrasound could be used to

determine if the kidney begins to develop and regresess, or if it fails to develop. We have previously used high-frequency ultrasound to assess heart development in embryonic mice.

Several groups have reported that the increased HA is associated with tissue fibrosis. However, how tissue homeostasis is regulated in the presence of HMM and LMM HA in *in vivo* has not been studied yet. Because the ECM of the heart valve is well characterized, heart valves in *Hyal2* KO and control mice could be used as a model tissue to explore the role of excess HA in tissue homeostasis. Our partial analysis of heart valves in Hyal2 KO mice demonstrated that the presence of excess HA disrupts the organization of collagen and elastin in HYAL2 KO mice compared to controls. Molecular and histochemical analysis of Hyal2 KO and control heart valves could determine the organization and expression of other ECM components including PGs, MMPs and TIMPs in detail. To determine the expression level of other genes and transcription factors due to increase HA in *Hyal2* KO mice compared to controls, the mRNA expression analysis on frozen heart valves could also perform. Briefly, valves from 3 adult mice of the same genotype will be dissected and pooled for RNA isolation. 100-200 ng of RNA will be used to generate cDNA and qRT-PCR will be performed. This information would be valuable to understand the molecular cause of a pathology associated with excess HA.

HYAL2 deficient mice demonstrated craniofacial abnormalities, increased serum HA, agenesis of a single kidney and cardiac abnormalities. Screening for these pathological features in the human population could allow HYAL2-deficient patients to be identified. A full evaluation of the phenotype in different human populations would be very useful in

defining the full range of the phenotype associated with HYAL2 deficiency in humans and whether a complete HYAL2 deficiency is likely to be compatible with human life.

Hearing loss is a common feature in several MPS patients and mice. The role of HA in inner ear development has been determined in *Xenopus laevis*. The viscoelastic properties of HA allow it to act as a propellant for the ECM and associated cell movements which are essential for the development of the semicircular canal in frogs [131]. *In situ hybridization* of E13.5 mouse embryos demonstrated the expression of both *Has2* and *Has3* genes in the semicircular canal and the cochlea respectively [28]. Further, histological analyses of the distribution of GAGs in the mouse ear showed HA is abundant in the inner and middle ear cavity [239]. However, no studies have been reported to describe how HYAL2 contributes to ear development. In preliminary studies, we have found the significant hearing loss in adult HYAL2 KO mice (not shown). Additional investigations of the structure of the ear using micro-CT, as well as histological studies of the inner ear structure would be useful in determining the cause of hearing loss in HYAL2 deficiency.

In our study of pre-weaning lethality in HYAL2 KO mice demonstrated that 1/3 of the KO mice died during postnatal (P) day1 (data not shown). The preliminary study of the cause of death in HYAL2 KO mice exhibited reduced ossification of palatal bones and abnormal skull bones compared to controls. Therefore, it will be interesting to study further the mechanism of ossification and the contribution of HYAL2 in this regard. During palatogenesis, the hydrated nature of HA provides intrinsic force to support palate elevation and fusion, and the condensed mesenchymal cells in the palate shelf differentiate into osteoblasts to form the hard palate. Palatal ossification requires a complex process of

spatiotemporal expression of growth factors, and differentiation factors including bone morphogenetic proteins (Bmps), core binding proteins (Cbf), Fgfs, TGfβ and hedgehog (hh) proteins that control the signaling pathways for the patterning and maturation of osteoblasts [240]. Using immunohistochemical approaches on embryonic tissue, one could determine the impact of HYAL2 deficiency on the molecular pathways of ossification during palate development. This information would be valuable for understanding the molecular mechanism of osteogenesis associated with excess HA.

The depolymerization of HA during heart development was evident in *ex vivo* studies of mouse cardiac explants; LMM-HA inhibited EMT and activated VEGF pathways [142]. In the absence of HYAL2, accumulation of HA was associated with increased mesenchymal cells, and presumably EMT in *Hyal2* KO heart and palate. The EMT process requires the activation or inhibition of different transcription factors and their regulatory signalling pathways to control cell proliferation, differentiation, invasion and migration [241]. Therefore, an examination of EMT pathways in *Hyal2* KO and control tissues would help to place where HYAL2 fits into these signal transduction pathways to regulate EMT. This study could utilize pre-existing oligonucleotide arrays to query the expression of EMT-related genes in the developing heart and palate of *Hyal2* KOs and controls. The different levels of expression of transcription factors, cell surface receptors, and other proteins will determine how HYAL2 regulate EMT at a particular time point. The mRNA expression data would be further verified with biochemical and histological analysis. This study would determine the importance of HA degradation during EMT *in vivo*.

Several *in vitro* and *ex vivo* studies have demonstrated a role for HMM-HA and LMM-HA in cardiogenesis. For example, increased HMM-HA promotes the invasive

activity of mesenchymal cells in a CD44-NFκB-Snail2-dependent pathway [242]. In the epicardium, HMM-HA activates the TGFβR3-Src pathway that is required for the cellular invasion of epicardial cells [243]. *Ex vivo* studies of mouse cardiac explants indicate that the formation of mesenchymal cells is promoted by HMM-HA. Whereas, LMM HA inhibits the formation of mesenchymal cells and increases VGEF production to promote the differentiation of the mesenchymal cells [244]. To determine the role of HYAL2 in this regard, *ex vivo* analysis of cardiac cushions from *Hyal2* KO and control mice could be performed. Briefly mouse AVC and endocardial cushion will be dissected out at E9.5 (during EMT) and 11.5 (after EMT), and cultured on collagen gels. The cellular migration and invasion will be measured using morphological characteristics of mesenchymal cells as described in a previous study [244]. Immunofluorescence and western blot will be performed to determine the localization and expression of VEGF and other signalling molecules on cultured cell lysate and media of *Hyal2* KO and control mice. This study would determine the role of HYAL2 in mesenchymal cell migration, invasion and activation of VEGF pathway in *ex vivo*.

Based on our knowledge, this is the only work that described cor-triatriatum in a mouse model. Cor-triatriatum is a rare genetic disorder associated with several cardiac abnormalities including mitral regurgitation, enlarged atrium, and valvular disease. The pathophysiology and molecular causes of cor-triatriatum are not well known. Therefore, our mouse model could be used to more fully understand the molecular causes of cor-triatriatum and whether there are possible approaches to treatment. Whether there are additional cardiac abnormalities that we did not identify in our studies remains to be determined. The histological analysis of the acute atrium demonstrated the presence of extra tissue mass. Our

preliminary study of the cell type in the extra mass suggested they were undiferentiated cardiac myocytes. Therefore, it would be interesting to further study this tissues using myocyte specific markers including α-SMA, alpha actin, and myosin heavy chain to confirm the cell type. Based on our analysis of embryonic lethality, cardiac defects could be a cause of pre-weaning lethality, as the embryos that died before birth appeared to die at approximately E15.5. A histological study of E14.5 *Hyal2* KO embryos might be helpful in identifying the cause of death in a small number of *Hyal2* KOs. In the longer term, creating a specific KO of HYAL2 in various cell populations that form the heart would help to understand the origins of the heart defects and whether they are the cause of lethality.

The localization of HYAL2 and HA distribution in the early embryonic (E8.5 -12.5) mouse heart suggested that these molecules were important during development. Using a similar approach, the correlation between the HA level and HYAL2 localization could be determined at other stages of embryonic development. The spatiotemporal localization of HYAL2 will determine where it is located during palate, ear and other tissues/organ development. The distribution pattern of HYAL2 in these organs and the correlation with HA accumulation in HYAL2 KOs is a key approach to providing the basis for further experiments to understand HYAL2's role in development. Further, studies of ECM organization in ear, palate, and heart using histochemical approach may light up how the excess HA disrupts the ECM homeostasis of those organs.

It would be interesting to study the impact of reducing the HA levels during development. Several studies have been reported that administration of dexamethasone or diphenylhydantoin reduced the HA levels in human and mouse [245]. A similar approach

could be tested female mice carrying HYAL2 KO embryos, starting with a low dose at E14.5, right after all the major organs are formed. The treated and control HYAL2 KO pups could be evaluated for heart and craniofacial defects at P1.

The current work demonstrated that HYAL2 is mainly expressed in endothelial and some specialized epithelial cells. According to the proposed model, HYAL2 interacts with a cell surface receptor and initiates HA endocytosis. Falkowski *et al*. has been reported that the HARE receptor is also expressed in endothelial cells [116]. Further, HARE KO mice also exhibited premature mortality, increased serum HA and dilated cardiomyopathy [118]. However, no studies have been done to determine if these proteins can interact to each other, and whether their interactions contribute to HA catabolism. The interaction between HYAL2 and HARE would be determined by performing an immunoprecipitation in mouse tissue. In this regard, HYAL2 KO mice can be used as an experimental control for HYAL2. The functional dependency of HARE and HYAL2 could be analyzed using *in vitro* studies. Briefly, endothelial cells from both HYAL2 KO and control mice could be isolated and cultured in the presence/absence of HARE blocking antibodies in the presence of exogenous fluorescently labelled HMM/LMM-HA. After incubation with exogenous HA, the uptake of HA will be monitored by microscopy and the size of the remaining HA in the media will be determined using agarose gel electrophoresis. If their activity depends on each other, then it will be interesting to generate a double KO (*Hyal2*$^{-/-}$ *Hare*$^{-/-}$) mouse and characterize the phenotypes.

Several *in vitro* studies have reported that HYAL2 can interact with the CD44 receptor. The co-localization of HYAL2 with CD44 or another receptor, LYVE-1, using a

commercial antibody to HYAL2 to analyze mouse tissues will provide insight into the potential *in vivo* relevance of interactions between HYAL2 and either receptor. If HYAL2 co-localizes with either receptor in a specific tissue or organ, this could suggest that they work together in HA catabolism. However, this would just be a starting point for many additional *in vitro* and *in vivo* experiments to assess their interdependence and importance in HA catabolism and uptake.

The HYAL2 KO mice have created a rich resource for future endeavors, only a few of which I have touched on this summary and discussion of future directions. It is clear that this model has the potential to dramatically advance our understanding of the role of HA and HA degradation in development and disease.

REFERENCES

1 Hynes, R. O. (2009) The extracellular matrix: Not just pretty fibrils. Science. **326**, 1216-1219. doi:10.1126/science.1176009; 10.1126/science.1176009

2 Rozario, T. and DeSimone, D. W. (2010) The extracellular matrix in development and morphogenesis: A dynamic view. Dev. Biol. **341**, 126-140. doi:10.1016/j.ydbio.2009.10.026; 10.1016/j.ydbio.2009.10.026

3 Dacks, J. B., Peden, A. A. and Field, M. C. (2009) Evolution of specificity in the eukaryotic endomembrane system. Int. J. Biochem. Cell Biol. **41**, 330-340. doi:10.1016/j.biocel.2008.08.041; 10.1016/j.biocel.2008.08.041

4 Frantz, C., Stewart, K. M. and Weaver, V. M. (2010) The extracellular matrix at a glance. J. Cell. Sci. **123**, 4195-4200. doi:10.1242/jcs.023820 [doi]

5 Tsipouras, P. and Ramirez, F. (1987) Genetic disorders of collagen. J. Med. Genet. **24**, 2-8

6 Heino, J. (2007) The collagen family members as cell adhesion proteins. Bioessays. **29**, 1001-1010. doi:10.1002/bies.20636

7 Halper, J. and Kjaer, M. (2014) Basic components of connective tissues and extracellular matrix: Elastin, fibrillin, fibulins, fibrinogen, fibronectin, laminin, tenascins and thrombospondins. Adv. Exp. Med. Biol. **802**, 31-47. doi:10.1007/978-94-007-7893-1_3 [doi]

8 Karnik, S. K., Brooke, B. S., Bayes-Genis, A., Sorensen, L., Wythe, J. D., Schwartz, R. S., Keating, M. T. and Li, D. Y. (2003) A critical role for elastin signaling in vascular morphogenesis and disease. Development. **130**, 411-423

9 Ewart, A. K., Morris, C. A., Atkinson, D., Jin, W., Sternes, K., Spallone, P., Stock, A. D., Leppert, M. and Keating, M. T. (1993) Hemizygosity at the elastin locus in a developmental disorder, williams syndrome. Nat. Genet. **5**, 11-16. doi:10.1038/ng0993-11

10 Li, D. Y., Brooke, B., Davis, E. C., Mecham, R. P., Sorensen, L. K., Boak, B. B., Eichwald, E. and Keating, M. T. (1998) Elastin is an essential determinant of arterial morphogenesis. Nature. **393**, 276-280. doi:10.1038/30522

11 Gandhi, N. S. and Mancera, R. L. (2008) The structure of glycosaminoglycans and their interactions with proteins. Chem. Biol. Drug Des. **72**, 455-482. doi:10.1111/j.1747-0285.2008.00741.x; 10.1111/j.1747-0285.2008.00741.x

12 Raman, R., Sasisekharan, V. and Sasisekharan, R. (2005) Structural insights into biological roles of protein-glycosaminoglycan interactions. Chem. Biol. **12**, 267-277. doi:S1074-5521(05)00042-6 [pii]

13 Schaefer, L. and Schaefer, R. M. (2010) Proteoglycans: From structural compounds to signaling molecules. Cell Tissue Res. **339**, 237-246. doi:10.1007/s00441-009-0821-y; 10.1007/s00441-009-0821-y

14 Gleghorn, L., Ramesar, R., Beighton, P. and Wallis, G. (2005) A mutation in the variable repeat region of the aggrecan gene (AGC1) causes a form of spondyloepiphyseal dysplasia associated with severe, premature osteoarthritis. Am. J. Hum. Genet. **77**, 484-490. doi:S0002-9297(07)63028-6 [pii]

15 Arikawa-Hirasawa, E., Le, A. H., Nishino, I., Nonaka, I., Ho, N. C., Francomano, C. A., Govindraj, P., Hassell, J. R., Devaney, J. M., Spranger, J., Stevenson, R. E., Iannaccone, S., Dalakas, M. C. and Yamada, Y. (2002) Structural and functional mutations of the perlecan gene cause schwartz-jampel syndrome, with myotonic myopathy and chondrodysplasia. Am. J. Hum. Genet. **70**, 1368-1375. doi:S0002-9297(07)62531-2 [pii]

16 Lu, P., Takai, K., Weaver, V. M. and Werb, Z. (2011) Extracellular matrix degradation and remodeling in development and disease. Cold Spring Harb Perspect. Biol. **3**, 10.1101/cshperspect.a005058. doi:10.1101/cshperspect.a005058 [doi]

17 Balazs, E. A., Laurent, T. C. and Jeanloz, R. W. (1986) Nomenclature of hyaluronic acid. Biochem. J. **235**, 903

18 Itano, N. (2008) Simple primary structure, complex turnover regulation and multiple roles of hyaluronan. J. Biochem. **144**, 131-137. doi:10.1093/jb/mvn046

19 Fraser, J. R., Laurent, T. C. and Laurent, U. B. (1997) Hyaluronan: Its nature, distribution, functions and turnover. J. Intern. Med. **242**, 27-33

20 C.G. Boeriu. (2013) Production methods for hyaluronan. International journal of carbohydrate chemistry. **2013**

21 Reed, R. K., Lilja, K. and Laurent, T. C. (1988) Hyaluronan in the rat with special reference to the skin. Acta Physiol. Scand. **134**, 405-411. doi:10.1111/j.1748-1716.1988.tb08508.x

22 Evanko, S. P. and Wight, T. N. (1999) Intracellular localization of hyaluronan in proliferating cells. J. Histochem. Cytochem. **47**, 1331-1342

23 Volpi, N., Schiller, J., Stern, R. and Soltes, L. (2009) Role, metabolism, chemical modifications and applications of hyaluronan. Curr. Med. Chem. **16**, 1718-1745

24 Kohda, D., Morton, C. J., Parkar, A. A., Hatanaka, H., Inagaki, F. M., Campbell, I. D. and Day, A. J. (1996) Solution structure of the link module: A hyaluronan-binding domain involved in extracellular matrix stability and cell migration. Cell. **86**, 767-775. doi:S0092-8674(00)80151-8 [pii]

25 Yang, B., Zhang, L. and Turley, E. A. (1993) Identification of two hyaluronan-binding domains in the hyaluronan receptor RHAMM. J. Biol. Chem. **268**, 8617-8623

26 Weigel, P. H. and DeAngelis, P. L. (2007) Hyaluronan synthases: A decade-plus of novel glycosyltransferases. J. Biol. Chem. **282**, 36777-36781. doi:10.1074/jbc.R700036200

27 Weigel, P. H., Hascall, V. C. and Tammi, M. (1997) Hyaluronan synthases. J. Biol. Chem. **272**, 13997-14000

28 Tien, J. Y. and Spicer, A. P. (2005) Three vertebrate hyaluronan synthases are expressed during mouse development in distinct spatial and temporal patterns. Dev. Dyn. **233**, 130-141. doi:10.1002/dvdy.20328

29 Spicer, A. P. and McDonald, J. A. (1998) Characterization and molecular evolution of a vertebrate hyaluronan synthase gene family. J. Biol. Chem. **273**, 1923-1932

30 Rilla, K., Oikari, S., Jokela, T. A., Hyttinen, J. M., Karna, R., Tammi, R. H. and Tammi, M. I. (2013) Hyaluronan synthase 1 (HAS1) requires higher cellular UDP-GlcNAc concentration than HAS2 and HAS3. J. Biol. Chem. **288**, 5973-5983. doi:10.1074/jbc.M112.443879; 10.1074/jbc.M112.443879

31 Kobayashi, N., Miyoshi, S., Mikami, T., Koyama, H., Kitazawa, M., Takeoka, M., Sano, K., Amano, J., Isogai, Z., Niida, S., Oguri, K., Okayama, M., McDonald, J. A., Kimata, K., Taniguchi, S. and Itano, N. (2010) Hyaluronan deficiency in tumor stroma impairs macrophage trafficking and tumor neovascularization. Cancer Res. **70**, 7073-7083. doi:10.1158/0008-5472.CAN-09-4687 [doi]

32 Arranz, A. M., Perkins, K. L., Irie, F., Lewis, D. P., Hrabe, J., Xiao, F., Itano, N., Kimata, K., Hrabetova, S. and Yamaguchi, Y. (2014) Hyaluronan deficiency due to Has3 knock-out causes altered neuronal activity and seizures via reduction in brain extracellular space. J. Neurosci. **34**, 6164-6176. doi:10.1523/JNEUROSCI.3458-13.2014; 10.1523/JNEUROSCI.3458-13.2014

33 Matsumoto, K., Li, Y., Jakuba, C., Sugiyama, Y., Sayo, T., Okuno, M., Dealy, C. N., Toole, B. P., Takeda, J., Yamaguchi, Y. and Kosher, R. A. (2009) Conditional inactivation of Has2 reveals a crucial role for hyaluronan in skeletal growth, patterning, chondrocyte maturation and joint formation in the developing limb. Development. **136**, 2825-2835. doi:10.1242/dev.038505; 10.1242/dev.038505

34 Mack, J. A., Feldman, R. J., Itano, N., Kimata, K., Lauer, M., Hascall, V. C. and Maytin, E. V. (2012) Enhanced inflammation and accelerated wound closure following tetraphorbol ester application or full-thickness wounding in mice lacking hyaluronan synthases Has1 and Has3. J. Invest. Dermatol. **132**, 198-207. doi:10.1038/jid.2011.248; 10.1038/jid.2011.248

35 Fraser, J. R., Appelgren, L. E. and Laurent, T. C. (1983) Tissue uptake of circulating hyaluronic acid. A whole body autoradiographic study. Cell Tissue Res. **233**, 285-293

36 Fraser, J. R. and Laurent, T. C. (1989) Turnover and metabolism of hyaluronan. Ciba Found. Symp. **143**, 41-53; discussion 53-9, 281-5

37 Laurent, T. C., Lilja, K., Brunnberg, L., Engstrom-Laurent, A., Laurent, U. B., Lindqvist, U., Murata, K. and Ytterberg, D. (1987) Urinary excretion of hyaluronan in man. Scand. J. Clin. Lab. Invest. **47**, 793-799

38 Kreil, G. (1995) Hyaluronidases--a group of neglected enzymes. Protein Sci. **4**, 1666-1669. doi:10.1002/pro.5560040902

39 Stern, R. (2003) Devising a pathway for hyaluronan catabolism: Are we there yet? **13**, 105-115

40 Hynes, W. L. and Walton, S. L. (2000) Hyaluronidases of gram-positive bacteria. FEMS Microbiol. Lett. **183**, 201-207. doi:S0378-1097(99)00669-2 [pii]

41 Csoka, A. B., Scherer, S. W. and Stern, R. (1999) Expression analysis of six paralogous human hyaluronidase genes clustered on chromosomes 3p21 and 7q31. Genomics. **60**, 356-361. doi:10.1006/geno.1999.5876

42 Csoka, A. B. and Stern, R. (2013) Hypotheses on the evolution of hyaluronan: A highly ironic acid. Glycobiology. **23**, 398-411. doi:10.1093/glycob/cws218; 10.1093/glycob/cws218

43 Csoka, A. B., Frost, G. I. and Stern, R. (2001) The six hyaluronidase-like genes in the human and mouse genomes. Matrix Biol. **20**, 499-508

44 Kim, E., Baba, D., Kimura, M., Yamashita, M., Kashiwabara, S. and Baba, T. (2005) Identification of a hyaluronidase, Hyal5, involved in penetration of mouse sperm through cumulus mass. Proc. Natl. Acad. Sci. U. S. A. **102**, 18028-18033. doi:10.1073/pnas.0506825102

45 Frost, G. I., Csoka, A. B., Wong, T. and Stern, R. (1997) Purification, cloning, and expression of human plasma hyaluronidase. Biochem. Biophys. Res. Commun. **236**, 10-15

46 Triggs-Raine, B., Salo, T. J., Zhang, H., Wicklow, B. A. and Natowicz, M. R. (1999) Mutations in HYAL1, a member of a tandemly distributed multigene family encoding disparate hyaluronidase activities, cause a newly described lysosomal disorder, mucopolysaccharidosis IX. Proc. Natl. Acad. Sci. U. S. A. **96**, 6296-6300

47 Shuttleworth, T. L., Wilson, M. D., Wicklow, B. A., Wilkins, J. A. and Triggs-Raine, B. L. (2002) Characterization of the murine hyaluronidase gene region reveals complex organization and cotranscription of Hyal1 with downstream genes, Fus2 and Hyal3. J. Biol. Chem. **277**, 23008-23018. doi:10.1074/jbc.M108991200

48 Puissant, E., Gilis, F., Dogne, S., Flamion, B., Jadot, M. and Boonen, M. (2014) Subcellular trafficking and activity of hyal-1 and its processed forms in murine macrophages. Traffic. **15**, 500-515. doi:10.1111/tra.12162 [doi]

49 Chao, K. L., Muthukumar, L. and Herzberg, O. (2007) Structure of human hyaluronidase-1, a hyaluronan hydrolyzing enzyme involved in tumor growth and angiogenesis. Biochemistry. **46**, 6911-6920. doi:10.1021/bi700382g [doi]

50 Markovic-Housley, Z., Miglierini, G., Soldatova, L., Rizkallah, P. J., Muller, U. and Schirmer, T. (2000) Crystal structure of hyaluronidase, a major allergen of bee venom. Structure. **8**, 1025-1035

51 Natowicz, M. R., Short, M. P., Wang, Y., Dickersin, G. R., Gebhardt, M. C., Rosenthal, D. I., Sims, K. B. and Rosenberg, A. E. (1996) Clinical and biochemical manifestations of hyaluronidase deficiency. N. Engl. J. Med. **335**, 1029-1033. doi:10.1056/NEJM199610033351405

52 Martin, D. C., Atmuri, V., Hemming, R. J., Farley, J., Mort, J. S., Byers, S., Hombach-Klonisch, S., Csoka, A. B., Stern, R. and Triggs-Raine, B. L. (2008) A mouse model of human mucopolysaccharidosis IX exhibits osteoarthritis. Hum. Mol. Genet. **17**, 1904-1915. doi:10.1093/hmg/ddn088

53 Imundo, L., Leduc, C. A., Guha, S., Brown, M., Perino, G., Gushulak, L., Triggs-Raine, B. and Chung, W. K. (2011) A complete deficiency of hyaluronoglucosaminidase 1 (HYAL1) presenting as familial juvenile idiopathic arthritis. J. Inherit. Metab. Dis. **34**, 1013-1022. doi:10.1007/s10545-011-9343-3

54 Hemming, R., Martin, D. C., Slominski, E., Nagy, J. I., Halayko, A. J., Pind, S. and Triggs-Raine, B. (2008) Mouse Hyal3 encodes a 45- to 56-kDa glycoprotein whose overexpression increases hyaluronidase 1 activity in cultured cells. Glycobiology. **18**, 280-289. doi:10.1093/glycob/cwn006

55 Harada, H. and Takahashi, M. (2007) CD44-dependent intracellular and extracellular catabolism of hyaluronic acid by hyaluronidase-1 and -2. J. Biol. Chem. **282**, 5597-5607. doi:10.1074/jbc.M608358200

56 Atmuri, V., Martin, D. C., Hemming, R., Gutsol, A., Byers, S., Sahebjam, S., Thliveris, J. A., Mort, J. S., Carmona, E., Anderson, J. E., Dakshinamurti, S. and Triggs-Raine, B. (2008) Hyaluronidase 3 (HYAL3) knockout mice do not display evidence of hyaluronan accumulation. Matrix Biol. **27**, 653-660. doi:10.1016/j.matbio.2008.07.006

57 Reese, K. L., Aravindan, R. G., Griffiths, G. S., Shao, M., Wang, Y., Galileo, D. S., Atmuri, V., Triggs-Raine, B. L. and Martin-Deleon, P. A. (2010) Acidic hyaluronidase activity is present in mouse sperm and is reduced in the absence of SPAM1: Evidence for a role for hyaluronidase 3 in mouse and human sperm. Mol. Reprod. Dev. **77**, 759-772. doi:10.1002/mrd.21217

58 Lepperdinger, G., Strobl, B. and Kreil, G. (1998) HYAL2, a human gene expressed in many cells, encodes a lysosomal hyaluronidase with a novel type of specificity. J. Biol. Chem. **273**, 22466-22470

59 Andre, B., Duterme, C., Van Moer, K., Mertens-Strijthagen, J., Jadot, M. and Flamion, B. (2011) Hyal2 is a glycosylphosphatidylinositol-anchored, lipid raft-associated hyaluronidase. Biochem. Biophys. Res. Commun. **411**, 175-179. doi:10.1016/j.bbrc.2011.06.125

60 Rai, S. K., Duh, F. M., Vigdorovich, V., Danilkovitch-Miagkova, A., Lerman, M. I. and Miller, A. D. (2001) Candidate tumor suppressor HYAL2 is a

glycosylphosphatidylinositol (GPI)-anchored cell-surface receptor for jaagsiekte sheep retrovirus, the envelope protein of which mediates oncogenic transformation. Proc. Natl. Acad. Sci. U. S. A. **98**, 4443-4448. doi:10.1073/pnas.071572898

61 Monzon, M. E., Manzanares, D., Schmid, N., Casalino-Matsuda, S. M. and Forteza, R. M. (2008) Hyaluronidase expression and activity is regulated by pro-inflammatory cytokines in human airway epithelial cells. Am. J. Respir. Cell Mol. Biol. **39**, 289-295. doi:10.1165/rcmb.2007-0361OC; 10.1165/rcmb.2007-0361OC

62 Albeiroti, S., Ayasoufi, K., Hill, D. R., Shen, B. and de la Motte, C. A. (2015) Platelet hyaluronidase-2: An enzyme that translocates to the surface upon activation to function in extracellular matrix degradation. Blood. **125**, 1460-1469. doi:10.1182/blood-2014-07-590513 [doi]

63 Jadin, L., Wu, X., Ding, H., Frost, G. I., Onclinx, C., Triggs-Raine, B. and Flamion, B. (2008) Skeletal and hematological anomalies in HYAL2-deficient mice: A second type of mucopolysaccharidosis IX? FASEB J. **22**, 4316-4326. doi:10.1096/fj.08-111997

64 Marei, W. F., Salavati, M. and Fouladi-Nashta, A. A. (2013) Critical role of hyaluronidase-2 during preimplantation embryo development. Mol. Hum. Reprod. **19**, 590-599. doi:10.1093/molehr/gat032 [doi]

65 Olofsson, B., Porsch, H. and Heldin, P. (2014) Knock-down of CD44 regulates endothelial cell differentiation via NFkappaB-mediated chemokine production. PLoS One. **9**, e90921. doi:10.1371/journal.pone.0090921 [doi]

66 Hida, D., Danielson, B. T., Knudson, C. B. and Knudson, W. (2015) CD44 knock-down in bovine and human chondrocytes results in release of bound HYAL2. Matrix Biol. . doi:S0945-053X(15)00062-1 [pii]

67 Bourguignon, L. Y., Singleton, P. A., Diedrich, F., Stern, R. and Gilad, E. (2004) CD44 interaction with na+-H+ exchanger (NHE1) creates acidic microenvironments leading to hyaluronidase-2 and cathepsin B activation and breast tumor cell invasion. J. Biol. Chem. **279**, 26991-27007. doi:10.1074/jbc.M311838200

68 Monzon, M. E., Fregien, N., Schmid, N., Falcon, N. S., Campos, M., Casalino-Matsuda, S. M. and Forteza, R. M. (2010) Reactive oxygen species and hyaluronidase 2 regulate airway epithelial hyaluronan fragmentation. J. Biol. Chem. **285**, 26126-26134. doi:10.1074/jbc.M110.135194 [doi]

69 Duterme, C., Mertens-Strijthagen, J., Tammi, M. and Flamion, B. (2009) Two novel functions of hyaluronidase-2 (Hyal2) are formation of the glycocalyx and control of CD44-ERM interactions. J. Biol. Chem. **284**, 33495-33508. doi:10.1074/jbc.M109.044362 [doi]

70 Hsu, L. J., Schultz, L., Hong, Q., Van Moer, K., Heath, J., Li, M. Y., Lai, F. J., Lin, S. R., Lee, M. H., Lo, C. P., Lin, Y. S., Chen, S. T. and Chang, N. S. (2009) Transforming growth factor beta1 signaling via interaction with cell surface hyal-2 and recruitment of WWOX/WOX1. J. Biol. Chem. **284**, 16049-16059. doi:10.1074/jbc.M806688200

71 Noble, P. W. (2002) Hyaluronan and its catabolic products in tissue injury and repair. Matrix Biol. **21**, 25-29

72 Fieber, C., Baumann, P., Vallon, R., Termeer, C., Simon, J. C., Hofmann, M., Angel, P., Herrlich, P. and Sleeman, J. P. (2004) Hyaluronan-oligosaccharide-induced transcription of metalloproteases. J. Cell. Sci. **117**, 359-367. doi:10.1242/jcs.00831

73 Taylor, K. R., Trowbridge, J. M., Rudisill, J. A., Termeer, C. C., Simon, J. C. and Gallo, R. L. (2004) Hyaluronan fragments stimulate endothelial recognition of injury through TLR4. J. Biol. Chem. **279**, 17079-17084. doi:10.1074/jbc.M310859200

74 Flannery, C. R., Little, C. B., Hughes, C. E. and Caterson, B. (1998) Expression and activity of articular cartilage hyaluronidases. Biochem. Biophys. Res. Commun. **251**, 824-829. doi:S0006-291X(98)99561-4 [pii]

75 Tanimoto, K., Kitamura, R., Tanne, Y., Kamiya, T., Kunimatsu, R., Yoshioka, M., Tanaka, N., Tanaka, E. and Tanne, K. (2010) Modulation of hyaluronan catabolism in chondrocytes by mechanical stimuli. J. Biomed. Mater. Res. A. **93**, 373-380. doi:10.1002/jbm.a.32540 [doi]

76 Yoshida, M., Sai, S., Marumo, K., Tanaka, T., Itano, N., Kimata, K. and Fujii, K. (2004) Expression analysis of three isoforms of hyaluronan synthase and hyaluronidase in the synovium of knees in osteoarthritis and rheumatoid arthritis by quantitative real-time reverse transcriptase polymerase chain reaction. Arthritis Res. Ther. **6**, R514-20. doi:10.1186/ar1223

77 Decleves, A. E., Caron, N., Voisin, V., Legrand, A., Bouby, N., Kultti, A., Tammi, M. I. and Flamion, B. (2012) Synthesis and fragmentation of hyaluronan in renal ischaemia. Nephrol. Dial. Transplant. **27**, 3771-3781. doi:10.1093/ndt/gfs098 [doi]

78 Wu, M., Cao, M., He, Y., Liu, Y., Yang, C., Du, Y., Wang, W. and Gao, F. (2015) A novel role of low molecular weight hyaluronan in breast cancer metastasis. FASEB J. **29**, 1290-1298. doi:10.1096/fj.14-259978 [doi]

79 Maierthaler, M., Kriegsmann, M., Peng, C., Jauch, S., Szabo, A., Wallwiener, M., Rom, J., Sohn, C., Schneeweiss, A., Sinn, H. P., Yang, R. and Burwinkel, B. (2015) S100P and HYAL2 as prognostic markers for patients with triple-negative breast cancer. Exp. Mol. Pathol. **99**, 180-187. doi:10.1016/j.yexmp.2015.06.010 [doi]

80 Siiskonen, H., Poukka, M., Tyynela-Korhonen, K., Sironen, R. and Pasonen-Seppanen, S. (2013) Inverse expression of hyaluronidase 2 and hyaluronan synthases 1-3 is associated with reduced hyaluronan content in malignant cutaneous melanoma. BMC Cancer. **13**, 181-2407-13-181. doi:10.1186/1471-2407-13-181 [doi]

81 Nykopp, T. K., Rilla, K., Tammi, M. I., Tammi, R. H., Sironen, R., Hamalainen, K., Kosma, V. M., Heinonen, S. and Anttila, M. (2010) Hyaluronan synthases (HAS1-3) and hyaluronidases (HYAL1-2) in the accumulation of hyaluronan in endometrioid endometrial carcinoma. BMC Cancer. **10**, 512-2407-10-512. doi:10.1186/1471-2407-10-512 [doi]

82 Weiss, I., Trope, C. G., Reich, R. and Davidson, B. (2012) Hyaluronan synthase and hyaluronidase expression in serous ovarian carcinoma is related to anatomic site and chemotherapy exposure. Int. J. Mol. Sci. **13**, 12925-12938. doi:10.3390/ijms131012925 [doi]

83 Yang, R., Pfutze, K., Zucknick, M., Sutter, C., Wappenschmidt, B., Marme, F., Qu, B., Cuk, K., Engel, C., Schott, S., Schneeweiss, A., Brenner, H., Claus, R., Plass, C., Bugert, P., Hoth, M., Sohn, C., Schmutzler, R., Bartram, C. R. and Burwinkel, B. (2015) DNA methylation array analyses identified breast cancer-associated HYAL2 methylation in peripheral blood. Int. J. Cancer. **136**, 1845-1855. doi:10.1002/ijc.29205 [doi]

84 Bouga, H., Tsouros, I., Bounias, D., Kyriakopoulou, D., Stavropoulos, M. S., Papageorgakopoulou, N., Theocharis, D. A. and Vynios, D. H. (2010) Involvement of hyaluronidases in colorectal cancer. BMC Cancer. **10**, 499-2407-10-499. doi:10.1186/1471-2407-10-499 [doi]

85 Tian, X., Azpurua, J., Hine, C., Vaidya, A., Myakishev-Rempel, M., Ablaeva, J., Mao, Z., Nevo, E., Gorbunova, V. and Seluanov, A. (2013) High-molecular-mass hyaluronan mediates the cancer resistance of the naked mole rat. Nature. **499**, 346-349. doi:10.1038/nature12234 [doi]

86 Wang, F., Grigorieva, E. V., Li, J., Senchenko, V. N., Pavlova, T. V., Anedchenko, E. A., Kudryavtseva, A. V., Tsimanis, A., Angeloni, D., Lerman, M. I., Kashuba, V. I., Klein, G. and Zabarovsky, E. R. (2008) HYAL1 and HYAL2 inhibit tumour growth in vivo but not in vitro. PLoS One. **3**, e3031. doi:10.1371/journal.pone.0003031 [doi]

87 Lepperdinger, G., Mullegger, J. and Kreil, G. (2001) Hyal2--less active, but more versatile? Matrix Biol. **20**, 509-514

88 Reitinger, S., Laschober, G. T., Fehrer, C., Greiderer, B. and Lepperdinger, G. (2007) Mouse testicular hyaluronidase-like proteins SPAM1 and HYAL5 but not HYALP1 degrade hyaluronan. Biochem. J. **401**, 79-85. doi:10.1042/BJ20060598

89 Miller, K. A., Shao, M. and Martin-DeLeon, P. A. (2007) Hyalp1 in murine sperm function: Evidence for unique and overlapping functions with other reproductive hyaluronidases. J. Androl. **28**, 67-76. doi:10.2164/jandrol.106.000356

90 Kimura, M., Kim, E., Kang, W., Yamashita, M., Saigo, M., Yamazaki, T., Nakanishi, T., Kashiwabara, S. and Baba, T. (2009) Functional roles of mouse sperm hyaluronidases, HYAL5 and SPAM1, in fertilization. Biol. Reprod. **81**, 939-947. doi:10.1095/biolreprod.109.078816; 10.1095/biolreprod.109.078816

91 Modelski, M. J., Menlah, G., Wang, Y., Dash, S., Wu, K., Galileo, D. S. and Martin-DeLeon, P. A. (2014) Hyaluronidase 2: A novel germ cell hyaluronidase with epididymal expression and functional roles in mammalian sperm. Biol. Reprod. **91**, 109. doi:10.1095/biolreprod.113.115857 [doi]

92 Yoshida, H., Nagaoka, A., Kusaka-Kikushima, A., Tobiishi, M., Kawabata, K., Sayo, T., Sakai, S., Sugiyama, Y., Enomoto, H., Okada, Y. and Inoue, S. (2013) KIAA1199, a deafness gene of unknown function, is a new hyaluronan binding protein involved in

hyaluronan depolymerization. Proc. Natl. Acad. Sci. U. S. A. **110**, 5612-5617. doi:10.1073/pnas.1215432110; 10.1073/pnas.1215432110

93 Abe, S., Usami, S. and Nakamura, Y. (2003) Mutations in the gene encoding KIAA1199 protein, an inner-ear protein expressed in deiters' cells and the fibrocytes, as the cause of nonsyndromic hearing loss. J. Hum. Genet. **48**, 564-570. doi:10.1007/s10038-003-0079-2

94 Roden, L., Campbell, P., Fraser, J. R., Laurent, T. C., Pertoft, H. and Thompson, J. N. (1989) Enzymic pathways of hyaluronan catabolism. Ciba Found. Symp. **143**, 60-76; discussion 76-86, 281-5

95 Gushulak, L., Hemming, R., Martin, D., Seyrantepe, V., Pshezhetsky, A. and Triggs-Raine, B. (2012) Hyaluronidase 1 and beta-hexosaminidase have redundant functions in hyaluronan and chondroitin sulfate degradation. J. Biol. Chem. **287**, 16689-16697. doi:10.1074/jbc.M112.350447; 10.1074/jbc.M112.350447

96 McAtee, C. O., Berkebile, A. R., Elowsky, C., Fangman, T., Barycki, J. J., Wahl, J. K.,3rd, Khalimonchuk, O., Naslavsky, N., Caplan, S. and Simpson, M. A. (2015) Hyaluronidase Hyal1 increases tumor cell proliferation and motility through accelerated vesicle trafficking. J. Biol. Chem. . doi:10.1074/jbc.M115.647446

97 Stern, R., Kogan, G., Jedrzejas, M. J. and Soltes, L. (2007) The many ways to cleave hyaluronan. Biotechnol. Adv. **25**, 537-557. doi:10.1016/j.biotechadv.2007.07.001

98 Gao, F., Koenitzer, J. R., Tobolewski, J. M., Jiang, D., Liang, J., Noble, P. W. and Oury, T. D. (2008) Extracellular superoxide dismutase inhibits inflammation by preventing oxidative fragmentation of hyaluronan. J. Biol. Chem. **283**, 6058-6066. doi:10.1074/jbc.M709273200; 10.1074/jbc.M709273200

99 Zelko, I. N. and Folz, R. J. (2010) Extracellular superoxide dismutase attenuates release of pulmonary hyaluronan from the extracellular matrix following bleomycin exposure. FEBS Lett. **584**, 2947-2952. doi:10.1016/j.febslet.2010.05.025; 10.1016/j.febslet.2010.05.025

100 Wheatley, S. C., Isacke, C. M. and Crossley, P. H. (1993) Restricted expression of the hyaluronan receptor, CD44, during postimplantation mouse embryogenesis suggests key roles in tissue formation and patterning. Development. **119**, 295-306

101 Bourguignon, L. Y., Zhu, D. and Zhu, H. (1998) CD44 isoform-cytoskeleton interaction in oncogenic signaling and tumor progression. Front. Biosci. **3**, d637-49

102 Wang, Q., Teder, P., Judd, N. P., Noble, P. W. and Doerschuk, C. M. (2002) CD44 deficiency leads to enhanced neutrophil migration and lung injury in escherichia coli pneumonia in mice. Am. J. Pathol. **161**, 2219-2228. doi:10.1016/S0002-9440(10)64498-7

103 de La Motte, C. A., Hascall, V. C., Calabro, A., Yen-Lieberman, B. and Strong, S. A. (1999) Mononuclear leukocytes preferentially bind via CD44 to hyaluronan on human intestinal mucosal smooth muscle cells after virus infection or treatment with poly(I.C). J. Biol. Chem. **274**, 30747-30755

104 Petrey, A. C. and de la Motte, C. A. (2014) Hyaluronan, a crucial regulator of inflammation. Front. Immunol. **5**, 101. doi:10.3389/fimmu.2014.00101; 10.3389/fimmu.2014.00101

105 Trochon, V., Mabilat, C., Bertrand, P., Legrand, Y., Smadja-Joffe, F., Soria, C., Delpech, B. and Lu, H. (1996) Evidence of involvement of CD44 in endothelial cell proliferation, migration and angiogenesis in vitro. Int. J. Cancer. **66**, 664-668. doi:10.1002/(SICI)1097-0215(19960529)66:5<664::AID-IJC14>3.0.CO;2-4 [pii]

106 Knudson, W., Chow, G. and Knudson, C. B. (2002) CD44-mediated uptake and degradation of hyaluronan. Matrix Biol. **21**, 15-23

107 Kennel, S. J., Lankford, T. K., Foote, L. J., Shinpock, S. G. and Stringer, C. (1993) CD44 expression on murine tissues. J. Cell. Sci. **104 (Pt 2)**, 373-382

108 Protin, U., Schweighoffer, T., Jochum, W. and Hilberg, F. (1999) CD44-deficient mice develop normally with changes in subpopulations and recirculation of lymphocyte subsets. J. Immunol. **163**, 4917-4923

109 Banerji, S., Ni, J., Wang, S. X., Clasper, S., Su, J., Tammi, R., Jones, M. and Jackson, D. G. (1999) LYVE-1, a new homologue of the CD44 glycoprotein, is a lymph-specific receptor for hyaluronan. J. Cell Biol. **144**, 789-801

110 Gordon, E. J., Gale, N. W. and Harvey, N. L. (2008) Expression of the hyaluronan receptor LYVE-1 is not restricted to the lymphatic vasculature; LYVE-1 is also expressed on embryonic blood vessels. Dev. Dyn. **237**, 1901-1909. doi:10.1002/dvdy.21605; 10.1002/dvdy.21605

111 Mouta Carreira, C., Nasser, S. M., di Tomaso, E., Padera, T. P., Boucher, Y., Tomarev, S. I. and Jain, R. K. (2001) LYVE-1 is not restricted to the lymph vessels: Expression in normal liver blood sinusoids and down-regulation in human liver cancer and cirrhosis. Cancer Res. **61**, 8079-8084

112 Gale, N. W., Prevo, R., Espinosa, J., Ferguson, D. J., Dominguez, M. G., Yancopoulos, G. D., Thurston, G. and Jackson, D. G. (2007) Normal lymphatic development and function in mice deficient for the lymphatic hyaluronan receptor LYVE-1. Mol. Cell. Biol. **27**, 595-604. doi:10.1128/MCB.01503-06

113 Luong, M. X., Tam, J., Lin, Q., Hagendoorn, J., Moore, K. J., Padera, T. P., Seed, B., Fukumura, D., Kucherlapati, R. and Jain, R. K. (2009) Lack of lymphatic vessel phenotype in LYVE-1/CD44 double knockout mice. J. Cell. Physiol. **219**, 430-437. doi:10.1002/jcp.21686; 10.1002/jcp.21686

114 Weigel, J. A., Raymond, R. C., McGary, C., Singh, A. and Weigel, P. H. (2003) A blocking antibody to the hyaluronan receptor for endocytosis (HARE) inhibits hyaluronan clearance by perfused liver. J. Biol. Chem. **278**, 9808-9812

115 Politz, O., Gratchev, A., McCourt, P. A., Schledzewski, K., Guillot, P., Johansson, S., Svineng, G., Franke, P., Kannicht, C., Kzhyshkowska, J., Longati, P., Velten, F. W.,

Johansson, S. and Goerdt, S. (2002) Stabilin-1 and -2 constitute a novel family of fasciclin-like hyaluronan receptor homologues. Biochem. J. **362**, 155-164

116 Falkowski, M., Schledzewski, K., Hansen, B. and Goerdt, S. (2003) Expression of stabilin-2, a novel fasciclin-like hyaluronan receptor protein, in murine sinusoidal endothelia, avascular tissues, and at solid/liquid interfaces. Histochem. Cell Biol. **120**, 361-369. doi:10.1007/s00418-003-0585-5

117 Kyosseva, S. V., Harris, E. N. and Weigel, P. H. (2008) The hyaluronan receptor for endocytosis mediates hyaluronan-dependent signal transduction via extracellular signal-regulated kinases. J. Biol. Chem. **283**, 15047-15055. doi:10.1074/jbc.M709921200

118 Schledzewski, K., Geraud, C., Arnold, B., Wang, S., Grone, H. J., Kempf, T., Wollert, K. C., Straub, B. K., Schirmacher, P., Demory, A., Schonhaber, H., Gratchev, A., Dietz, L., Thierse, H. J., Kzhyshkowska, J. and Goerdt, S. (2011) Deficiency of liver sinusoidal scavenger receptors stabilin-1 and -2 in mice causes glomerulofibrotic nephropathy via impaired hepatic clearance of noxious blood factors. J. Clin. Invest. **121**, 703-714. doi:10.1172/JCI44740 [doi]

119 Assmann, V., Marshall, J. F., Fieber, C., Hofmann, M. and Hart, I. R. (1998) The human hyaluronan receptor RHAMM is expressed as an intracellular protein in breast cancer cells. J. Cell. Sci. **111 (Pt 12)**, 1685-1694

120 Entwistle, J., Hall, C. L. and Turley, E. A. (1996) HA receptors: Regulators of signalling to the cytoskeleton. J. Cell. Biochem. **61**, 569-577. doi:10.1002/(SICI)1097-4644(19960616)61:4<569::AID-JCB10>3.0.CO;2-B [pii]

121 Toole, B. P. (2001) Hyaluronan in morphogenesis. Semin. Cell Dev. Biol. **12**, 79-87. doi:10.1006/scdb.2000.0244

122 Solis, M. A., Chen, Y. H., Wong, T. Y., Bittencourt, V. Z., Lin, Y. C. and Huang, L. L. (2012) Hyaluronan regulates cell behavior: A potential niche matrix for stem cells. Biochem. Res. Int. **2012**, 346972. doi:10.1155/2012/346972; 10.1155/2012/346972

123 Cordero, D. R., Brugmann, S., Chu, Y., Bajpai, R., Jame, M. and Helms, J. A. (2011) Cranial neural crest cells on the move: Their roles in craniofacial development. Am. J. Med. Genet. A. **155A**, 270-279. doi:10.1002/ajmg.a.33702; 10.1002/ajmg.a.33702

124 Kalluri, R. and Weinberg, R. A. (2009) The basics of epithelial-mesenchymal transition. J. Clin. Invest. **119**, 1420-1428. doi:10.1172/JCI39104 [doi]

125 Nieto, M. A. (2001) The early steps of neural crest development. Mech. Dev. **105**, 27-35

126 Camenisch, T. D., Spicer, A. P., Brehm-Gibson, T., Biesterfeldt, J., Augustine, M. L., Calabro, A.,Jr, Kubalak, S., Klewer, S. E. and McDonald, J. A. (2000) Disruption of hyaluronan synthase-2 abrogates normal cardiac morphogenesis and hyaluronan-mediated transformation of epithelium to mesenchyme. J. Clin. Invest. **106**, 349-360. doi:10.1172/JCI10272

127 Casini, P., Nardi, I. and Ori, M. (2012) Hyaluronan is required for cranial neural crest cells migration and craniofacial development. Dev. Dyn. **241**, 294-302. doi:10.1002/dvdy.23715; 10.1002/dvdy.23715

128 Kultti, A., Zhao, C., Singha, N. C., Zimmerman, S., Osgood, R. J., Symons, R., Jiang, P., Li, X., Thompson, C. B., Infante, J. R., Jacobetz, M. A., Tuveson, D. A., Frost, G. I., Shepard, H. M. and Huang, Z. (2014) Accumulation of extracellular hyaluronan by hyaluronan synthase 3 promotes tumor growth and modulates the pancreatic cancer microenvironment. Biomed. Res. Int. **2014**, 817613. doi:10.1155/2014/817613; 10.1155/2014/817613

129 Li, Y., Toole, B. P., Dealy, C. N. and Kosher, R. A. (2007) Hyaluronan in limb morphogenesis. Dev. Biol. **305**, 411-420. doi:10.1016/j.ydbio.2007.02.023

130 Pohl, M., Sakurai, H., Stuart, R. O. and Nigam, S. K. (2000) Role of hyaluronan and CD44 in in vitro branching morphogenesis of ureteric bud cells. Dev. Biol. **224**, 312-325. doi:10.1006/dbio.2000.9783

131 Haddon, C. M. and Lewis, J. H. (1991) Hyaluronan as a propellant for epithelial movement: The development of semicircular canals in the inner ear of xenopus. Development. **112**, 541-550

132 Galloway, J. L., Jones, S. J., Mossey, P. A. and Ellis, I. R. (2013) The control and importance of hyaluronan synthase expression in palatogenesis. Front. Physiol. **4**, 10. doi:10.3389/fphys.2013.00010; 10.3389/fphys.2013.00010

133 Copp, A. J. and Bernfield, M. (1988) Accumulation of basement membrane-associated hyaluronate is reduced in the posterior neuropore region of mutant (curly tail) mouse embryos developing spinal neural tube defects. Dev. Biol. **130**, 583-590

134 Toole, B. P. and Gross, J. (1971) The extracellular matrix of the regenerating newt limb: Synthesis and removal of hyaluronate prior to differentiation. Dev. Biol. **25**, 57-77

135 Nandadasa, S., Foulcer, S. and Apte, S. S. (2014) The multiple, complex roles of versican and its proteolytic turnover by ADAMTS proteases during embryogenesis. Matrix Biol. **35**, 34-41. doi:10.1016/j.matbio.2014.01.005; 10.1016/j.matbio.2014.01.005

136 Gakunga, P., Frost, G., Shuster, S., Cunha, G., Formby, B. and Stern, R. (1997) Hyaluronan is a prerequisite for ductal branching morphogenesis. Development. **124**, 3987-3997

137 Taneyhill, L. A. and Bronner-Fraser, M. (2005) Recycling signals in the neural crest. J. Biol. **4**, 10. doi:10.1186/jbiol31

138 Etchevers, H. C., Amiel, J. and Lyonnet, S. (2006) Molecular bases of human neurocristopathies. Adv. Exp. Med. Biol. **589**, 213-234. doi:10.1007/978-0-387-46954-6_14

139 Hinton, R. B. and Yutzey, K. E. (2010) Heart valve structure and function in development and disease. Annu. Rev. Physiol. . doi:10.1146/annurev-physiol-012110-142145

140 de la Pompa, J. L. and Epstein, J. A. (2012) Coordinating tissue interactions: Notch signaling in cardiac development and disease. Dev. Cell. **22**, 244-254. doi:10.1016/j.devcel.2012.01.014; 10.1016/j.devcel.2012.01.014

141 Bernanke, D. H. and Orkin, R. W. (1984) Hyaluronidase activity in embryonic chick heart muscle and cushion tissue and cells. Dev. Biol. **106**, 351-359

142 Rodgers, L. S., Lalani, S., Hardy, K. M., Xiang, X., Broka, D., Antin, P. B. and Camenisch, T. D. (2006) Depolymerized hyaluronan induces vascular endothelial growth factor, a negative regulator of developmental epithelial-to-mesenchymal transformation. Circ. Res. **99**, 583-589. doi:10.1161/01.RES.0000242561.95978.43

143 Keyte, A. and Hutson, M. R. (2012) The neural crest in cardiac congenital anomalies. Differentiation. **84**, 25-40. doi:10.1016/j.diff.2012.04.005 [doi]

144 High, F. A. and Epstein, J. A. (2008) The multifaceted role of notch in cardiac development and disease. Nat. Rev. Genet. **9**, 49-61. doi:nrg2279 [pii]

145 Mulholland, D. L. and Gotlieb, A. I. (1996) Cell biology of valvular interstitial cells. Can. J. Cardiol. **12**, 231-236

146 Rodriguez, K. J., Piechura, L. M. and Masters, K. S. (2010) Regulation of valvular interstitial cell phenotype and function by hyaluronic acid in 2-D and 3-D culture environments. Matrix Biol. . doi:10.1016/j.matbio.2010.09.001

147 Masters, K. S., Shah, D. N., Leinwand, L. A. and Anseth, K. S. (2005) Crosslinked hyaluronan scaffolds as a biologically active carrier for valvular interstitial cells. Biomaterials. **26**, 2517-2525. doi:10.1016/j.biomaterials.2004.07.018

148 Al'Qteishat, A., Gaffney, J., Krupinski, J., Rubio, F., West, D., Kumar, S., Kumar, P., Mitsios, N. and Slevin, M. (2006) Changes in hyaluronan production and metabolism following ischaemic stroke in man. Brain. **129**, 2158-2176. doi:awl139 [pii]

149 Turino, G. M. and Cantor, J. O. (2003) Hyaluronan in respiratory injury and repair. Am. J. Respir. Crit. Care Med. **167**, 1169-1175. doi:10.1164/rccm.200205-449PP [doi]

150 Toole, B. P., Wight, T. N. and Tammi, M. I. (2002) Hyaluronan-cell interactions in cancer and vascular disease. J. Biol. Chem. **277**, 4593-4596. doi:10.1074/jbc.R100039200 [doi]

151 Rangel, M. P., de Sa, V. K., Martins, V., Martins, J. R., Parra, E. R., Mendes, A., Andrade, P. C., Reis, R. M., Longatto-Filho, A., Oliveira, C. Z., Takagaki, T., Carraro, D. M., Nader, H. B. and Capelozzi, V. L. (2015) Tissue hyaluronan expression, as reflected in the sputum of lung cancer patients, is an indicator of malignancy. Braz. J. Med. Biol. Res. **48**, 557-567. doi:10.1590/1414-431X20144300 [doi]

152 Posey, J. T., Soloway, M. S., Ekici, S., Sofer, M., Civantos, F., Duncan, R. C. and Lokeshwar, V. B. (2003) Evaluation of the prognostic potential of hyaluronic acid and hyaluronidase (HYAL1) for prostate cancer. Cancer Res. **63**, 2638-2644

153 Anttila, M. A., Tammi, R. H., Tammi, M. I., Syrjanen, K. J., Saarikoski, S. V. and Kosma, V. M. (2000) High levels of stromal hyaluronan predict poor disease outcome in epithelial ovarian cancer. Cancer Res. **60**, 150-155

154 Frenkel, J. S. (2014) The role of hyaluronan in wound healing. Int. Wound. J. **11**, 159-163. doi:10.1111/j.1742-481X.2012.01057.x; 10.1111/j.1742-481X.2012.01057.x

155 West, D. C., Shaw, D. M., Lorenz, P., Adzick, N. S. and Longaker, M. T. (1997) Fibrotic healing of adult and late gestation fetal wounds correlates with increased hyaluronidase activity and removal of hyaluronan. Int. J. Biochem. Cell Biol. **29**, 201-210

156 Grande-Allen, K. J., Griffin, B. P., Ratliff, N. B., Cosgrove, D. M. and Vesely, I. (2003) Glycosaminoglycan profiles of myxomatous mitral leaflets and chordae parallel the severity of mechanical alterations. J. Am. Coll. Cardiol. **42**, 271-277

157 Gupta, V., Barzilla, J. E., Mendez, J. S., Stephens, E. H., Lee, E. L., Collard, C. D., Laucirica, R., Weigel, P. H. and Grande-Allen, K. J. (2009) Abundance and location of proteoglycans and hyaluronan within normal and myxomatous mitral valves. Cardiovasc. Pathol. **18**, 191-197. doi:10.1016/j.carpath.2008.05.001

158 Guo, M. S., Wu, Y. Y. and Liang, Z. B. (2012) Hyaluronic acid increases MMP-2 and MMP-9 expressions in cultured trabecular meshwork cells from patients with primary open-angle glaucoma. Mol. Vis. **18**, 1175-1181

159 Coutinho, M. F., Lacerda, L. and Alves, S. (2012) Glycosaminoglycan storage disorders: A review. Biochem. Res. Int. **2012**, 471325. doi:10.1155/2012/471325; 10.1155/2012/471325

160 Muenzer, J. (2011) Overview of the mucopolysaccharidoses. Rheumatology (Oxford). **50 Suppl 5**, v4-12. doi:10.1093/rheumatology/ker394; 10.1093/rheumatology/ker394

161 Bach, G., Friedman, R., Weissmann, B. and Neufeld, E. F. (1972) The defect in the hurler and scheie syndromes: Deficiency of -L-iduronidase. Proc. Natl. Acad. Sci. U. S. A. **69**, 2048-2051

162 Johnson, B. A., van Diggelen, O. P., Dajnoki, A. and Bodamer, O. A. (2013) Diagnosing lysosomal storage disorders: Mucopolysaccharidosis type II. Curr. Protoc. Hum. Genet. **79**, Unit 17.14. doi:10.1002/0471142905.hg1714s79 [doi]

163 Scott, H. S., Blanch, L., Guo, X. H., Freeman, C., Orsborn, A., Baker, E., Sutherland, G. R., Morris, C. P. and Hopwood, J. J. (1995) Cloning of the sulphamidase gene and identification of mutations in sanfilippo A syndrome. Nat. Genet. **11**, 465-467. doi:10.1038/ng1295-465 [doi]

164 Neufeld, E. F. and Muenzer, J. (2001) The mucopolysaccharidoses. In The Metabolic & Molecular Bases of Inherited Disease (Scriver, C. R., Beaudet, A. L., Sly, W. S. and Valle, D., eds.), pp. 3421-3451, McGraw–Hil

165 Tomatsu, S., Orii, K. O., Vogler, C., Nakayama, J., Levy, B., Grubb, J. H., Gutierrez, M. A., Shim, S., Yamaguchi, S., Nishioka, T., Montano, A. M., Noguchi, A., Orii, T., Kondo,

N. and Sly, W. S. (2003) Mouse model of N-acetylgalactosamine-6-sulfate sulfatase deficiency (galns-/-) produced by targeted disruption of the gene defective in morquio A disease. Hum. Mol. Genet. **12**, 3349-3358. doi:10.1093/hmg/ddg366 [doi]

166 Fidzianska, E., Abramowicz, T., Czartoryska, B., Glogowska, I., Gorska, D. and Rodo, M. (1984) Assignment of the gene for human arylsulfatase B, ARSB, to chromosome region 5p11----5qter. Cytogenet. Cell Genet. **38**, 150-151

167 Miller, R. D., Hoffmann, J. W., Powell, P. P., Kyle, J. W., Shipley, J. M., Bachinsky, D. R. and Sly, W. S. (1990) Cloning and characterization of the human beta-glucuronidase gene. Genomics. **7**, 280-283

168 Grande-Allen, K. J., Calabro, A., Gupta, V., Wight, T. N., Hascall, V. C. and Vesely, I. (2004) Glycosaminoglycans and proteoglycans in normal mitral valve leaflets and chordae: Association with regions of tensile and compressive loading. Glycobiology. **14**, 621-633. doi:10.1093/glycob/cwh076

169 Fesslova, V., Corti, P., Sersale, G., Rovelli, A., Russo, P., Mannarino, S., Butera, G. and Parini, R. (2009) The natural course and the impact of therapies of cardiac involvement in the mucopolysaccharidoses. Cardiol. Young. **19**, 170-178. doi:10.1017/S1047951109003576; 10.1017/S1047951109003576

170 Braunlin, E. A., Harmatz, P. R., Scarpa, M., Furlanetto, B., Kampmann, C., Loehr, J. P., Ponder, K. P., Roberts, W. C., Rosenfeld, H. M. and Giugliani, R. (2011) Cardiac disease in patients with mucopolysaccharidosis: Presentation, diagnosis and management. J. Inherit. Metab. Dis. **34**, 1183-1197. doi:10.1007/s10545-011-9359-8

171 Haskins, M., Casal, M., Ellinwood, N. M., Melniczek, J., Mazrier, H. and Giger, U. (2002) Animal models for mucopolysaccharidoses and their clinical relevance. Acta Paediatr. Suppl. **91**, 88-97

172 Okuyama, T., Tanaka, A., Suzuki, Y., Ida, H., Tanaka, T., Cox, G. F., Eto, Y. and Orii, T. (2010) Japan elaprase treatment (JET) study: Idursulfase enzyme replacement therapy in adult patients with attenuated hunter syndrome (mucopolysaccharidosis II, MPS II). Mol. Genet. Metab. **99**, 18-25. doi:10.1016/j.ymgme.2009.08.006; 10.1016/j.ymgme.2009.08.006

173 Braunlin, E. A., Berry, J. M. and Whitley, C. B. (2006) Cardiac findings after enzyme replacement therapy for mucopolysaccharidosis type I. Am. J. Cardiol. **98**, 416-418. doi:10.1016/j.amjcard.2006.02.047

174 Oussoren, E., Brands, M. M., Ruijter, G. J., der Ploeg, A. T. and Reuser, A. J. (2011) Bone, joint and tooth development in mucopolysaccharidoses: Relevance to therapeutic options. Biochim. Biophys. Acta. **1812**, 1542-1556. doi:10.1016/j.bbadis.2011.07.013; 10.1016/j.bbadis.2011.07.013

175 Stanton, H., Melrose, J., Little, C. B. and Fosang, A. J. (2011) Proteoglycan degradation by the ADAMTS family of proteinases. Biochim. Biophys. Acta. **1812**, 1616-1629. doi:10.1016/j.bbadis.2011.08.009; 10.1016/j.bbadis.2011.08.009

176 Colige, A., Sieron, A. L., Li, S. W., Schwarze, U., Petty, E., Wertelecki, W., Wilcox, W., Krakow, D., Cohn, D. H., Reardon, W., Byers, P. H., Lapiere, C. M., Prockop, D. J. and Nusgens, B. V. (1999) Human ehlers-danlos syndrome type VII C and bovine dermatosparaxis are caused by mutations in the procollagen I N-proteinase gene. Am. J. Hum. Genet. **65**, 308-317. doi:10.1086/302504

177 Dagoneau, N., Benoist-Lasselin, C., Huber, C., Faivre, L., Megarbane, A., Alswaid, A., Dollfus, H., Alembik, Y., Munnich, A., Legeai-Mallet, L. and Cormier-Daire, V. (2004) ADAMTS10 mutations in autosomal recessive weill-marchesani syndrome. Am. J. Hum. Genet. **75**, 801-806. doi:10.1086/425231

178 Dubail, J. and Apte, S. S. (2015) Insights on ADAMTS proteases and ADAMTS-like proteins from mammalian genetics. Matrix Biol. . doi:10.1016/j.matbio.2015.03.001; 10.1016/j.matbio.2015.03.001

179 Kern, C. B., Wessels, A., McGarity, J., Dixon, L. J., Alston, E., Argraves, W. S., Geeting, D., Nelson, C. M., Menick, D. R. and Apte, S. S. (2010) Reduced versican cleavage due to Adamts9 haploinsufficiency is associated with cardiac and aortic anomalies. Matrix Biol. **29**, 304-316. doi:10.1016/j.matbio.2010.01.005

180 Chow, G., Knudson, C. B. and Knudson, W. (2006) Expression and cellular localization of human hyaluronidase-2 in articular chondrocytes and cultured cell lines. Osteoarthritis Cartilage. **14**, 849-858. doi:10.1016/j.joca.2006.02.009

181 Armstrong, E. J. and Bischoff, J. (2004) Heart valve development: Endothelial cell signaling and differentiation. Circ. Res. **95**, 459-470. doi:10.1161/01.RES.0000141146.95728.da

182 Jordan, M. C., Zheng, Y., Ryazantsev, S., Rozengurt, N., Roos, K. P. and Neufeld, E. F. (2005) Cardiac manifestations in the mouse model of mucopolysaccharidosis I. Mol. Genet. Metab. **86**, 233-243. doi:10.1016/j.ymgme.2005.05.003

183 Atmuri, V., Martin, D. C., Hemming, R., Gutsol, A., Byers, S., Sahebjam, S., Thliveris, J. A., Mort, J. S., Carmona, E., Anderson, J. E., Dakshinamurti, S. and Triggs-Raine, B. (2008) Hyaluronidase 3 (HYAL3) knockout mice do not display evidence of hyaluronan accumulation. Matrix Biol. **27**, 653-660. doi:10.1016/j.matbio.2008.07.006

184 Proohet EB, Mills B, Arrington JB,Sobin LH. (1994) Armed forces institute of pathology laboratory methods in histopathology. , American Registry of Pathology, Washinton, D.C.

185 Plaas, A. H., West, L., Midura, R. J. and Hascall, V. C. (2001) Disaccharide composition of hyaluronan and chondroitin/dermatan sulfate. analysis with fluorophore-assisted carbohydrate electrophoresis. Methods Mol. Biol. **171**, 117-128. doi:10.1385/1-59259-209-0:117

186 Gordon, L. B., Harten, I. A., Calabro, A., Sugumaran, G., Csoka, A. B., Brown, W. T., Hascall, V. and Toole, B. P. (2003) Hyaluronan is not elevated in urine or serum in hutchinson-gilford progeria syndrome. Hum. Genet. **113**, 178-187. doi:10.1007/s00439-003-0958-9

187 Camenisch, T. D., Biesterfeldt, J., Brehm-Gibson, T., Bradley, J. and McDonald, J. A. (2001) Regulation of cardiac cushion development by hyaluronan. Exp. Clin. Cardiol. **6**, 4-10

188 Camenisch, T. D., Schroeder, J. A., Bradley, J., Klewer, S. E. and McDonald, J. A. (2002) Heart-valve mesenchyme formation is dependent on hyaluronan-augmented activation of ErbB2-ErbB3 receptors. Nat. Med. **8**, 850-855. doi:10.1038/nm742

189 Stephens, E. H., Chu, C. K. and Grande-Allen, K. J. (2008) Valve proteoglycan content and glycosaminoglycan fine structure are unique to microstructure, mechanical load and age: Relevance to an age-specific tissue-engineered heart valve. Acta Biomater. **4**, 1148-1160. doi:10.1016/j.actbio.2008.03.014

190 Strauch, O. F., Stypmann, J., Reinheckel, T., Martinez, E., Haverkamp, W. and Peters, C. (2003) Cardiac and ocular pathologies in a mouse model of mucopolysaccharidosis type VI. Pediatr. Res. **54**, 701-708. doi:10.1203/01.PDR.0000084085.65972.3F

191 Stephens, E. H., Saltarrelli, J. G., Baggett, L. S., Nandi, I., Kuo, J. J., Davis, A. R., Olmsted-Davis, E. A., Reardon, M. J., Morrisett, J. D. and Grande-Allen, K. J. (2011) Differential proteoglycan and hyaluronan distribution in calcified aortic valves. Cardiovasc. Pathol. **20**, 334-342. doi:10.1016/j.carpath.2010.10.002 [doi]

192 Vyavahare, N., Ogle, M., Schoen, F. J., Zand, R., Gloeckner, D. C., Sacks, M. and Levy, R. J. (1999) Mechanisms of bioprosthetic heart valve failure: Fatigue causes collagen denaturation and glycosaminoglycan loss. J. Biomed. Mater. Res. **46**, 44-50

193 Hoffmeister, A., Hetzel, J., Sander, S., Kron, M., Hombach, V. and Koenig, W. (1999) Plasma viscosity and fibrinogen in relation to haemodynamic findings in chronic congestive heart failure. Eur. J. Heart Fail. **1**, 293-295. doi:S1388-9842(99)00030-6 [pii]

194 Underhill, C. B., Nguyen, H. A., Shizari, M. and Culty, M. (1993) CD44 positive macrophages take up hyaluronan during lung development. Dev. Biol. **155**, 324-336. doi:S0012-1606(83)71032-8 [pii]

195 Csoka, A. B., Frost, G. I., Heng, H. H., Scherer, S. W., Mohapatra, G. and Stern, R. (1998) The hyaluronidase gene HYAL1 maps to chromosome 3p21.2-p21.3 in human and 9F1-F2 in mouse, a conserved candidate tumor suppressor locus. Genomics. **48**, 63-70. doi:S0888754397951582 [pii]

196 Stern, R. (2004) Hyaluronan catabolism: A new metabolic pathway. Eur. J. Cell Biol. **83**, 317-325. doi:S0171-9335(04)70400-8 [pii]

197 Pierpont, M. E., Basson, C. T., Benson, D. W.,Jr, Gelb, B. D., Giglia, T. M., Goldmuntz, E., McGee, G., Sable, C. A., Srivastava, D., Webb, C. L. and American Heart Association Congenital Cardiac Defects Committee, Council on Cardiovascular Disease in the Young. (2007) Genetic basis for congenital heart defects: Current knowledge: A scientific statement from the american heart association congenital cardiac defects committee, council on cardiovascular disease in the young: Endorsed by the american academy of pediatrics. Circulation. **115**, 3015-3038. doi:10.1161/CIRCULATIONAHA.106.183056

198 Payne, R. M., Johnson, M. C., Grant, J. W. and Strauss, A. W. (1995) Toward a molecular understanding of congenital heart disease. Circulation. **91**, 494-504

199 Chowdhury, B., Hemming, R., Hombach-Klonisch, S., Flamion, B. and Triggs-Raine, B. (2013) Murine hyaluronidase 2 deficiency results in extracellular hyaluronan accumulation and severe cardiopulmonary dysfunction. J. Biol. Chem. **288**, 520-528. doi:10.1074/jbc.M112.393629; 10.1074/jbc.M112.393629

200 Lin, C. J., Lin, C. Y., Chen, C. H., Zhou, B. and Chang, C. P. (2012) Partitioning the heart: Mechanisms of cardiac septation and valve development. Development. **139**, 3277-3299. doi:10.1242/dev.063495; 10.1242/dev.063495

201 Hinton, R. B.,Jr, Lincoln, J., Deutsch, G. H., Osinska, H., Manning, P. B., Benson, D. W. and Yutzey, K. E. (2006) Extracellular matrix remodeling and organization in developing and diseased aortic valves. Circ. Res. **98**, 1431-1438. doi:10.1161/01.RES.0000224114.65109.4e

202 Mjaatvedt, C. H., Yamamura, H., Capehart, A. A., Turner, D. and Markwald, R. R. (1998) The Cspg2 gene, disrupted in the hdf mutant, is required for right cardiac chamber and endocardial cushion formation. Dev. Biol. **202**, 56-66. doi:S0012-1606(98)99001-7 [pii]

203 Corrigan, N., Brazil, D. P. and Auliffe, F. M. (2010) High-frequency ultrasound assessment of the murine heart from embryo through to juvenile. Reprod. Sci. **17**, 147-157. doi:10.1177/1933719109348923; 10.1177/1933719109348923

204 Metscher, B. D. (2009) MicroCT for comparative morphology: Simple staining methods allow high-contrast 3D imaging of diverse non-mineralized animal tissues. BMC Physiol. **9**, 11-6793-9-11. doi:10.1186/1472-6793-9-11 [doi]

205 Armistead, J., Patel, N., Wu, X., Hemming, R., Chowdhury, B., Basra, G. S., Del Bigio, M. R., Ding, H. and Triggs-Raine, B. (2015) Growth arrest in the ribosomopathy, bowen-conradi syndrome, is due to dramatically reduced cell proliferation and a defect in mitotic progression. Biochim. Biophys. Acta. **1852**, 1029-1037. doi:10.1016/j.bbadis.2015.02.007 [doi]

206 Schindelin, J., Arganda-Carreras, I., Frise, E., Kaynig, V., Longair, M., Pietzsch, T., Preibisch, S., Rueden, C., Saalfeld, S., Schmid, B., Tinevez, J. Y., White, D. J., Hartenstein, V., Eliceiri, K., Tomancak, P. and Cardona, A. (2012) Fiji: An open-source platform for biological-image analysis. Nat. Methods. **9**, 676-682. doi:10.1038/nmeth.2019 [doi]

207 Fenderson, B. A., Stamenkovic, I. and Aruffo, A. (1993) Localization of hyaluronan in mouse embryos during implantation, gastrulation and organogenesis. Differentiation. **54**, 85-98

208 Zhu, X., Deng, X., Huang, G., Wang, J., Yang, J., Chen, S., Ma, X. and Wang, B. (2014) A novel mutation of hyaluronan synthase 2 gene in chinese children with ventricular septal defect. PLoS One. **9**, e87437. doi:10.1371/journal.pone.0087437 [doi]

209 Araki, T., Chan, G., Newbigging, S., Morikawa, L., Bronson, R. T. and Neel, B. G. (2009) Noonan syndrome cardiac defects are caused by PTPN11 acting in endocardium to

enhance endocardial-mesenchymal transformation. Proc. Natl. Acad. Sci. U. S. A. **106**, 4736-4741. doi:10.1073/pnas.0810053106 [doi]

210 Frieden, L. A., Townsend, T. A., Vaught, D. B., Delaughter, D. M., Hwang, Y., Barnett, J. V. and Chen, J. (2010) Regulation of heart valve morphogenesis by eph receptor ligand, ephrin-A1. Dev. Dyn. **239**, 3226-3234. doi:10.1002/dvdy.22458 [doi]

211 Stork, T., Mockel, M., Danne, O., Voller, H., Eichstadt, H. and Frei, U. (1995) Left ventricular hypertrophy and diastolic dysfunction: Their relation to coronary heart disease. Cardiovasc. Drugs Ther. **9 Suppl 3**, 533-537

212 Murdoch, C. E., Chaubey, S., Zeng, L., Yu, B., Ivetic, A., Walker, S. J., Vanhoutte, D., Heymans, S., Grieve, D. J., Cave, A. C., Brewer, A. C., Zhang, M. and Shah, A. M. (2014) Endothelial NADPH oxidase-2 promotes interstitial cardiac fibrosis and diastolic dysfunction through proinflammatory effects and endothelial-mesenchymal transition. J. Am. Coll. Cardiol. **63**, 2734-2741. doi:10.1016/j.jacc.2014.02.572; 10.1016/j.jacc.2014.02.572

213 Zaid, R. R., Barker, C. M., Little, S. H. and Nagueh, S. F. (2013) Pre- and post-operative diastolic dysfunction in patients with valvular heart disease: Diagnosis and therapeutic implications. J. Am. Coll. Cardiol. **62**, 1922-1930. doi:10.1016/j.jacc.2013.08.1619; 10.1016/j.jacc.2013.08.1619

214 Borlaug, B. A. and Paulus, W. J. (2011) Heart failure with preserved ejection fraction: Pathophysiology, diagnosis, and treatment. Eur. Heart J. **32**, 670-679. doi:10.1093/eurheartj/ehq426 [doi]

215 Leung, D. Y., Boyd, A., Ng, A. A., Chi, C. and Thomas, L. (2008) Echocardiographic evaluation of left atrial size and function: Current understanding, pathophysiologic correlates, and prognostic implications. Am. Heart J. **156**, 1056-1064. doi:10.1016/j.ahj.2008.07.021 [doi]

216 Tei, C. (1995) New non-invasive index for combined systolic and diastolic ventricular function. J. Cardiol. **26**, 135-136

217 Bruch, C., Schmermund, A., Marin, D., Katz, M., Bartel, T., Schaar, J. and Erbel, R. (2000) Tei-index in patients with mild-to-moderate congestive heart failure. Eur. Heart J. **21**, 1888-1895. doi:10.1053/euhj.2000.2246 [doi]

218 Poulsen, S. H., Nielsen, J. C. and Andersen, H. R. (2000) The influence of heart rate on the doppler-derived myocardial performance index. J. Am. Soc. Echocardiogr. **13**, 379-384. doi:S0894731700215629 [pii]

219 Marian, A. J. (2002) Modifier genes for hypertrophic cardiomyopathy. Curr. Opin. Cardiol. **17**, 242-252

220 Dupuis, L. E., McCulloch, D. R., McGarity, J. D., Bahan, A., Wessels, A., Weber, D., Diminich, A. M., Nelson, C. M., Apte, S. S. and Kern, C. B. (2011) Altered versican cleavage in ADAMTS5 deficient mice; a novel etiology of myxomatous valve disease. Dev. Biol. **357**, 152-164. doi:10.1016/j.ydbio.2011.06.041; 10.1016/j.ydbio.2011.06.041

221 Laurent, T. C., Laurent, U. B. and Fraser, J. R. (1996) The structure and function of hyaluronan: An overview. Immunol. Cell Biol. **74**, A1-7. doi:10.1038/icb.1996.32

222 Laurent, T. C. and Fraser, J. R. (1992) Hyaluronan. FASEB J. **6**, 2397-2404

223 Itano, N., Sawai, T., Miyaishi, O. and Kimata, K. (1999) Relationship between hyaluronan production and metastatic potential of mouse mammary carcinoma cells. Cancer Res. **59**, 2499-2504

224 Laurent, T. C., Laurent, U. B. and Fraser, J. R. (1996) Serum hyaluronan as a disease marker. Ann. Med. **28**, 241-253

225 Morales, T. I. and Hascall, V. C. (1989) Factors involved in the regulation of proteoglycan metabolism in articular cartilage. Arthritis Rheum. **32**, 1197-1201

226 Schiller, S. and Dorfman, A. (1957) The metabolism of mucopolysaccharides in animals: The effect of cortisone and hydrocortisone on rat skin. Endocrinology. **60**, 376-381. doi:10.1210/endo-60-3-376 [doi]

227 Prevo, R., Banerji, S., Ferguson, D. J., Clasper, S. and Jackson, D. G. (2001) Mouse LYVE-1 is an endocytic receptor for hyaluronan in lymphatic endothelium. J. Biol. Chem. **276**, 19420-19430. doi:10.1074/jbc.M011004200

228 Culty, M., Nguyen, H. A. and Underhill, C. B. (1992) The hyaluronan receptor (CD44) participates in the uptake and degradation of hyaluronan. J. Cell Biol. **116**, 1055-1062

229 Hirose, Y., Saijou, E., Sugano, Y., Takeshita, F., Nishimura, S., Nonaka, H., Chen, Y. R., Sekine, K., Kido, T., Nakamura, T., Kato, S., Kanke, T., Nakamura, K., Nagai, R., Ochiya, T. and Miyajima, A. (2012) Inhibition of stabilin-2 elevates circulating hyaluronic acid levels and prevents tumor metastasis. Proc. Natl. Acad. Sci. U. S. A. **109**, 4263-4268. doi:10.1073/pnas.1117560109 [doi]

230 Gerdin, B. and Hallgren, R. (1991) Localisation of hyaluronan in the human intestinal wall. Gut. **32**, 760-762

231 Butikofer, P., Malherbe, T., Boschung, M. and Roditi, I. (2001) GPI-anchored proteins: Now you see 'em, now you don't. FASEB J. **15**, 545-548. doi:10.1096/fj.00-0415hyp [doi]

232 Cherr, G. N., Meyers, S. A., Yudin, A. I., VandeVoort, C. A., Myles, D. G., Primakoff, P. and Overstreet, J. W. (1996) The PH-20 protein in cynomolgus macaque spermatozoa: Identification of two different forms exhibiting hyaluronidase activity. Dev. Biol. **175**, 142-153. doi:S0012-1606(96)90102-5 [pii]

233 de la Motte, C., Nigro, J., Vasanji, A., Rho, H., Kessler, S., Bandyopadhyay, S., Danese, S., Fiocchi, C. and Stern, R. (2009) Platelet-derived hyaluronidase 2 cleaves hyaluronan into fragments that trigger monocyte-mediated production of proinflammatory cytokines. Am. J. Pathol. **174**, 2254-2264. doi:10.2353/ajpath.2009.080831 [doi]

234 Jadin, L., Bookbinder, L. H. and Frost, G. I. (2012) A comprehensive model of hyaluronan turnover in the mouse. Matrix Biol. **31**, 81-89. doi:10.1016/j.matbio.2011.11.002; 10.1016/j.matbio.2011.11.002

235 Fraser, J. R., Kimpton, W. G., Laurent, T. C., Cahill, R. N. and Vakakis, N. (1988) Uptake and degradation of hyaluronan in lymphatic tissue. Biochem. J. **256**, 153-158

236 McCourt, P. A., Smedsrod, B. H., Melkko, J. and Johansson, S. (1999) Characterization of a hyaluronan receptor on rat sinusoidal liver endothelial cells and its functional relationship to scavenger receptors. Hepatology. **30**, 1276-1286. doi:S0270913999004887 [pii]

237 Belsky, E. and Toole, B. P. (1983) Hyaluronate and hyaluronidase in the developing chick embryo kidney. Cell Differ. **12**, 61-66

238 Colombaro, V., Jadot, I., Decleves, A. E., Voisin, V., Giordano, L., Habsch, I., Flamion, B. and Caron, N. (2015) Hyaluronidase 1 and hyaluronidase 2 are required for renal hyaluronan turnover. Acta Histochem. **117**, 83-91. doi:10.1016/j.acthis.2014.11.007 [doi]

239 Pawlowski, K. S., Wright, C. G. and Meyerhoff, W. L. (1998) Histologic demonstration of glycosaminoglycans in inner ear fluids. Acta Otolaryngol. **118**, 505-510

240 Yu, W., Serrano, M., Miguel, S. S., Ruest, L. B. and Svoboda, K. K. (2009) Cleft lip and palate genetics and application in early embryological development. Indian. J. Plast. Surg. **42 Suppl**, S35-50. doi:10.4103/0970-0358.57185 [doi]

241 Lamouille, S., Xu, J. and Derynck, R. (2014) Molecular mechanisms of epithelial-mesenchymal transition. Nat. Rev. Mol. Cell Biol. **15**, 178-196. doi:10.1038/nrm3758 [doi]

242 Craig, E. A., Parker, P. and Camenisch, T. D. (2009) Size-dependent regulation of Snail2 by hyaluronan: Its role in cellular invasion. Glycobiology. **19**, 890-898. doi:10.1093/glycob/cwp064; 10.1093/glycob/cwp064

243 Allison, P., Espiritu, D., Barnett, J. V. and Camenisch, T. D. (2015) Type III TGFbeta receptor and src direct hyaluronan-mediated invasive cell motility. Cell. Signal. **27**, 453-459. doi:10.1016/j.cellsig.2014.11.037 [doi]

244 Dor, Y., Klewer, S. E., McDonald, J. A., Keshet, E. and Camenisch, T. D. (2003) VEGF modulates early heart valve formation. Anat. Rec. A. Discov. Mol. Cell. Evol. Biol. **271**, 202-208. doi:10.1002/ar.a.10026 [doi]

245 Bosi, G., Evangelisti, R., Valeno, V., Carinci, F., Pezzetti, F., Calastrini, C., Bodo, M. and Carinci, P. (1998) Diphenylhydantoin affects glycosaminoglycans and collagen production by human fibroblasts from cleft palate patients. J. Dent. Res. **77**, 1613-1621